Markerless motion capture applied to the analysis of locomotor kinematics in the semi-aquatic hunting spider, *Dolomedes aquaticus*

Kiri Frances Pullar

A thesis submitted for the degree of

Master of Science in Zoology

at the University of Otago, Dunedin,

New Zealand.

Date: October 6, 2009

Abstract

This thesis focuses on two key goals. Firstly, developing a markerless motion capture technique for the examination of joint angles during spider locomotion. Secondly, applying this technique to understanding gait and gait generating mechanisms in the semi-aquatic hunting spider, *Dolomedes aquaticus*.

I present a markerless technique for reconstructing 2D joint angles during locomotion based on information contained in video frames and a spider model based on the relative lengths of segments and joint angle limits. This algorithm allows gait analysis without the need for a sophisticated lab setup. Analysis is based on the subject filmed by a stationary video camera. Techniques that recover body pose from video sequences with little user intervention have numerous applications such as motion capture, gesture recognition, surveillance of people or animals and animation for movies or computer games. The spiders' pose is estimated in every frame of a video sequence. The basic elements of my tracking approach include an articulated body model, extracted features from video frames and various constraints. These components are combined in a Bayesian framework, which segments the frame into foreground and subject and estimates the pose of the subject.

Joint angles are used to investigate gait and gait generating mechanisms underlying locomotion in the spider. Firstly, kinematic parameters were compared to mass and body length of spiders. Stride length was the only kinematic parameter to yield significant results compared to spider size, however non-significant scaling relationships were similar in magnitude to those in the literature.

Secondly, kinematic parameters were analysed in relation to speed of locomotion. Stride frequency showed a greater correlation with normalized speed than absolute speed and stride length showed a greater correlation with absolute speed than normalized speed. This suggests that larger animals increase their speed by increasing stride length, whereas it is possible for smaller animals to increase their speed by increasing stride frequency. Contrary to the relationship frequently observed in insects, both protraction and retraction periods decreased with speed.

Thirdly, changes in velocity and acceleration were compared across the trajectory of each pair of legs and the ipsilateral and contralateral coordination of legs was investigated. Each leg was found to contribute in a specific manner to locomotion. Movements of front legs were random, suggesting they play some other role, possibly sensory, rather than contributing to stability. Legs 2 and 3 appeared to play a more dominant role in generating propulsive force, with hind legs probably contributing more to stability than propulsion.

Acknowledgements

I would like to begin by thanking my supervisor, Mike Paulin. Thank you for your time and support, particularly when things were not going as planned. Thank you for encouraging me to attempt things I though at the time I were impossible and general guidance on developing myself as a scientist.

A huge thank you to Rasmus Jensen for allowing me access to his human tracking code, without him I would possibly still be staring at a computer screen wondering where to begin. Thanks also to Jordi Moya-Laraño for supplying me with speed vs. size data from other spider species. Additionally, anyone else who I contacted over the duration of my thesis for things ranging from code to copies of papers, everyone was so accommodating of a Masters student from a University that most people have probably never heard of.

I am grateful to all the staff and students at the Zoology Department at the University of Otago. In particular, Ken Miller and Murray McKenzie for their technical assistance and Phil Bishop for his spider advice. To Stefan Reussenzehn, your data made my life considerably easier when trying to construct a model spider. Thanks for sharing the lab space and spiders with me. We may be a small "lab group", but having someone who understood some of my challenges along the way was invaluable.

Thanks to Joshua Gagnon, for his assistance with diagrams, for proofreading and for providing a sometimes unwelcome distraction from work. Finally, I am grateful to all my friends and family who have supported me in different ways as I worked on my thesis over the last couple of years.

Contents

List of Figures

List of Tables

List of Abbreviations

Abbreviation or symbol	Meaning/Description
AEP	Anterior extreme position
Co	Coxa
CRF	Conditional Random Field
DOF	Degrees of Freedom
f_c	Cut-off frequency for Butterworth filter
Fe	Femur
F_S	Stride frequency
L1	Left leg 1
L2	Left leg 2
L3	Left leg 3
L4	Left leg 4
L_S	Stride length
M	Mass
MAP	Maximum-a-Posteriori
Me	Metatarsus
MRF	Markov Random Field
Pa	Patella
PEP	Posterior extreme position
R1	Right leg 1
R2	Right leg 2
R3	Right leg 3
R4	Right leg 4
Ta	Tarsus
Ti	Tibia
Tr	Trochanter
V_a	Absolute velocity
V_n	Normalized velocity

Chapter 1

Introduction

1.1 Legged locomotion

All active locomotory strategies are based around the principle that when an organism exerts a force on the external environment it will accelerate in the opposite direction. Additionally, there are external forces to consider which differ depending on the environment and mode of locomotion. Terrestrial vertebrates have been shaped by evolution so their brains and bodies exploit the interaction between gravity and inertia producing agile locomotion. Despite major morphological and physiological differences, birds and mammals produce similar force patterns and energy fluctuations during legged locomotion.

In the past, the dominant hypothesis for the motor control of locomotion was servo control. Servo control is a static control scheme, where the central nervous system specifies a target limb position for each phase of the step cycle (Loeb, 1989). This hypothesis maintained its dominance for many years, partly due to the arrangement of proprioceptive sensory feedback having similarities with feedback loops used in industrial torque motors (Loeb, 1989). More recently, there has been a shift away from the view that limbs are actively forced along a specified trajectory; rather locomotion can be achieved through natural mechanisms or 'passive dynamics' which do not require continuous forcing (McGeer, 1990a; McGeer, 1990b). The passive dynamic model of bipedal walking is similar to a wheel rolling on a frictional surface without slipping, in that it can move down a gentle slope and gain energy from gravity so that the essential cost of locomotion is zero (McGeer, 1990a). Running requires that energy must be stored and recovered from muscles which act like springs and facilitate cyclic energy exchange (McGeer, 1990b).Variation in force over time is explained using two mechanisms of minimizing energy expenditure: the inverted pendulum for the walking animal and the spring-mass model for the run-

ning animal.

The inverted pendulum model of walking involves the cyclic transformation of energy. This exchange process is most easily characterized for bipedal animals. In the first half of the step the body's centre of mass gains height and loses speed, thus kinetic energy is converted into gravitational potential energy. The body then falls forward and downward converting much of the gravitational potential energy back into kinetic energy (Cavagna et al., 1976). While bipeds behave like a single inverted pendulum, animals with additional legs behave like multiple inverted pendulums e.g. quadrupeds behave like two inverted pendulums with an inverted pendulum located in the fore and hind quarters (Griffin et al., 2004).

During walking, there is a cyclic exchange between gravitational potential and kinetic energy with each being in opposite phase. During running, trotting or hopping gaits, these energies are in phase, comparable to a bouncing on a pogo stick which reduces the proportion of energy recovered over the stepping cycle (Dickinson et al., 2000). During initial contact with the ground, the leg is storing kinetic and gravitational potential energy as elastic energy in the muscles, tendons and ligaments. This is followed by the propulsive phase where the leg pushes the body up and forward using the recoiled elastic energy from the previous phase (Cavagna et al., 1976). Finally, during galloping a combination of these two mechanisms is employed (Taylor, 1978). It was originally hypothesized that transition between gaits occurs when the energetic cost of maintaining a given gait became too high (Hoyt & Taylor, 1981). More recently it has been suggested that these transitions may instead occur when musculoskeletal forces reach a critical level (Farley & Taylor, 1991).

The relationships between energetics, mechanics and the scale of various bipeds and quadrupeds ranging in size from rats to horses have been investigated, resulting in several general trends for birds and mammals. Firstly, metabolic power has a positive, linear relationship with speed and as body mass increases the cost of moving a gram of body mass a given distance decreases (Taylor et al., 1982). Secondly, the mechanical power required for changes in kinetic energy of limbs and body relative to the centre of mass increases by the 1.55 power of speed but is independent of body size (Fedak et al., 1982). Thirdly, the mechanical work required to lift and re-accelerate the centre of mass within a step, in order to sustain a constant average speed, increases nearly linearly with average speed in all animals (Heglund et al., 1982a). Mechanical work expressed in mass-specific terms is independent of body size (Heglund et al., 1982a). Additionally, walking, running, trotting and hopping gaits produce similar time-dependent fluctuations in the total energy of the centre of mass for both large and small animals; whereas galloping seems to differ with

small animals using front legs mainly for braking and hind legs for re-acceleration and large animals using both sets of legs for both purposes. This result suggests that locomotory mechanics allow the utilization of elastic energy in the legs of large animals but not in small ones (Heglund et al., 1982a). Finally, in contrast to the metabolic energy results of the paper by Taylor et al., (1982), the mass-specific total mechanical work required of muscles and tendons to maintain oscillations of the total mechanical energy increases curvilinearly with speed and is independent of body mass (Heglund et al., 1982b). This means that while the metabolic energy consumed is significantly greater for a small animal than a large animal travelling the same speed, their muscles are performing work at about the same rate. No simple explanation was found for either the linear relationship between speed and metabolic rate or the trend in changing cost of locomotion with body size; however the authors hypothesised that these trends were likely due to the energetic costs of generating force and activating muscles (Heglund et al., 1982b).

There are four competing theories predicting how speed should scale with body mass. These hypotheses state that maximal speed in large and small animals should be predicted by geometric similarity, elastic similarity, static stress similarity or dynamic similarity (for discussion of the assumptions involved see McMahon (1975)). The geometric similarity hypothesis states that animals are geometrically similar if one can be made indistinguishable from the other by multiplying all dimensions by the same factor, i.e. to go from a small animal to a large one both length and diameter of a particular bone or muscle are multiplied by the same factor (Alexander, 2003). Conceptually related to geometric similarity, dynamic similarity implies if all lengths are multiplied by a factor λ, all times are multiplied by a factor τ, and all forces are multiplied by a factor ϕ, then two motions can be made identical (Alexander & Jayes, 1983). Elastic similarity implies that animals are geometrically designed so that their bodies deform under gravity in a similar manner (Alexander, 2003). The final hypothesis, static stress similarity, state that stress is approximately equal (or static) in corresponding parts of the body of animals in equivalent gaits (McMahon, 1975). Both the elastic and statics stress models require geometric distortions where length dimensions are multiplied by one factor and diameters by another factor with changes in body size.

Over the last 20 years, the growing body of evidence suggests that terrestrial animals produce movement patterns that are dynamically similar. Results obtained from studies on ghost crabs (Blickhan & Full, 1987) and cockroaches (Full & Tu, 1990, 1991) suggest that energy conserving mechanisms utilized by vertebrates may be characteristic of all legged locomotion. Thus, movement kinematics (stepping patterns, gaits etc) should be predicted from the mechanical design of the animal rather than morphology and physiology unique to vertebrates.

The purpose of the first half of this chapter is to introduce some of the terminology involved in studies of legged locomotion, to identify the major relevant findings from locomotion studies of the different arthropod subphyla and to briefly examine the anatomy and kinematics of spiders. The purpose of the second half of this chapter is to discuss the motivation for using markerless tracking techniques and present the thesis objectives, to examine some markerless techniques which are currently state of the art and finally to briefly describe the structure of the remaining chapters of this thesis.

1.2 Terminology

To facilitate the comparison of gaits among species there are several different classification schemes, most of which include a distinction between walking and running. In this study, I was interested in kinematic and dynamic distinctions between walking and running. A large amount of terminology is involved in studies of locomotion. In order to keep this section brief, further definitions required for interpretation of results are contained in a glossary (Appendix A.).

1.2.1 Dynamic definitions of gait

Recent studies have used force plates to describe the dynamic (mechanical energy) fluctuations of the animal's centre of mass in order to distinguish between walking and running gaits. These fluctuations were described above using two models: the inverted pendulum and pogo stick. Specifically, a gait is considered running (pogo stick) when the kinetic energy and gravitational potential energy of the centre of mass are in phase, whereas a gait is considered walking (inverted pendulum) when kinetic energy and gravitational potential energy oscillate out of phase. Kinematic techniques were chosen for this study, rather than measurement of forces and energy, because they allow the examination of gaits from a single camera recording. I assume however, that the kinematics involved in locomotion are functioning under dynamic constraints.

1.2.2 Kinematic definitions of gait

In order to compare observations from spiders with as many other species as possible, we require kinematic definitions of gait that have been applied to a large number of very different animals. One such definition characterises walking by at least one limb being in

contact with the substrate at all times during the stride cycle; whereas running requires the presence of an aerial phase where all limbs are off the substrate (e.g. Full & Tu, 1991). Using a footfall-based gait definition (Hildebrand, 1985), animals are walking if the duty factor is greater than 0.5 and running if duty factor drops below 0.5. Footfall pattern also indicates which limbs are currently supporting the centre of mass; therefore alterations to footfall pattern affect an animal's stability. If an animal's centre of mass falls outside its support polygon, it becomes unstable and has the tendency to fall over. However, falling is not necessarily a bad idea. Walking and running can be considered controlled falling, where an animal can utilize such falling movement by altering its footfall pattern to keep the centre of mass near the front end of a shifting support polygon (Cartmill et al., 2002).

1.3 Arthropod locomotion

Arthropods have long been used as models to examine the neural mechanisms underlying locomotion. Much of the historical literature focuses on stepping patterns and gait, with more recent studies expanding to cover fields including inter-limb coordination, kinematics, muscle activity, reflexes associated with locomotion and computational or robotic models. Arthropods are viewed as the classic example of a statically stable design (Koditschek et al., 2004). Arthropods have a low centre of mass, sprawling posture and a large number of legs, meaning that six legged arthropods generally have at least three legs supporting the centre of mass at a time and eight legged arthropods generally have at least four. There are two characteristic types of gaits exhibited by arthropods, the metachronal wave and the alternating gait. In alternating gaits, diagonal legs act as a single leg of a bipedal animal. For example, the alternating tripod in which the left front and hind legs and the right middle leg operate at the same time and vice versa, comparable to a single leg in bipedal animals. With a metachronal wave, the contralateral leg phase coupling is not as strong and a "wave" of leg movements ripples down each side of the animal.

One of the reasons for the success of arthropods is the ability of their body plan to adapt to locomotion in many varied terrains. Such adaptation has resulted in arthropods becoming the most abundant (both in terms of number of species and individuals) and morphologically diverse animal phylum. Arthropods' external skeletons and multi-jointed, multi-limbed body plan allows efficient movement and manipulation under water, through the air or on land, despite limited neural mechanisms in some cases (Ritzmann et al., 2004). There are four currently extant subphyla: hexapods, crustaceans, myriapods, and chelicerates (Cook et al., 2001).

1.3.1 Hexapods

Among arthropods, hexapods have been most widely studied. Ants operate with an alternating tripod gait at speeds ranging from slow walking to fast running. Increasing speed has no effect on the geometry of the tripod (distance between the tarsal imprints belonging to the tripod and distance of the tarsal imprints from the longitudinal axis of the body); they are simply placed further apart from each other by extending stride length (Zollikofer, 1994a). Gait is only altered at very low speeds, when restarting locomotion after a stop or when following very sharp curves, in which case the tripod is replaced by a metachronal wave (Zollikofer, 1994a). Further analysis revealed at highest speeds distance between tripods is often greater than leg length, indicating an aerial phase which is characteristic of a bouncing gait (Zollikofer, 1994b). In fact in one species of ant, *Cataglyphis bombycina*, increasing speed decreases the foreleg contact, eventually leading to a diagonal quadrupedal pattern where the two forelegs are completely lifted off the ground (Zollikofer, 1994b).

Similar gait patterns were observed in conjunction with measurements of ground reaction force for the American cockroach, *Periplaneta americana*. Aerial phases were observed at faster speeds indicted by the ground reaction forces frequently approaching zero. At rapid speeds the animals' forelegs again lift off the ground, causing a switch to quadrupedal or even bipedal running (Full & Tu, 1991). Increases in speed were found to correspond to increases in stride length, with changes in stride frequency having little effect (Full & Tu, 1991). Force measurements allowed for the calculation of kinetic and gravitational potential energy, which were found to be nearly in phase, indicative of a running or bouncing type gait (Full & Tu, 1991). In the more slowly moving death head cockroach, *Blaberus discoidalis*, no aerial phase was attained. However, there is still a range of speeds which produced the pattern of energy fluctuation characteristic of a bouncing gait (Full & Tu, 1990).

Examination of stick insects appears to be the only evidence suggesting fundamental differences between arthropod and vertebrate locomotory behaviour. During forward movement certain legs exert braking forces whilst others simultaneously exert propulsive forces (Graham, 1983). It is suggested that it is necessary for the animal to achieve a static support for the centre of mass, resulting in 'lurching' walking behaviour (Graham, 1983). However, the statically stable design of arthropods does not eliminate dynamic effects at faster speeds (Ting et al., 1994) and this result may be limited to slow walking speeds. Alternatively, this may be an oddity of stick insect behaviour as they are often observed to exhibit a lateral swinging, which is suggested to be a form of camouflage where movement mimics leaves and small branches being blown by the wind (Stockard, 1908).

1.3.2 Crustaceans

Compared to the other arthropod groups, crustaceans are often considered to be slow walkers. It is interesting to note that in the arthropod literature the ghost crab, *Ocypode quadrata*, was the only species to exhibit energy exchange patterns consistent with the inverted pendulum type gait, with fluctuations in gravitational potential energy out of phase with kinetic energy (Blickhan & Full, 1987). Percentage energy recovery for this gait reached up to 55%, which is similar to results obtained from walking birds and mammals (Blickhan & Full, 1987). Despite being decapods, crabs only usually use eight legs in locomotion resulting in an alternating tetrapod stepping pattern during walking. During slow walking certain legs in the tetrapod were slightly out of phase, suggesting that in some cases the stepping pattern may be better described as a metachronal wave (Blickhan & Full, 1987). The same stepping pattern is maintained during slow running. However, the potential and kinetic energies are in phase with each other, reducing the energy recovery to an average of 9% (Blickhan & Full, 1987). Finally, at fastest speeds recordings reveal an aerial phase when all legs are off the ground and both horizontal and vertical forces decreased to zero and energy recovery is reduced to around 7% (Blickhan & Full, 1987).

Like crabs, crayfish, *Procambarus clarkii*, only use the four most posterior pairs of legs in locomotion which operate in a metachronal manner. Both alternate and in-phase patterns were reported in free moving crayfish which differs from treadmill results which only have an alternating gait (Jamon & Clarac, 1995). This highlights the importance of being aware of the constraints experimental conditions may impose in locomotion research. Analysis of leg trajectories revealed each leg plays a specific role in locomotion, with leg 4 appearing to be dominant due to its larger strides and stable cycling movement (Jamon & Clarac, 1995). Data suggests that normally legs 3 and 4 are the main legs contributing to locomotion; however this was sometimes substituted for legs 4 and 5 which was hypothesised to result from increased velocity (Jamon & Clarac, 1995). It is interesting to note that legs 4 and 5 have very different movement amplitudes which suggest that continuous adaptation is required to maintain a coordinated stepping pattern; leg 4 appears to move independently, while legs 3 and 5 are probably under the influence of movement of other legs (Jamon & Clarac, 1995).

1.3.3 Myriapods

Like other arthropods, myriapods' primary form of propulsion is their many legs. However, unlike other arthropods (with the exception of some larvae) they flex their body

segments in a wave-like pattern in order to achieve some of the fastest velocities observed in the arthropod phylum (Anderson et al., 1995). The muscle activity of the giant desert centipede, *Scolopendra heros*, was analyzed in synchrony with video recordings of treadmill locomotion by Anderson et al. (1995). Body segments were chosen as the unit of interest for kinematic investigations which revealed that waves were propagated posteriorly along the body regardless of speed. Speed of wave propagation longitudinally and amplitude and wavelength of lateral flexion and lateral displacement all increase with increasing speeds. As is commonly the case in legged locomotion, the number of legs in contact with the ground decreased at higher speeds. In conjunction with muscle activity recordings these results suggest that lateral bending and lateral displacement are actively produced by axial muscles rather than resulting from mechanical forces produced by high speed stepping patterns (Anderson et al., 1995).

1.3.4 Chelicerates

Despite arachnids being one of the largest arthropod groups, study of their locomotory behaviour has been somewhat neglected compared to insects and crustaceans. There are however limited studies generally focusing on basics such as stepping pattern rather than more in depth kinematic and dynamic studies. Like crabs, scorpions' walking is not limited to the forward direction, they also move laterally and backward over short distances (Bowerman, 1975). Phase relationships are variable, with the stepping patterns of scorpions walking revealing both an alternating tripod stepping pattern (Bowerman, 1975) and a metachronal pattern (Bowerman, 1981).

Although they possess eight legs, Harvestmen behave as a hexapod with the second pair of legs from the front acting as a sensory apparatus. Like hexapods they operate at all speeds with an alternating tripod stepping pattern which provides a stable base for support throughout the cycle (Sensenig & Shultz, 2006). Kinetic and potential energies are in phase indicating a bouncing gait. The centre of mass was found to undergo large vertical and lateral displacements; however these were consistent with models for energetic efficiency and dynamic stability (Sensenig & Shultz, 2006).

Wilson (1967) investigated stepping patterns in tarantula spiders. There is a large variation in phase relationships revealing use of both metachronal and alternating tetrapod gaits, but this variation is not correlated with speed. Spider studies often have adopted a comparative approach, looking at how different habitats and life style shape locomotion. Vagrant wolf spider, *Trochosa ruricola*, was compared with burrow dwelling wolf spider, *Lycosa tarantula*. Results found that *T. ruricola* uses an alternating gait but this is not achie-

ved even at the highest speeds for *L. tarantula* (Ward & Humphreys, 1981). Analysis of phase lags suggests that the front pair of legs act primarily as a sensory organ and that this role is more evident in the burrow dwelling species. Shultz (1987) compared a terrestrial spider, *Lycosa rabida*, and a semi-aquatic spider, *Dolomedes triton*, walking on land and on the water surface. Both species operated with an alternating tetrapod gait on the solid surface and this gait was maintained somewhat by *L. rabida* when walking on water. *D. trition* showed greater specialization for this habitat, adopting a 'rowing' method of locomotion, with the fourth leg, which is not used for propulsion on aquatic surfaces, being used to correct for yaw (Shultz, 1987).

Pendulum mechanics have been hypothesized to not only impact on conservation of energy principals affecting terrestrial locomotion but also suspensory locomotion. An investigation was carried out by Moya-Laraño et al. (2008) to see if pendulum mechanics could be used to predict the morphological evolution of spiders. A large group of predatory spiders who had lost and gained suspensory locomotion a number of times throughout their evolution were compared. Suspensory spiders which hang upside down from their webs during locomotion were found to have disproportionally longer legs relative to body size than their terrestrial counterparts. Within suspensory species, longer legs allowed spiders to run faster during suspensory locomotion (i.e. pendulum gait) but caused these same spiders to run more slowly when running on the ground (i.e. inverted pendulum gait). Additionally, larger suspensory spiders running on the ground achieved much lower speeds than terrestrial spiders of a similar size (Moya-Laraño et al., 2008).

1.4 Spider anatomy

Spiders belong to the order Araneae within the class Arachnida. The body of spiders is made up of two major parts, the cephalothorax and the abdomen (Fig. 1.1). The anterior part is the cephalothorax, which mainly functions as the site of the central nervous system but also has a major role in both locomotion and feeding as this is where all appendages are attached. The posterior part is the abdomen, which contains the majority of the internal organs and has an important role in a variety of tasks including respiration, circulation, excretion, reproduction and the production of silk (Foelix, 1982). Spiders have eight legs arranged in pairs which are attached to the cephalothorax between the carapace and sternum.

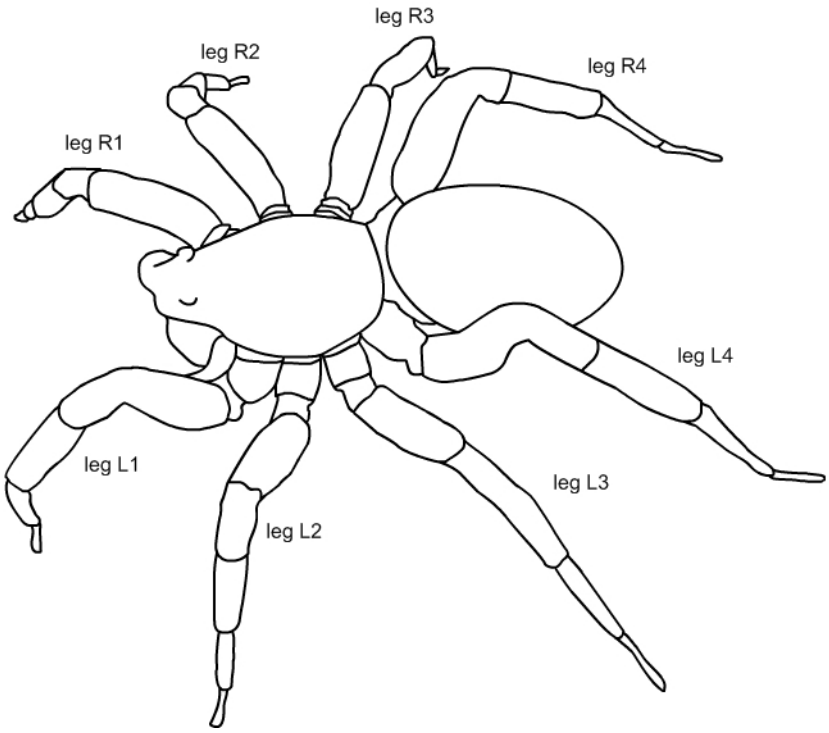

Figure 1.1: Basic external anatomy of a spider

1.4.1 Kinematic analysis of a spider's leg

The spider's leg consists of seven segments called podomeres: coxa (Co), trochanter (Tr), femur (Fe), patella (Pa), tibia (Ti), metatarsus (Me) and tarsus (Ta) (Fig. 1.2). Muscles attached to most of the joints to allow articulation of the podomeres by either bending the joint (flexors) or stretching it (extensors) (Foelix, 1982). The notable exception to this is the Fe-Pa and Ti-Me joints which lack extensor muscles. The extension of these joints is mediated by the hydrostatic mechanism, where haemolymph is pumped into chambers in the joints causing an increase in hydrostatic pressure (Parry & Brown, 1959). Spiders move their legs quickly and with large amplitudes so it is advantageous to have long slender legs with most of the mass concentrated near where the appendage joins the body, in order to reduce the problem of inertial forces (Blickhan & Barth, 1985). Podomeres are reasonably rigid in structure, thus it is possible to think of them from a mechanical point of view in order to investigate moments and rotations (Table 1.1). Joints with several degrees of freedom (ball and socket joints) are located in segments close to the trunk. Hinge or universal joints with limited rotation, are found in the middle portion of the leg. These joints are articulated along the dorsal hinge line and do not require muscles for stabilization perpendicular to the main plane of movement (Blickhan & Barth, 1985). The tarsus, which is the most distal segment of the leg is free of muscles and instead is activated by

tendons. This reduces active manoeuvrability but errors in the position of this segment can only lead to small errors in the overall position of the spider (Blickhan & Barth, 1985). Legs in free flight can be considered a 7-link manipulator with the overall configuration of joints depending on the number of legs in contact with the ground (Gasparetto et al., 2008).

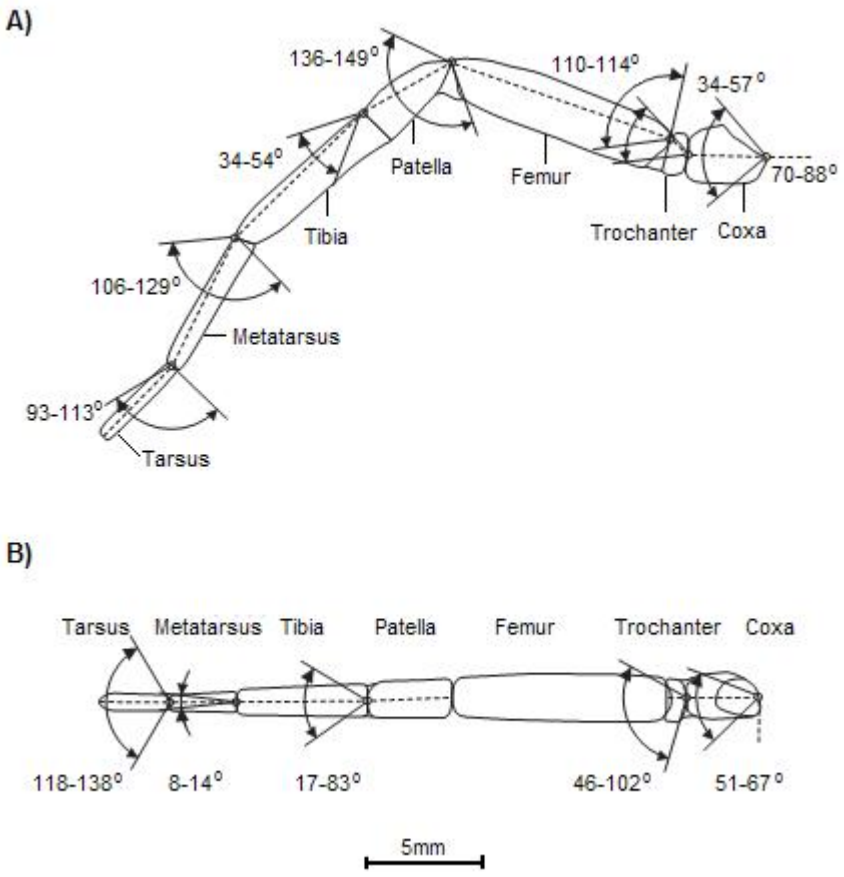

Figure 1.2: Ranges of motion for joints of *Dolomedes aquaticus*, (a) in the Y-Z plane, (b) in the X-Y plane modified from Reussenzehn (2008).

1.4.2 The water spider, *Dolomedes aquaticus*

The present study investigates the joint kinematics of *Dolomedes aquaticus*, during locomotion. This species is found throughout Otago, New Zealand, where its abundance among the water races constructed during the gold rush lead to miners naming it the water spider (Goyen, 1887). It is commonly found near water on or under surrounding objects such as plants, stones and pieces of wood. *D. aquaticus* sense their prey both on water and land by detecting vibrations using the two front pairs of legs (Forster & Forster, 1999). These spiders sit and wait until they sense aquatic insects or sometimes even small verte-

Table 1.1: Mechanical properties of a spider's legs, after (Gasparetto et al., 2008).

Spider joint	Mechanical counterpart	DOF
Body-Co	Ball and socket	3
Co-Tr	Ball and socket	3
	OR saddle	2
Tr-Fe	Universal	2
Fe-Pa	Hinge	1
Pa-Ti	Universal	2
	OR hinge	1
Ti-Me	Universal	2
	OR hinge	1
Me-Ta	Universal	2

brates approaching then chase them down in rapid bursts of speed. Agile locomotion is of particular importance to spiders that hunt their prey rather than constructing a web or tunnel.

D. aquaticus are able to run rapidly on land and the water surface, posing interesting questions about how the mechanical design of their body has evolved in order to exploit differing terrains. Ranges of movement for leg joints of *D. aquaticus* have been determined experimentally (Fig. 1.2), (Reussenzehn, 2008). With these measurements acting as constraints, video analysis can be used to reveal what ranges of movement are actually exploited by each joint and their cyclic pattern during locomotion at different speeds.

1.5 Motivation

In this field of study, problems are usually solved by placing markers on the subject of interest and tracking these markers over several views to gain a representation of 3D pose. However this approach, although widely accepted comes along with intrinsic problems e.g. incorrect tracking of markers, occlusions of markers, identification of correct placement can be unreliable, markers can move or become completely removed during locomotion, the need for specialized lab environments and lighting conditions. A number of companies have developed software packages to assist in video analysis. These packages are generally focused on clinical studies of human gait and are inadequate for use in our research disciplines.

Recently, two papers have been published with a focus on developing marker based video tracking techniques with applications to invertebrates. Zakotnik et al. (2004) created software which reconstructs the animals' posture through a process called simulated an-

nealing. This approach consists of a kinematic body model including joint constraints and video recordings from an arbitrary number of views. Rather than the traditional approach of tracking the marker trajectories over time this software works by projecting the predicted model to recorded views and then trying to minimize the error between the two. Additionally, this approach analyses each frame independently and so the tracker is able to recover from incorrect and occluded markers. When applied to the tracking of an animated locus in two views, this algorithm was able to reconstruct joint angles with errors between 0.7^o and 4.9^o with accuracy restricted by the pixel resolution of the video.

Hedrick (2008) broke the objective of pose estimation down into two coupled problems. Firstly, features must be identified in the video frames. In this case the features of interest can be the entire animal or the markers located at the centre of a joint or tip of a limb. An automatic tracking option is presented, however it is limited to tightly controlled lab setup and generally tracking the entire animal rather than specific joint angles. Secondly, either 2D or 3D coordinates are reconstructed from image data. This requires a calibration of camera(s) by direct linear transformation, and is robust enough to resolve 3D pose from multiple cameras while correcting for distortion. The advantage of the Zakotnik et al. (2004) approach is that it allows for the reconstruction of 3D pose from a single camera view whereas with the Hedrick (2008) software a single camera will only give 2D pose and multiple cameras are required if the goal is 3D reconstruction.

Single camera or 'monocular' techniques come with various advantages and drawbacks. Monocular techniques are particularly beneficial when multiple views are not able to be obtained e.g. archival footage or web-cam recordings (Sidenbladh, 2001). They also reduce the need for costly equipment and can allow for a more natural setting rather than laboratory conditions. The key problem to overcome when tracking in 3D with such approaches is 2D-3D projection ambiguities. Depth information is lost when a 3D object is projected into the 2D image plane and must be replaced by prior knowledge or other image cues (Sidenbladh, 2001). In highly articulated objects, such as spiders, self occlusions of limbs occur frequently, which becomes problematic when only observing from a single view. Additionally, the search space required for full 3D reconstruction of spider motion is very large, with up to 110 degrees of freedom required (6 for global position and rotation, up to 13 for each leg). Thus, it becomes necessary to develop mathematical/statistical models of the motion. Tracking works by predicting the positions of the objects in the next frame and then dynamically adjusting the model using data extracted from each frame of the video.

The ability to track moving objects is of vital importance in the evolution of biological sensory systems. Predators need some sort of internal representation of not only their state

(position and speed etc) but also the prey state in order to plan a trajectory and decide when to strike at their prey. It is reasonable to assume that our brain uses both observation and motion models. Take for instance a fielder running to catch a flying cricket ball, within the first 840 ms of the ball leaving the bat most fielders have already started running forwards or backwards depending on the height of the trajectory (McLeod & Dienes, 1996). At this stage the difference between the two flights is small and noisy estimates of variables such as the projection angle, velocity of the ball and wind resistance mean that precise calculation of trajectory is impossible. So how does the brain decide where to move your hands in order to catch the ball? Our brain helps us through these situations by creating a dynamic model of the motion, which not only estimates the position, but also the speed and direction of the objects tracked. I intend to take inspiration from the brain and incorporate both observations and dynamic models of legged locomotion in order to reconstruct the 2D pose of running spiders. The motivation for this thesis is twofold. Firstly, to investigate to what extent the general problem of tracking a spider in 2D can be solved. That is, can a computational approach be constructed that tracks and reconstructs the motion of a spider in 2D, using a monocular gray-scale video sequence and dynamics based predictions rather than physical markers? Secondly, is the 2D motion of the spiders consistent with results viewed from vertebrates and other arthropods?

1.6 Current state of the art

Computer vision based approaches to human motion capture have been around since the 1980's (reviewed in Moeslund & Granum, 2001). Over the last two decades, the number of papers published within this field has rapidly increased mainly due to two reasons: a) computers have become more accessible and faster and b) the potential applications (e.g. surveillance, control and analysis) of these approaches have been realized. A great variety of computer vision based techniques have been proposed for tracking human motion in 3D. These procedures vary in camera configuration, the types of algorithm used, the use of various anatomic and kinematic models, the focus on either particular regions of the subject or the whole body and the representation of captured data. For comprehensive reviews of human motion capture techniques see (Moeslund & Granum, 2001; Moeslund et al., 2006).

While human motion capture is moving from the laboratory to the real world, studies on other animals still tend to favour traditional marker techniques rather than passive sensing of natural features. The following sections will briefly examine some techniques applicable to this thesis, which are currently state of the art. The tracking problem can be

divided into two key parts. Firstly the pixels of the image need to be separated into those that belong to the subject and those that belong to the background and secondly based on the subject pixels we desire an estimation of the pose of the subject. In order to discuss some techniques which are currently state of the art I briefly introduce two key concepts, Markov Random Fields (MRF) and graph cuts, these are discussed in more depth in the chapter 3.

In the literature, image segmentation problems are frequently formulated in terms of MRFs. MRFs allow a probabilistic framework where contextual information can be incorporated with pixel information (Li, 1994). In the case of segmentation, MRFs model the probability of observed data and the corresponding labels. In more specific terminology, given $\boldsymbol{y} = \{y_1, y_2, ..., y_n\}$, where y_i represents the colour intensity of pixel i of an image consisting of n pixels, the corresponding labels form the vector $\boldsymbol{x} = \{x_1, x_2, ..., x_n\}$ where x_i represents the label of pixel i. Using Bayes' rule, the posterior over the labels given the data becomes $p(\mathbf{x} \mid \mathbf{y}) \propto p(\mathbf{x},\mathbf{y}) = p(\mathbf{x})p(\mathbf{y} \mid \mathbf{x})$, where $p(\mathbf{x})$ is modelled as a MRF (Kumar & Hebert, 2003). Segmentation becomes an optimization problem, where the best labelling is found by minimizing the energy corresponding to the MRF configuration.

Graph cuts have established themselves as a fast, accurate technique for minimizing the energy of a MRF. A graph consists of a set of a set of nodes V, directed edges E and some weight or cost C. Generally the nodes correspond to pixels and there are some additional special nodes called terminals (Boykov & Kolmogorov, 2004). Terminals correspond to the set of labels that can be assigned to pixels. We focus on the two terminal case, specifically terminal nodes are the source s and sink t. Fig. 1.3. shows an example of such a graph, based on a 3x3 image with binary labelling. The edges of the graph are assigned a cost, where the cost may differ between directed edge (p, q) and the reverse edge (q, p) (Boykov & Kolmogorov, 2004). In general, edges can be considered one of two types, t-edges which connect a pixel with a label and n-edges which connect pairs of neighbouring pixels. Thus, the costs associated with edges can be split into the penalty for assigning the corresponding label to a pixel and the penalty for discontinuity between pixels respectively (Boykov & Kolmogorov, 2004). A cut divides the graph into subsets of pixels, S that contains the source and T that contains the sink (Fig. 1.3). The cost of a cut is given by the sum of the edges (p,q), such the $p \in S$ and $q \in T$. The graph cuts' problem is then solved by finding the cut with the smallest cost. By the Ford-Fulkerson algorithm, this is equivalent to finding the maximum flow from the source, s, to the sink, t, with the capacity of each edge equal to edge weights (Boykov & Kolmogorov, 2004).

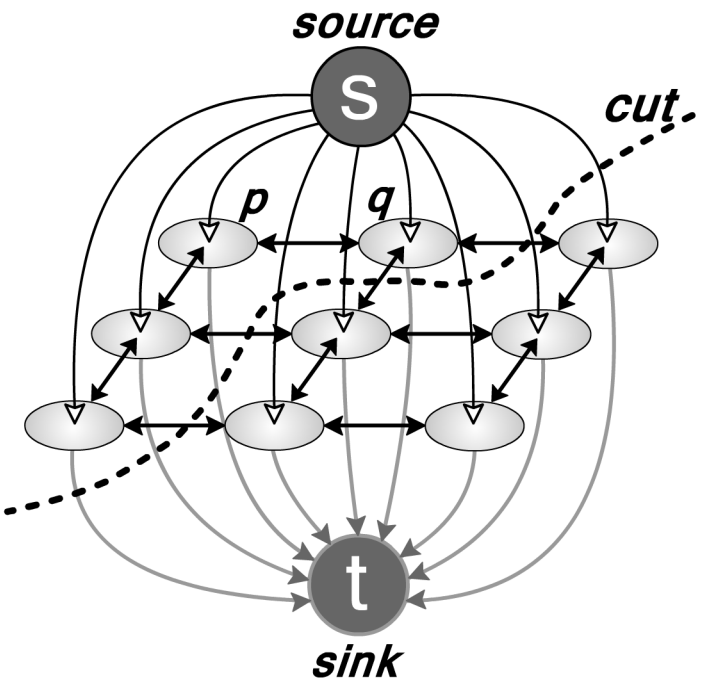

Figure 1.3: Example of graph representation of an image. A cut is used to divide the image into two parts. Each node represents a pixel and is connected by edges to its neighbours and to the terminals (source and sink). A terminal (source and sink) corresponds to label that defines to which part the pixel belongs. A cut divides the graph into subsets of pixels, S that contains the source and T that contains the sink. Created after Boykov & Kolmogorov (2004).

1.6.1 Segmentation and shape priors

Graph cuts are widely used in computer vision as a way of finding the minimum cut on a specialised graph that minimizes the energy of a MRF. Boykov and Jolly (2001) presented a technique for segmentation using binary graph cuts. The effectiveness of this technique is illustrated by the large number of recent publications that cite and build upon this paper (cited by 608 according to Google scholar 06/08/09). This paper demonstrated that rough user defined region cues and boundary cues based on edge detection are sufficient for accurate segmentation. A fast implementation of the min-cut/max-flow segmentation is described in Boykov & Kolmogorov (2004). Having found an initial solution to a MRF using graph cuts the algorithm can be extended to being dynamic rather than static; that is, a given solution can aid in the solving of a similar MRF with slightly different energy terms (Kohli & Torr, 2007). The algorithm performs well when changes are small and is much faster than its static counterpart. This is a major benefit when segmenting video sequences, assuming changes between successive frames are relatively small, as it can allow real time image segmentation.

It was noted by Kumar et al. (2005) that segmentation resulting from MRFs, where information about the image edges and colour distributions of subject and background was included, often resulted in unrealistic shapes for the subject. This motivated the development of the Obj-Cut approach (Kumar et al., 2005). The Obj-Cut algorithm attacks the segmentation problem by combining MRF with layered pictorial structures which provide a realistic shape prior. While the segmentation results are impressive, it is computationally intensive to learn the exemplars of the layered pictorial structures from the video and these exemplars have to be learnt in advance, prior to detection and segmentation.

Graph based methods can be modified to include a shape prior; however this typically results in an energy that is more difficult to optimise. One framework that includes a shape prior is the Branch-and-Mincut approach, which efficiently transverses the solution space using two powerful techniques: graph cut and branch-and-bound (Lempitsky et al., 2008). The shape prior is a set of image masks defining a given binary segmentation. This technique was applied to segmenting a coffee mug undergoing 3D pose changes against a cluttered background. Results indicated that in this case the algorithm was much more accurate than the standard graph cut segmentation mainly due to significant overlap in the intensity distributions of the mug and background (Lempitsky et al., 2008).

1.6.2 Pose inference

More recently techniques are being developed that use a shape prior not only for segmentation but also pose estimation. The shape prior used in the MRF is pose specific and is generally either learnt from the video sequence or consists of a simplified kinematic model where body parts are represented geometrically e.g. stick figures or ellipsoids. One such approach that has proven successful is POSECUT (Bray et al., 2006). This technique uses image information including background and foreground pixel intensity distributions and edges. Additionally, a shape prior is added that consists of a stickman and theses features are combined in a Bayesian framework. Segmentation depends on the subjects' estimated pose which requires an initial guess for optimization of each frame. In this case, the pose in the previous frame was used rather than more sophisticated methods to save on computation time. Results illustrated that accurate shape models are not required and a simplified articulated shape model suffices for accurate segmentation (Bray et al., 2006).

As mentioned previously, tracking 3D pose of subjects in monocular images suffers from ambiguity. This problem is alleviated by the use of multiple views of the subject. These can be easily added to the optimization framework by minimizing the sum of the minimum pose specific energy across all views (Kohli et al., 2008). Segmentation accuracy has been investigated quantitatively, with 97.43% subject pixels and 99.4% of all pixels being labelled correctly where ground truth is generated by hand labelling of images (Kohli et al., 2008). Pose estimation results are not compared to ground truth but rather accuracy of the technique is demonstrated by images comparing the pose of the optimized stickman to the original and segmented images.

The above papers focused mainly on segmentation aspects of the POSECUT algorithm. This technique has also been utilized for pose estimation with the practical application of human gait analysis for physiotherapists (Jensen, 2008). The key goals of this paper were to present an algorithm that allows for gait analysis based on video footage from a stationary camera with no special requirements for the type of camera, background or clothing of the subject and minimal interaction from the user. The pose is calculated in 2D using the optimization described above, problems when one leg passes over the other are corrected using logical operations and the angles are smoothed using a high order Fourier series. Gait analysis outputs step length, stride length, cadence, speed and range of motion of the joints. Evaluation of the accuracy of the algorithm is based on visual inspection of figures and video sequences due to lack of quantitative reference data. This technique was further adapted to use Time-of-flight camera depth image sequences and automatic initialization, which results in good output data for gait analysis and requires

no user interaction (Jensen et al., 2009)

Rather than correcting the problem of limbs becoming stuck on the wrong part that occurs at times when body parts pass close to each other in post processing, it is possible to build in solutions into the optimization framework. One such approach involves incorporating colour constraints into the pose estimation process (Li et al., 2009). In this paper multiple web cameras are used to get silhouettes which are then used to create a 3D voxel-based visual hull. A representative colour is assigned to each surface voxel. The colour model consists of a mean value and covariance matrix for each body part and based on this model colour constraints are incorporated into the energy calculation as part of the unary term. This constraint proved successful in overcoming some self-occlusions, but its applicability is limited to cases where most of the body parts are different in colour.

1.7 Thesis overview

A brief outline of the remaining sections of the thesis follows.

Chapter 2 In this chapter I describe the collection and maintenance of spiders used in analysis. The experimental setup consisting of a light source, behavioural apparatus, camera and computer is described in detail.

Chapter 3 The construction of tracking code is explained in this chapter. I begin with the theory and implementation of segmentation and pose estimation, followed by smoothing of raw data, gait analysis and finally the statistics involved in comparisons.

Chapter 4 The accuracy of the tracking algorithm is briefly examined. This is followed by the kinematic analysis of spider locomotion including scaling of kinematic parameters with size and speed, analysis of spider leg movements, phase relationships between legs and finally the range of movement of each of the joints in the spider leg.

Chapter 5 In the last and concluding chapter of this thesis, I first review the tracking algorithm and highlight future improvements. I examine the kinematics relating to organisation of the stride in general, and then discuss inter-leg coordination comparing our results to data previously obtained for spiders, arthropods and vertebrates. I end the chapter with a summary of this work and list its main contributions.

Appendices Three appendices are included to assist the reader in their understanding of this thesis. Firstly, a glossary containing some specific terminology in the locomotion research is included. Secondly, the components of the graphical user interface for tracking are explained. Finally, the files included on the attached CD are described.

Chapter 2

Experimental setup

2.1 Animals

Spiders were collected from a stream bank located southwest of Macraes Flat Village (45°26'S 170°25'E) in Otago, New Zealand. Individuals were maintained in 25 cm × 15 cm × 10 cm plastic containers with holes drilled in the lid to allow air supply. Holding enclosures were lined on one half with a moist paper towel and the remaining half contained a piece of bark and plastic container of water. Spiders were fed weekly with crickets (*Teleogryllus commodus*) and locusts (*Locusta migratoria*) (Biosuppliers Live Insects, Auckland, NZ). Enclosures were cleaned weekly and fresh water was provided to eliminate the build-up of food and waste products. Spiders were kept out of direct sunlight, under natural light conditions and were maintained at laboratory temperature (approximately 10-20°C). Only relatively large spiders were used for filming (mass between 0.59-1.71 g). All spiders investigated possessed eight walking legs; if a leg was injured or removed the spider was not used in gait analysis.

2.2 Lab setup

Behavioural arenas consisted of a custom made 40 cm× 10 cm × 2 cm glass aquaria (Metro Glasstech, Dunedin); this size was selected as large enough for free locomotion but small enough to encourage spiders to run in a relatively straight line. The arena was lit from below using three 10 × 10 arrays of ultra bright LEDs (SCL Limited, Dunedin). In order to achieve a more uniform light intensity, layers of frosted glass and/or frosted paper were used to scatter the light from the LEDs. A piece of cardboard covered the last 5 cm at

the opposite end to the spider to act as a refuge from the bright light. A 1 cm grid was printed onto an overhead projector transparency to allow for calibration of measurements from pixels to cm. The video camera was positioned in the middle, above the arena to allow filming of the spider from a dorsal viewpoint (Fig. 2.1). Trials were recorded using a high-speed video camera (125 fps, 1/625 s shutter speed, 1280 × 1024 pixels with a Troubleshooter 1000 HR, Fastec Imaging, San Diego, USA).

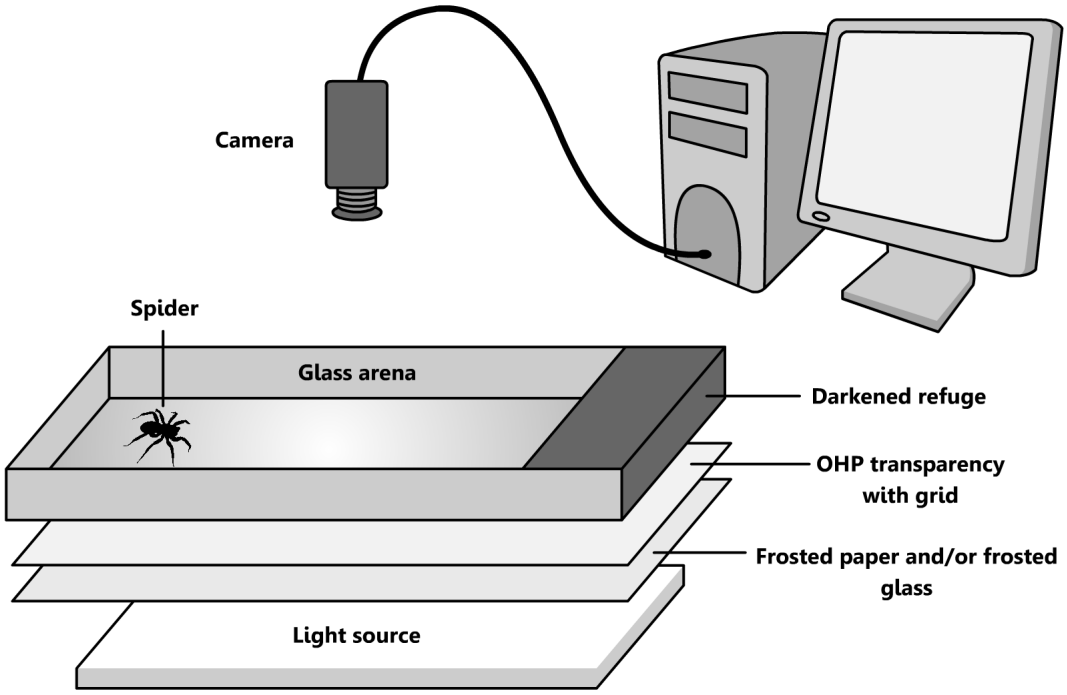

Figure 2.1: Experimental setup consists of a glass arena with a darkened refuge at one end. The arena is lit by LED arrays scattered using frosted paper and/or frosted glass. A video camera films the spider from above. The camera was attached to a computer, which was used for image capture, storage and analysis. For further details see text.

Spiders were occasionally stimulated to move from one end of the arena to the other by either prodding them with tweezers or gently blowing on them. The resulting locomotion did not appear to differ from normal running in unstimulated animals. Each animal was run no more than five consecutive times. Short rest periods were given between each trial while data was transferred from the camera to the computer and converted into HD resolution avi files using the camera software (CamLink, Fastec Imaging, San Diego, USA). Trials where the animal did not run in a straight line or at a constant speed were rejected. The animals were not observed slipping on the glass surface and did not appear to have any difficulty running. Starting and stopping sequences were not used in analysis.

Chapter 3

Constructing tracking code

Probabilistic approaches to image analysis are based around the assumption that there exists some probability distribution that describes the variability and interactions of different sets of image features (Perez, 1998). Therefore, we are able to consider the variables of the problem as a set of discrete random variables $\{X_1, X_2, \ldots, X_n\}$ with joint probability distribution P_X. I use the POSECUT approach (Bray et al., 2006). This involves optimising a cost function based on a Markov Random Field (MRF), in order to estimate pose in each frame of a video sequence. The core code was based around modifying the techniques used for human gait analysis by Jensen (2008). A graphical user interface was developed, which allows the user to modify input parameters with ease and batch process multiple files (Appendix B.). Key components involved in this energy minimisation problem are briefly described below.

3.1 Input data

Each frame is read into MATLAB (Student version R2009a, The MathWorks, USA), where the video stream is treated as a sequence of images. Videos were gray-scale, so each frame was represented by a single m-by-n matrix; that is the image is composed of m pixels in the vertical direction and n pixels in the horizontal direction. At the original video resolution this matrix must contain information regarding 1310720 pixels for each frame analyzed. This requires a lot of memory, so the resolution of the videos was reduced from 1280 × 1024 pixels to 640 × 512 pixels using a 3 x 3 overlapping matrix and areas outside the region of interest were removed using VirtualDub (Version 1.8.8; http://www.virtualdub.org/). Each element in the matrix has a value corresponding to how bright/dark the intensity of the pixel at the given position is. The value of 0 corresponds to black and 255 to white.

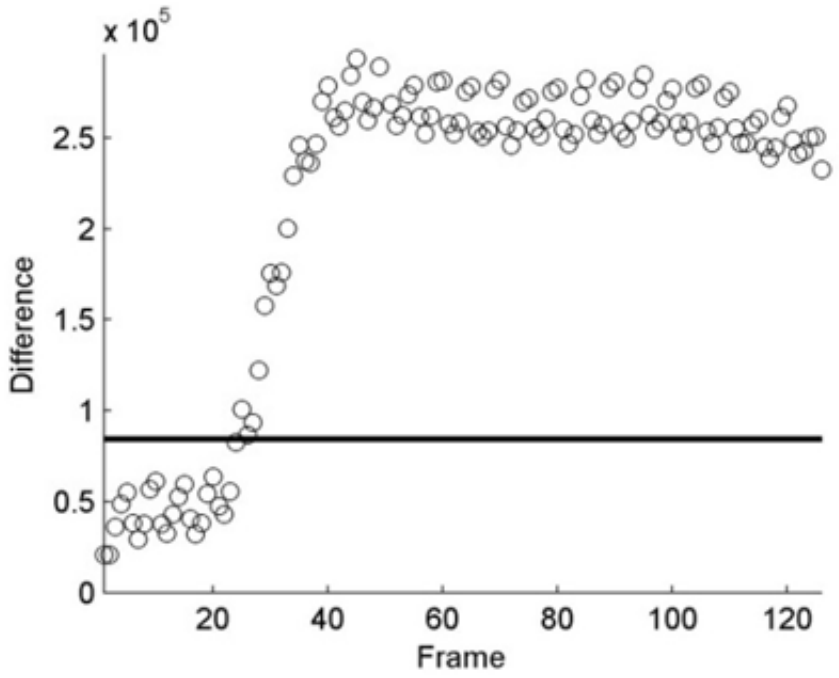

Figure 3.1: Sum of differences for every frame and threshold ($\bar{X} + t_{0.99}$) used to determine subject entering and exiting the arena.

Videos always contained at least five frames of background before the subject entered the arena. The absolute difference between the intensity value of pixel i in the current frame and pixel *i* in the first frame was summed across the n pixels in the frame. These values were compared to a threshold (upper limit of the 99% confidence interval about the mean difference from known background frames), which allowed the estimation of frames containing the subject and frames containing only background. Fig. 3.1 shows the difference across video frames and the threshold. Frames with a difference above the threshold value are likely to contain the subject, whereas those below the mean value are likely to contain only background. Fig. 3.2 shows the estimated frames with subject entering and exiting the arena.

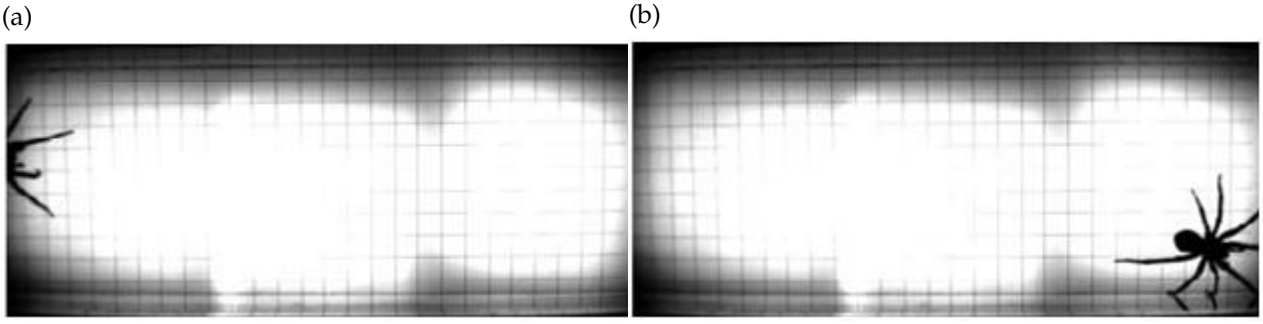

Figure 3.2: Frames with the subject entering (a) and exiting (b) the arena.

3.2 Image segmentation

Image segmentation in this case is a binary problem where particular regions of the image are labelled 'subject' and 'background'. Given a vector $\mathbf{y} = y_1, y_2, ..., y_n$ where each y_i represents the intensity of the pixel i of an image containing n pixels, the solution to our problem becomes finding the value of the vector $\mathbf{x} = x_1, x_2, ..., x_n$ where each x_i represents the assigned label of pixel i. Each x_i takes its value from the label set $L = l_1, l_2, ..., l_m$, which in this case only consists of 'background' and 'subject'. The posterior probability of $\mathbf{x}$ given $\mathbf{y}$ can be written as:

$$P(\mathbf{x}|\mathbf{y}) = \frac{(P(\mathbf{y}|\mathbf{x})P(\mathbf{x}))}{P(\mathbf{y})} \propto P(\mathbf{y}|\mathbf{x})P(\mathbf{x}) \tag{3.1}$$

Each configuration of the MRF, denoted by $\mathbf{x}$, defines a segmentation. Taking only pixel intensities into account, the energy corresponding to the configuration $\mathbf{x}$ is the data log likelihood, defined as:

$$E(x) = \sum_i -\log P(\mathbf{x}|\mathbf{y}) = \sum_i \left(\phi\left(\mathbf{x}, \mathbf{y}\right) + \psi\left(\mathbf{x}\right)\right) \tag{3.2}$$

where $\phi\left(\mathbf{x}, \mathbf{y}\right) = -\log P(\mathbf{y}|\mathbf{x})$ and $\psi\left(\mathbf{x}\right) = -\log P(\mathbf{x})$.

The aim of the maximum-a-posterior (MAP) MRF formulation becomes minimizing the energy *E(x)* corresponding to the configuration, $\mathbf{x}$, of the MRF given observed data $\mathbf{y}$. For further background on Markov random fields in computer vision see Li (1994). Within this framework we can further decompose the energy function into unary and pairwise terms. Using only log likelihood terms results in pixels being incorrectly labelled due to the similarity between subject distribution and some background pixels (Fig. 3.6 (b)), thus it is necessary to introduce additional terms to the energy function in order to achieve a more accurate segmentation. After adding contrast dependent terms, the energy of the MRF becomes:

$$E(x) = \sum_i \left(\phi_i\left(x_i, \mathbf{y}\right) + \psi_i\left(x_i\right)\right) + \sum_{i,j} \left(\left(\phi_{i,j}\left(x_i, x_j, \mathbf{y}\right) + \psi_{i,j}\left(x_i, x_j\right)\right)\right) \tag{3.3}$$

Generally, the value of the unary prior term $\psi_i\left(x_i\right)$ is set to a constant, which is equivalent to assuming a uniform prior. Later in section 3.3 we will show how a shape prior $\psi_i\left(x_i|\mathbf{y}\right)$ can be incorporated into the framework to improve segmentation and estimate pose. Fig. 3.3 shows the final shape specific MRF consisting of unary terms: log likelihood based on

colour, $\phi_i(x_i, \mathbf{y})$, and shape prior, $\psi_i(x_i|\mathbf{y})$, which favours pixels falling close to the shape being labelled 'subject'; as well as pairwise terms: contrast term, $\phi_{i,j}(x_i, x_j, \mathbf{y})$, which favours edges detected in the image matching labelling boundaries and smoothness prior, $\psi_{i,j}(x_i, x_j)$, which favours neighbours having the same labels. Each of the terms involved in this energy function will be described in more detail below.

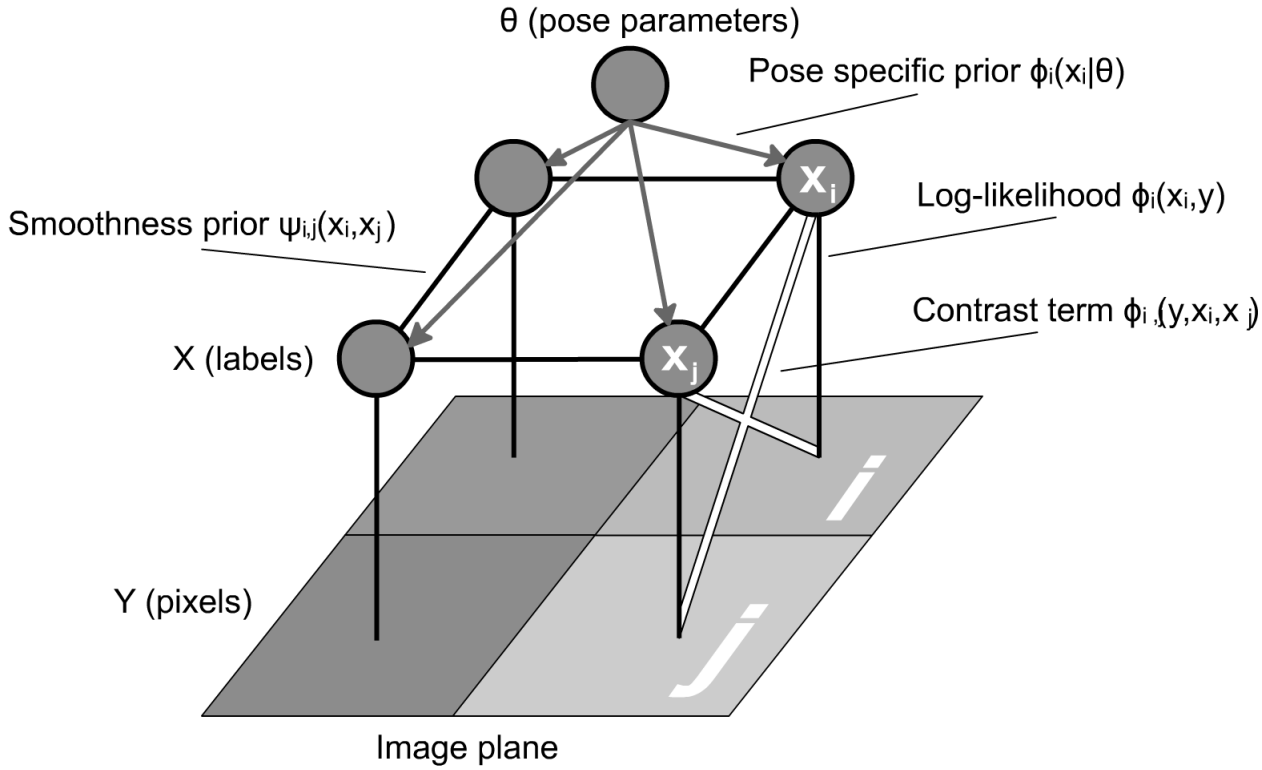

Figure 3.3: The shape specific Markov Random Field for image segmentation. Given a set of labels $\mathbf{x}$, observations $\mathbf{y}$ and pose parameters θ, the figure shows each of the terms involved in calculating the energy of the MRF: log likelihood, contrast term, smoothness prior and pose specific prior.

3.2.1 Likelihood term

The unary likelihood terms $\phi(x_i, \mathbf{y})$ of the energy function are calculated using the pixel intensity distributions for the subject and background. Assuming two different distributions with mean, μ, and standard deviation, σ, the probability that observed data, $\mathbf{y}$, belongs to either background or subject is given by:

$$P(\mathbf{y}|x) \begin{cases} \frac{1}{\sqrt{2\pi\sigma_B^2}} \exp\left(-\frac{(y-\mu_B)^2}{\sigma_B^2}\right), & x = background \\ \frac{1}{\sqrt{2\pi\sigma_S^2}} \exp\left(-\frac{(y-\mu_S)^2}{\sigma_S^2}\right), & x = subject \end{cases} \tag{3.4}$$

By taking the negative log of the probability function and discarding the constants $\log\left(\sqrt{2\pi\sigma}\right)$, we are given the log likelihood function:

$$\phi(x_i, \mathbf{y}) \begin{cases} \left(\frac{(y-\mu_B)^2}{\sigma_B^2}\right), & x = background \\ \left(\frac{(y-\mu_S)^2}{\sigma_S^2}\right), & x = subject \end{cases} \tag{3.5}$$

Implemenation

Since frames have been sorted into background and those containing the subject, the mean of every pixel across background frames provides a good estimate of the background mean across all frames.

$$\bar{x}_i \approx \frac{1}{n_B} \sum_{j=1}^{n_B} x_{i,j} \tag{3.6}$$

where n_B is the number of background frames and $x_{i,j}$ is the value of the ith pixel in the jth background frame. The standard deviation of intensity of each pixel across background frames is also calculated to estimate the background standard deviation across all frames:

$$\sigma_B \approx \sqrt{\frac{1}{n_B - 1} \sum_{j=1}^{n_B} \left(x_{i,j} - \bar{x}_i\right)^2} \tag{3.7}$$

These values are substituted into equation (3.5) to calculate the likelihood function for background and (3.3) to calculate its energy.

Calculating the mean and standard deviation of the subject is a little less intuitive. There are a range of techniques available to tackle this image segmentation problem e.g. Grabcut (Rother et al., 2004), but these often require user input and can be computationally intensive, so we opt for a simpler function. The background log likelihood is summed across the rows and the columns for the initial frame (Fig. 3.4, a & b). Pixels with intensity above the threshold value are likely to contain the subject, whereas those below the threshold are likely to contain only background. Fig. 3.4 (c) shows the bounding box containing the subject. These values are again thresholded to remove remaining background (Fig. 3.4, d), and subject statistics are calculated on the result. While this technique is a little cumbersome, it provides a quick, reasonable estimate to mean and standard deviation of

the subject, because the background pixels are closer to white and subject pixels are closer to black.

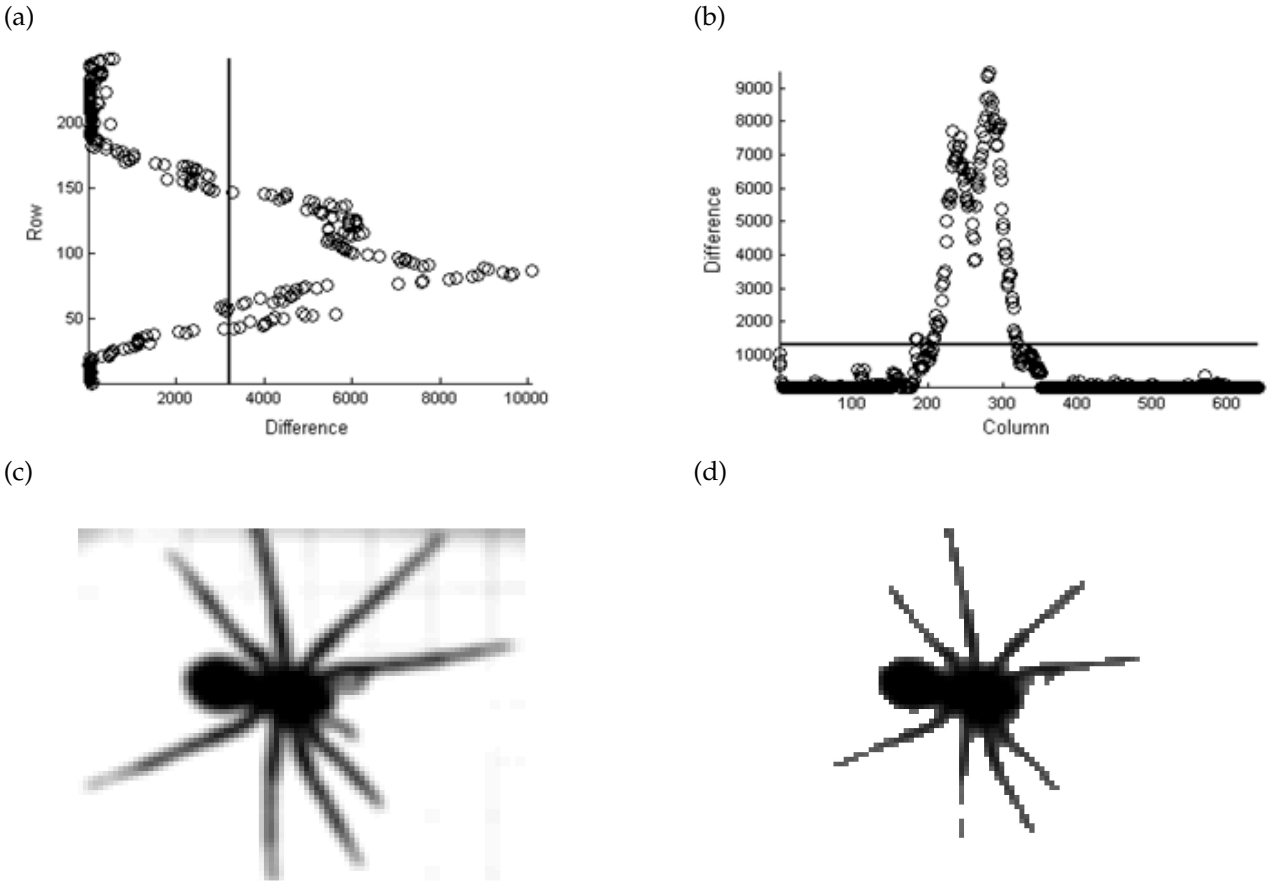

Figure 3.4: Finding the subject. (a) Sum of background likelihood over rows; (b) Sum of background likelihood over columns; (c) Bounding box of the subject; (d) Subject pixels.

$$\bar{x}_S \approx \frac{1}{n_S} \sum_{i=1}^{n_S} x_i \tag{3.8}$$

$$\sigma_s \approx \sqrt{\frac{1}{n_s - 1} \sum_{i=1}^{n_s} (x_i - \bar{x}_s)^2} \tag{3.9}$$

where n_S is the number of subject pixels and x_i is the intensity value of the ith pixel.

The likelihood function gives high values for data unlikely to be in the given distribution (light pixels) and low values for data likely to be in the distribution (dark pixels). Fig. 3.5 shows the background and foreground log likelihoods. The foreground likelihood gives little information about where the subject is due to the similarity between the intensity distribution of the subject and the darker area near the outside of the arena. Like Jen-

(a) (b)

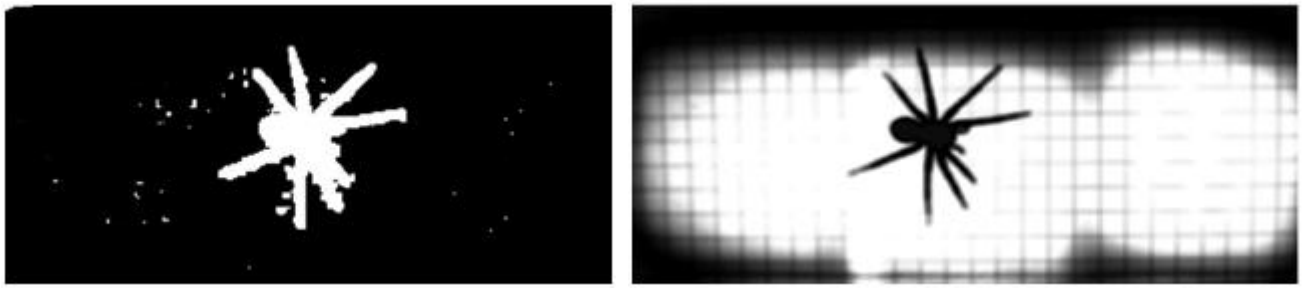

Figure 3.5: Negative log likelihood for background and foreground. (a) Background likelihood; (b) Foreground likelihood.

sen (2008), I find using only the background distribution held against its own mean, i.e $\phi\left(x_i = subject, \mathbf{y}\right) = mean\left(\phi\left(x_i = background, \mathbf{y}\right)\right)$ resulted in more accurate labelling of subject and background (Fig. 3.6).

(a) (b)

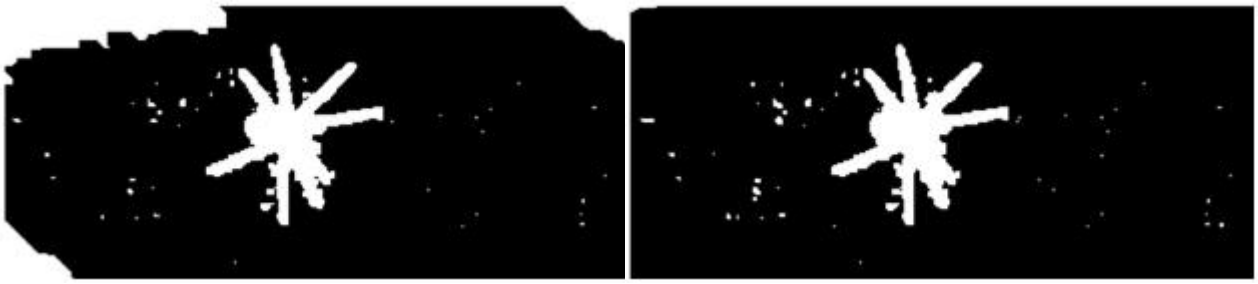

Figure 3.6: Segmentation based only on negative log likelihood. (a) Segmentation using subject and background distributions; (b) Segmentation using background distribution held against its own mean.

3.2.2 Smoothness prior

It is reasonable to assume data is not totally random, so generally neighbours will have a higher probability of having the same label. The prior $\psi\left(x_i, x_j\right)$ is a pairwise term which takes the form of a Generalized Potts model (Bray et al., 2006):

$$\psi\left(x_i, x_j\right) = \begin{cases} K_{i,j}, & x_i \neq x_j \\ 0, & x_i = x_j \end{cases} \tag{3.10}$$

where $K_{i,j}$ is a term that penalizes adjacent neighbours which have different labels. Because we are dealing with the binary situation of segmenting between background and

subject the problem is referred to as an Ising model (Greig et al., 1989).

Implementation

Due to my inexperience with other programming languages, I originally desired all code to be programmed in MATLAB. Energy with the smoothness term included was implemented using general sliding-neighbourhood operations (nlfilter()) to apply functions that compared the value of the centre pixel x_i, to its 4-neighbourhood (each pixel is connected to the 4 pixels surrounding it). Unfortunately this implementation was far too slow (MATLAB is notoriously slow when you use for-loops), with each calculation of energy taking ~2.5 min, resulting in a single frame taking hours to process. Comparatively, the C++ implementation by Jensen (2008) took ~0.016 sec per energy calculation resulting in a frame taking ~2 minutes to process. From this point onwards any calculations of total energy use Jensen's C++ functions via the mex function, which enables C++ code to be called into a MATLAB executable file.

3.2.3 Contrast term

The final term to be added to the energy of the image segmentation problem is a contrast term, which favours pixels with similar colours having the same label. This term is incorporated by increasing the cost within the Ising model (for two neighbours being different) proportionally to the similarity in intensity of the corresponding pixels. In these experiments a pairwise, likelihood term $\gamma(x_i, x_j)$ is used:

$$\gamma(x_i, x_j) = \lambda \exp\left(\frac{-g\,(i,j)}{2\sigma^2}\right) \frac{1}{dist(i,j)} \tag{3.11}$$

where $g^2(i,j)$ measures the difference in intensity values between pixels i and $j$and $dist(i,j)$ is the spatial distance between the two. The contrast term has the form:

$$\phi\left(x_i, x_j, \mathbf{y}\right) = \begin{cases} \gamma(x_i, x_j), & x_i \neq x_j \\ 0, & x_i = x_j \end{cases} \tag{3.12}$$

Adding this final term to the energy causes the formulation to depart from the strict definition of a MRF, with the resulting energy now characteristic of a Conditional Random

Field (CRF). A CRF can be viewed as an MRF globally conditioned on the data (Kohli, 2007).

Implementation

As for the smoothness prior, we use a 4-neighbourhood and this conveniently sets the value of $dist(i,j)$to one. The gradient g^2, is approximated using a Sobel operator, G, for every pixel, in both in horizontal and vertical directions:

$$G_x = \begin{vmatrix} 1 & 0 & -1 \\ 2 & 0 & -2 \\ 1 & 0 & -1 \end{vmatrix} \tag{3.13}$$

G_y is the transpose of G_x, giving the gradient magnitude $g^2 \approx \sqrt{G_x^2 + G_y^2}$ and the range of $\gamma(x_i, x_j)$ is (0, λ).

3.3 Pose-specific segmentation

The framework for image segmentation described above uses likelihood terms which are based solely on pixel intensity and contrast. Though the above energy formulation provides a reasonable segmentation, there is no prior on the segmentation to look spider-like. A spider shape prior is added to the algorithm in order to achieve more accurate segmentation results. This simple model ensures the resulting subject actually resembles the spider form by removing artefacts such as reflections and later plays an important role in pose estimation.

3.3.1 The stick spider

An articulated stick spider is used to generate a pose-specific shape prior on the segmentation. The stick spider is based on measurements of each leg segment of *D. aquaticus* (Reussenzehn, 2008), (Table 3.1). This model is scaled to aproixmate the size of the spider in a given video. Additionally, for a spider of this leg span the cephalothorax was estimated to be 14 mm long by 12 mm wide and the abdomen was estimated to be 14 mm long by 10 mm wide.

Table 3.1: Lengths (mm) used in shape model, data from Reussenzehn (2008).

Segment	Leg 1	Leg 2	Leg 3	Leg 4
Co	2.9	3.1	3.0	3.4
Tr	1.1	1.1	1.2	1.4
Fe	8.2	8.5	8.4	9.3
Pa	4.4	4.4	4.1	4.2
Ti	7.1	7.3	6.8	8.0
Me	6.3	6.5	6.8	8.8
Ta	4.2	4.1	3.6	4.9

The model has 43 degrees of freedom defining the global position and orientation of the cephalothorax-abdomen (2 DOF for x-y position, 1 DOF for rotation) and the various joint angle values for rotation in the plane of the experimental arena (about the dorsal-ventral axis; 5 DOF for each leg). Joint- limits were imposed so that the angle could not exceed the known maximum range for *D. aquaticus* (Reussenzehn, 2008), (Table 3.2). For the body-coxa joints, angles were zero for natural orientation of the coxae (coxa 1 = 55^o, coxa 2 = 76^o, coxa 3 = $108^o$and coxa 4 =117^o, where angles were measured in relation to the symmetry line of the cephalothorax (Reussenzehn, 2008)). The remaining angles are reported as rotation about the joint axis.

Table 3.2: Maximum joint angles (^{o}) used in the shape model, data from Reussenzehn (2008).

Joint	Leg 1	Leg 2	Leg 3	Leg 4
Body-Co	51	65	67	54
Co-Tr	102	102	46	56
Tr-Fe	0	0	0	0
Fe-Pa	0	0	0	0
Pa-Ti	83	68	36	17
Ti-Me	14	13	13	8
Me-Ta	119	120	118	138

3.3.2 Pose-specific prior

Given an estimate of the location and shape of the subject, the pose specific prior is constructed so that pixels falling close to the shape have a higher probability of being labelled 'subject' while those falling further away have a higher probability of being labelled 'background'. The uniform prior, $\psi(x_i)$ in Eq. (3.3) , is replaced by a shape prior:

$$\psi\left(x_i\right) = \phi\left(x_i|\theta\right) = -\log P\left(x_i|\theta\right) \tag{3.14}$$

where θ contains the configuration of the stick spider (position, orientation and leg span). The probability $P(x_i|\theta)$ of x being labelled as foreground or background is defined as:

$$(x_i = subject|\theta) = 1 - P(x_i = background|\theta) = \frac{1}{1 + \exp\left(\mu \times \left(d\left(i, \theta\right) - d_r\right)\right)} \tag{3.15}$$

where *d(i, θ)* the distance of pixel i from the shape defined by θ, d_r is the thickness of the shape and μ contains the magnitude of the cost for points outside of the shape. Our final energy function now takes the form:

$$E(x) = \sum_i \left(\phi_i\left(x_i, \mathbf{y}\right) + \psi_i\left(x_i|\theta\right)\right) + \sum_{i,j} \left(\left(\phi_{i,j}\left(x_i, x_j, \mathbf{y}\right) + \psi_{i,j}\left(x_i, x_j\right)\right)\right) \tag{3.16}$$

This is the energy minimization formulation that is used both to segment the frames and estimate the pose of the shape model.

Implementation

In order to find the distance map, the shape model in its given configuration undergoes rasterization. The result is binary image, where the subject is represented by ones and the background zeros; the cephalothorax and abdomen are ellipses and each leg segment consists of a line. This has the advantage of speeding up the process (which is rather time intensive because it has to be completed for every change in pose) by avoiding vector calculations for each body segment and then finding the distance. The distance transform calculates for each pixel i the distance to the nearest pixel that contains a one (i.e. is part of the shape model). The resulting matrix contains the distance map where pixels that are part of the shape get value zero; those adjacent to the shape get value 1 and so on. My algorithm uses the Euclidean distance transform, where the distance between two points (x1,y1) and (x2, y2) is defined as:

$$dist = \sqrt{(x1 - x2)^2 + (y1 - y2)^2} \tag{3.17}$$

This formula is implemented in MATLAB using bwdist(), which finds the distance from i to the nearest nonzero pixel. Fig. 3.7 shows the rasterization and the corresponding distance map overlaid with the stick spider model.

(a) (b)

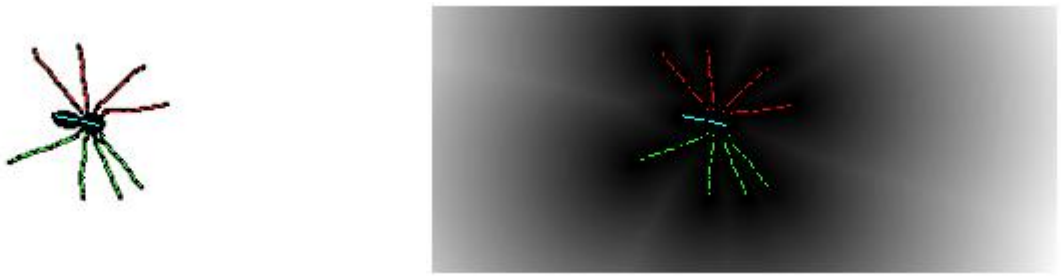

Figure 3.7: The rasterization of the shape model and the corresponding Euclidean Distance Transform overlaid with the spider shape model (note: colours have been inverted for (a) to avoid large black background). (a) Raster body; (b) Distance map.

3.4 Pose estimation

The pose of the subject is not only important to the final energy minimization for image segmentation, but it also contains the information desired for gait analysis. In this section of the methods I return to my original aim of estimating the pose of a spider in a given image. In order to solve this problem, some sort of initial guess of the subject pose is required to optimize in order to find the correct pose.

3.4.1 Pose initialization

Finding the initial pose is definitely not a trivial task. Automated initialization procedures, while becoming more common, are generally rejected in order to simplify the problem. The majority of computer vision-based human motion capture systems reduce the problem by either initially having the subject in some known start pose or by having the user specify the configuration (Moeslund & Granum, 2001). I opt for the latter because having a known start pose is infeasible in this case due to uncooperative subjects and their many leg segments. After the video is loaded and cropped to contain the tracking region of interest, the graphical user interface (Appendix B) allows the user to adjust the global position, angles and leg span of the spider. For estimating the angles, it generally suffices to only set the body-coxa joint for each leg and global rotation. The body segment lengths defined in the shape model are used to create a model of the spider that has been adjusted for leg span, but retains the relative proportions of each segment.

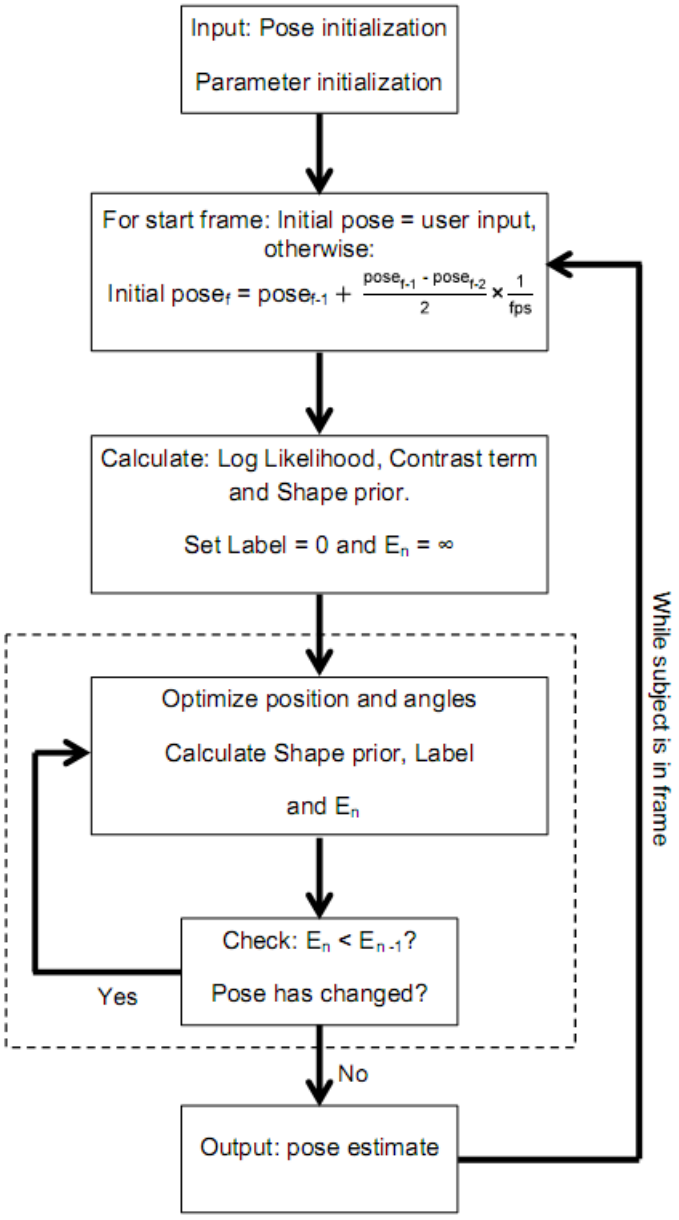

Figure 3.8: Pose estimation algorithm described in text.

3.4.2 Pose inference in every frame

To find the pose in a given frame the algorithm needs an initial guess of the subject pose which is optimized to find the correct pose. This guess is either the initial pose from above or the pose of the subject in the previous frame updated under the assumption of smooth motion. This simple model assumes that the global velocity of the subject and the angular velocity of the joints are constant over time. Although the assumption of constant velocity is naïve it provides a reasonable initial guess, assuming filming was done at a high enough speed that the difference in pose between successive frames is small. The algorithm for pose inference is summarized below in the flow diagram (Fig. 3.8).

The algorithm follows the POSECUT approach (Bray et al., 2006), where given an image of the subject the pose inference can be formulated in terms of an optimization problem over the CRF energy, which can be minimize via graph cuts. To solve the energy minimization $\theta_{opt} = \arg\min_{\theta}\left(\min_{x} \psi\left(x, \theta\right)\right)$, steps contained in the dashed box (Fig. 3.8), are repeated until the energy is no longer lowered or the pose no longer changes. This should cause the loop to terminate close to an optimal solution.

The best position for a given configuration is estimated by repositioning the shape model to each of the four neighbouring positions and finding which one gives the least energy. Angles are optimized one limb at a time for the given labelling of background and subject. There is one angle change for the global position of the cephalothorax-abdomen in 2D and five angle changes for the leg segments (two of the seven joint angles are fixed at zero based on experimental data, Table 3.2). Optimization of angles is done outwards from the body, so each chain of rotations starts with the body-coxa joint and finishes with the metatarsus-tarsus joint. This prevents the algorithm getting stuck at a point where decreasing one angle and increasing another result in a lower cost. Angular changes made to the limb are represented by random combinations of -1,1 and 0, where (0, 0, 0, 0, 0) is the current configuration of the limb, and other values either increase (1) or decrease (-1) the angle by 1°. Angle changes multiplied by increasingly small constants, generally starting with 5 and decreasing to 1, this allows larger angular changes near the start of minimization followed by small changes towards the end when the pose is close to its optimal configuration.

Fig. 3.9 shows an example of the pose inference parameters and results for a single frame. In particular Fig. 3.9 (b) shows that this algorithm performs well at image segmentation and Fig. 3.9 (a) shows that pose estimates match the original images reasonably accurately.

(a) (b)

Figure 3.9: Pose specific terms and the segmentation result for a single frame. (a) The shape prior corresponding to the optimal pose of the stick spider; (b) Segmentation result based on energy minimization.

3.4.3 Initializing parameters

Various parameters for energy calculations need to be set prior to tracking. During tracking, the image overlaid with the shape model and the shape prior energies were displayed during to allow the user to observe the effects of altering different parameter values. Values described in Table 3.3 generally provided a good balance between the various terms involved in the segmentation and pose estimation problem, but these sometimes required tinkering to achieve accurate results.

Table 3.3: Input parameters for segmentation and energy calculations.

Parameter	Estimation	Description
Subject log likelihood	In text	The mean of the background log likelihood is used instead of a random distribution. Generally pixels above this threshold will be subject and those below it will be background.
Ising parameter	$K = \frac{\sigma}{2}$	Sets the penalty of having two neighbouring pixels with different labels. Set to half the standard deviation of the background log likelihood of the start frame.
Contrast term parameter	$\lambda = 2\sigma$	Controls the magnitude of the penalty along the edges of segmentation. The penalty for neighbouring pixels having different labels decreases from λ to 0 as difference in intensity increases. Set to twice the standard deviation of the background log likelihood of the start frame.
Body size	$d_r = \frac{span}{200}$	Controls the thickness (in pixels) of the shape prior model. We set this to a fraction of the leg span. Having a low value reduces the risk of false positives outside the body causing the algorithm to fail.
Body size	$\mu = \frac{sigma}{d_r}$	Controls the magnitude of the shape prior cost. Needs to be high enough to give a large penalty for incorrectly labelling pixels as subject which are not close to the shape.

3.5 Data smoothing

Raw kinematic data contains noise from various sources; this causes the resulting trajectories to be not as smooth as we would expect. Errors may be small when investigating only positional data. However differentiated noise increases linearly with frequency, causing errors to increase significantly in magnitude when raw positional data is used to calculate velocity and acceleration (Biewener & Full, 1992). This is illustrated below in Fig. 3.10; note the range of values on the y-axis is orders of magnitude larger for acceleration compared to velocity and velocity compared to position. These comparisons emphasize the importance of properly filtering data prior to differentiation.

A fourth-order zero-lag Butterworth filter is commonly used to reduce noise from raw kinematic data. In general, a low-pass filter is used to remove noise above a given cut-off frequency. The filter produces a weighted average of the immediate (*i*) and past (*i-1,i-2*) raw data plus a weighted average of the past (*i-1, i-2*) filtered output:

$$F_i = a_0 F_{i-2} + a_1 F_{i-1} + a_2 R_i + b_1 R_{i-2} + b_2 R_{i-1} \tag{3.18}$$

where F is the filtered value, R is the raw value, a and b are the filter coefficients and

i is the current frame. The coefficients are determined by the ratio of the sampling frequency (frames per second) to the cut-off frequency (f_c). However, this requires that we first specify f_c, which can be determined via residual analysis (Biewener & Full, 1992). This involves comparing the residual between filtered and raw data over a wide range of values of f_c, then selecting the value that minimises noise passing through the filter and the signal distortion (Fig. 3.11). Filtering can introduce a phase shift to the data. To remove this distortion, we need to pass the data through the filter in the forward direction followed by the reverse direction. The use of this procedure and equation (3.18), results in a fourth-order, zero-lag, Butterworth filter.

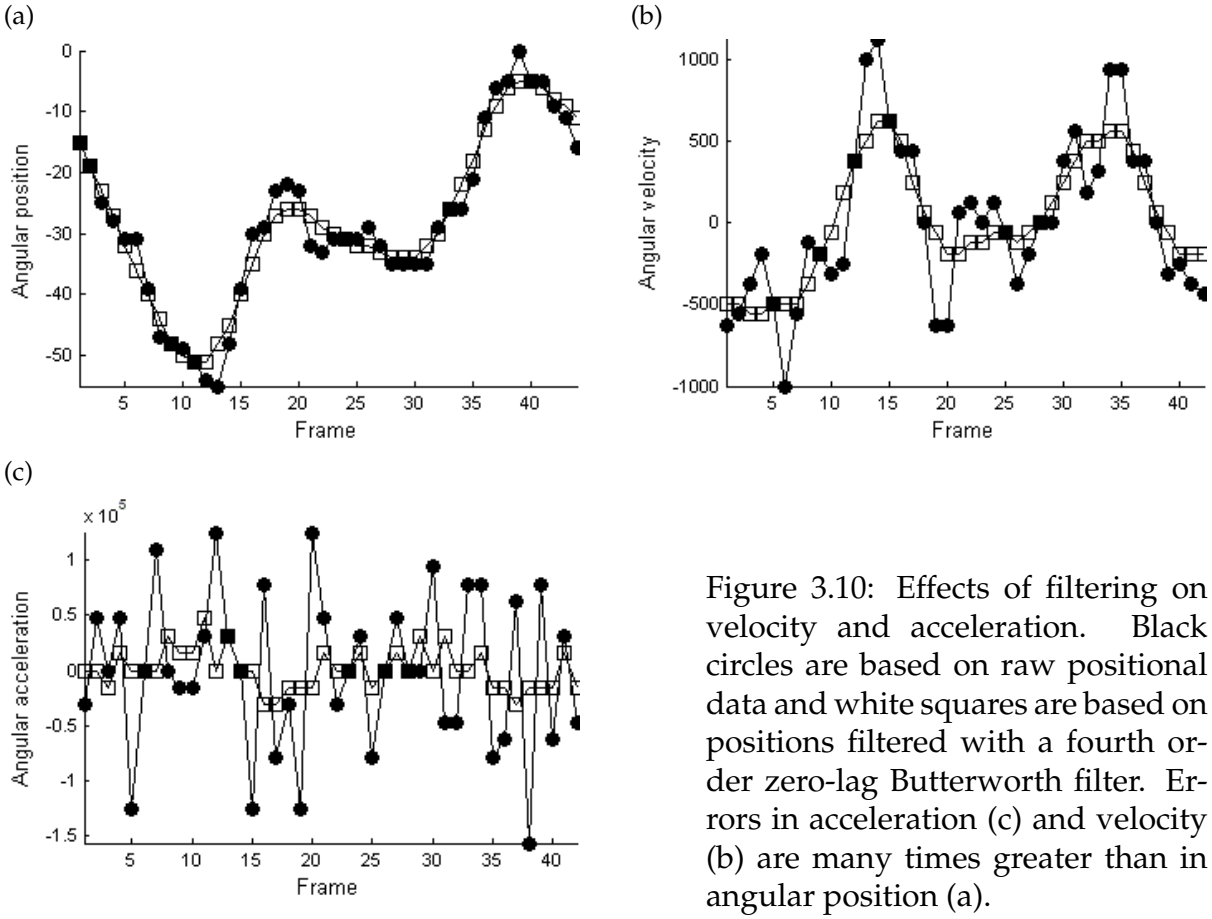

Figure 3.10: Effects of filtering on velocity and acceleration. Black circles are based on raw positional data and white squares are based on positions filtered with a fourth order zero-lag Butterworth filter. Errors in acceleration (c) and velocity (b) are many times greater than in angular position (a).

Once data has been digitally smoothed, we can return to finding the linear and angular derivatives (velocity and acceleration). It is common practice to perform a numerical procedure called finite differences on position data to obtain values for velocity (3.19) and acceleration (3.20) as functions of time:

$$\dot{x}(i) = \frac{x_{i+1} - x_{i-1}}{2(\Delta t)} \tag{3.19}$$

$$\ddot{x}(i) = \frac{x_{i+1} - 2x_i + x_{i-1}}{(\Delta t)^2} \tag{3.20}$$

where $\ddot{x}(i)$ is an acceleration value, $\dot{x}(i)$ is a velocity value, $x(i)$ is the filtered position value, i is the current frame and Δt is the time between frames. Analysis of these values will be discussed further in the following section on gait analysis.

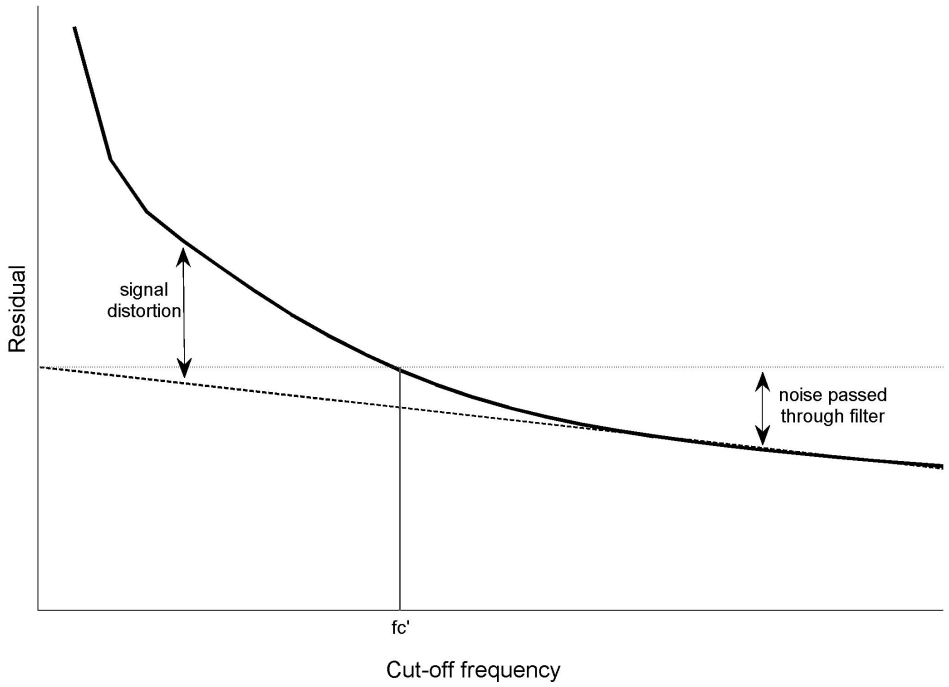

Figure 3.11: Residual analysis for determination of an appropriate filter cut-off frequency. f_c' is the frequency that balances the amount of noise versus signal distortion.

3.6 Gait analysis

In our coordinate system, the overall direction of forward movement of the spider (length of the behavioural arena) was used to define the x-axis, and lateral movement to the right was in the positive y direction. By convention, positive angles of body rotation indicate the body is turning clockwise and negative indicate turning in the anticlockwise direction. For the body-coxa joints, angles are reported with zero being perpendicular to the symmetry line of the cephalothorax. The remaining angles are reported as rotation about the joint axis. These angles increased when the joint moved forwards reaching a maximum corresponding to the anterior extreme point (AEP) and decreased when the joint moved backwards reaching a minimum corresponding to the posterior extreme point (PEP).

Linear speed was measured by the change in position of the cephalothorax-abdomen joint using equation (3.19) and acceleration equation (3.20) . Angular velocity and acceleration were also calculated for global rotation and each leg joint using the same equations.

The extreme positions of the leg movement are denoted by AEP for anterior extreme position and by PEP for posterior extreme position. The angular position of the legs was approximated by the angle delimited by the tarsus, the body-Co joint between the leg and the body and the body-Co joint of the contralateral leg. This angle was equal to 0^0 when the leg was perpendicular to the cephalo-caudal axis of the body. Its value increased when the leg moved forwards towards the AEP and decreased when the leg moved backwards towards the PEP.

The period of the stride was defined as the time elapsing between two successive AEPs of the same leg. It could only be measured to within 8 ms because of the film speed. The period consisted of one stance phase and one swing phase. The stride frequencies were calculated by 1/stride duration and presented as the number of strides per second. Stride length was calculated by dividing the average speed by the stride frequency. The kinematic duty factor (stance duration/stride duration) was expressed as percentage of stride duration. Within a given sequence, stride duration measurements did not differ between legs ($p>0.05$ ANOVA), however the movements of legs 1 and 4 are more ambiguous for functional reasons i.e. dragging being included as part of protraction. Thus, unless stated otherwise, stride data is presented using leg L2 for comparisons.

Phase relationships between legs during locomotion were calculated by the time at which an AEP occurred for a given leg relative within the period of the reference leg (Jamon & Clarac, 1995):

$$\phi_{n:n'} = (AEP_n - AEP_{n'})/P_{n'} \tag{3.21}$$

where $P_{n'}$ is the stride period of the reference leg.

Values of Φ less than 0.25 or greater than 0.75 represent simultaneous in-phase stepping and values of Φ between 0.25 and 0.75 represent alternate anti-phase stepping.

For the comparisons between size and speed across a variety of spider species, data was obtained from (Moya-Laraño et al., 2008). For comparisons with other arthropods and vertebrates data came from a variety of sources: mammals (Iriarte-Diaz, 2002); lizards (Bonine & Garland, 1999); turtle (Zani & Claussen, 1994); birds (Blanco & Jones, 2005); cockroaches (Full & Tu, 1991; Ting et al., 1994); crab (Blickhan & Full, 1987); frog (Ahn et al., 2004). This does not represent an exhaustive search of the literature, but does span

the major vertebrate groups which use terrestrial locomotion and includes the species of arthropods which have been studied in greatest depth. I follow the guidelines of (Iriarte-Diaz, 2002) and present the single fastest running speed documented if more than one value had been reported for the same species, along with the mean mass reported for animals involved in the experiment.

3.7 Statistical Analysis

I selected 29 trials from 15 subjects (mass = 1.194g ± 0.376), based on the requirements of reasonably constant velocity and little deviation in heading angle. The usable data was obtained from about one in ten trials with spiders preferring to stay close to walls while running, resulting in legs frequently hitting the wall; also spiders often decelerated and stopped part way through the trial. For comparisons of kinematic parameters with mass and body length, data from the same subject was treated as a single data point (mean, minimum or maximum) to avoid pseudoreplication (N=15). For comparisons of kinematic parameters with speed, data is presented for each trial (N=29). Analysis of phase lags required that at least two full strides of each leg were observed during the trial, reducing the number of acceptable trials (N=27).

All graphing and statistical analyses were performed in MATLAB (Student version R2009a, The MathWorks, USA). Comparisons between kinematic variables and size parameters (mass and body length) were made using regression on log transformed data. Values of the slope, a, were corrected for log transformation following Sprugel (1983). Comparisons between speed and kinematic variables were made using linear regression.

For phase lag data, each phase value was multiplied by 360 to convert from phase range (0-1) to degrees (0-360). The mean angle (phase) of leg lag was calculated in MATLAB as:

$$\mu_p = atan2(y, x) \tag{3.22}$$

where atan2 is a variant of the arctangent function, $X = \sum_{i=1}^{n} \cos\left(\frac{a_i}{n}\right)$, $Y = \sum_{i=1}^{n} \sin\left(\frac{a_i}{n}\right)$, and n is the sample size (Fisher, 1995). This value is then divided by 360 to convert the result back to the original range. The circular standard deviation was calculated as:

$$s_p = \frac{180}{\pi}\sqrt{-2\ln r} \tag{3.23}$$

where r is the length of the mean vector, $r = \sqrt{X^2 + Y^2}$ (Zar, 1996). Again, this value is then divided by 360 to convert the result back to the original range. Phase distributions were tested for uniformity of distribution using the Rayleigh test. Rayleigh's z:

$$z = \frac{R^2}{n} \tag{3.24}$$

where $R = nr$ (Zar, 1996). The p value associated with Rayleigh's R is approximated by:

$$p = \exp\left[\sqrt{1 + 4n + 4\left(n^2 - R^2\right)} - (1 + 2n)\right] \tag{3.25}$$

which is accurate to three decimal places for samples sizes as small as ten (Zar, 1996). To determine if any relationship existed between phase lags and speed, data was examined for angular-linear correlation. The correlation coefficient was calculated as:

$$r_{al} = \sqrt{\frac{r_{XC}^2 + r_{XS}^2 - 2r_{XC}r_{XS}r_{CS}}{1 - r_{CS}^2}} \tag{3.26}$$

where r_{XC} is the correlation between X (speed) and the cosine of a (phase), r_{XS} is the correlation between X and the sine of a and r_{CS} is the correlation between the sine and cosine of a (Zar, 1996). The significance of the correlation is assessed by comparing the test statistic nr_{al}^2 to X^2 distribution with 2 degrees of freedom (Zar, 1996).

Chapter 4

Results

4.1 Evaluation of tracking algorithm

Images included in the previous section show that segmentation of frames into subject and background improves significantly as additional terms increase the amount of information in our CRF framework. The final CRF is successful at isolating the spider in a given frame (Fig. 3.9). Videos included on the DVD in appendix 3 illustrate that the algorithm appears to do a reasonable job of tracking the motion of the spiders' joints across frames. Generally motion capture techniques have their accuracy assessed by comparing results to ground truth data. Because we don't have access to a data set for our study species, we attempt a quantitative evaluation through other techniques below.

Analysing 46 frames where the spider appeared to not be moving resulted in slightly "jiggly" looking results. The maximum and minimum position in x coordinates differed by 2 pixels and y coordinates differed by 1 pixel. Translated in to cm x coordinate measurements differed by 0.083 cm and y coordinate measurements differed by 0.042 cm. Alternatively, looking at one standard deviation gave 0.557 pixels (0.023 cm) for x coordinates and 0.487 pixels (0.020 cm) for y coordinates. Individual joint angles were somewhat less accurate than total angle of the leg (Table 4.1), suggesting that at times the pose estimation fitting results in one angle increasing/decreasing and a joint further down the chain does the opposite.

Table 4.1: Difference between maximum and minimum values (°) for each joint averaged over leg pairs. Values in parentheses are the standard deviation for each joint and the total leg configuration across all frames, averaged over leg pairs.

Joint	Leg 1	Leg 2	Leg 3	Leg 4
Body-Co	5 (1.502)	13 (3.468)	6 (1.814)	5 (1.268)
Co-Tr	9 (2.581)	14 (3.865)	8 (2.465)	2 (0.643)
Pa-Ti	5 (1.730)	14 (3.793)	3 (0.643)	7 (2.248)
Ti-Me	9 (3.279)	13 (2.899)	3 (0.856)	3 (1.167)
Me-Ta	10 (3.528)	9 (2.771)	13 (5.019)	6 (2.464)
Total leg	3 (0.707)	3 (0.909)	2 (0.662)	3 (0.872)

Comparing the results tracking in one direction and then the reverse direction yielded similar results to above. Position data showed reasonable accuracy with root mean squared difference for position in x coordinates of 2.300 pixels and y coordinates 0.983 pixels. Translated in to cm x coordinate measurements differed by 0.096 cm and y coordinate measurements differed by 0.041 cm. Again the angle for total leg configuration was more accurate than the angles for individual joints (Table 4.2). Thus, from here on, results will focus mainly on total leg configuration with the exception of presenting maximum and minimum values for each of the joints in the leg.

Table 4.2: Root mean squared differences (°) between forward and reverse tracking for each joint and the total leg configuration averaged over leg pairs.

Joint	Leg 1	Leg 2	Leg 3	Leg 4
Body-Co	4.739	5.395	5.185	5.827
Co-Tr	6.760	5.604	7.050	5.594
Pa-Ti	6.417	3.969	4.636	3.988
Ti-Me	2.006	1.882	1.408	1.225
Me-Ta	15.851	14.035	7.689	7.521
Total leg	6.166	4.311	3.311	3.252

4.2 Analysis of spider locomotion

The locomotion speed measured in 15 individuals during a total of 29 sequences averaged 24.807 ± 6.698 cm s^{-1} (S.D.) and ranged between 5.000 and 49.548 cm s^{-1}. Speed varied both within different trials with the same individual and between individuals. Thus, correlations between the size of the animal and the speed at which it moved were examined.

4.2.1 Kinematic variables and size

No correlation was found between average, maximum, or minimum absolute or normalized speeds and mass or body length (Fig. 4.1 (a-d); Table 4.3). The only kinematic parameter to have any relationship with either size parameter was stride length. Relationships between mass and maximum, minimum and average stride length were all significant (Fig. 4.2 (c); Table 4.3). All comparisons except minimum stride length were also significantly related to body length (Fig. 4.2 (d); Table 4.3). Stride frequency had no significant relationship with size (Fig. 4.2 (a & b); Table 4.3).

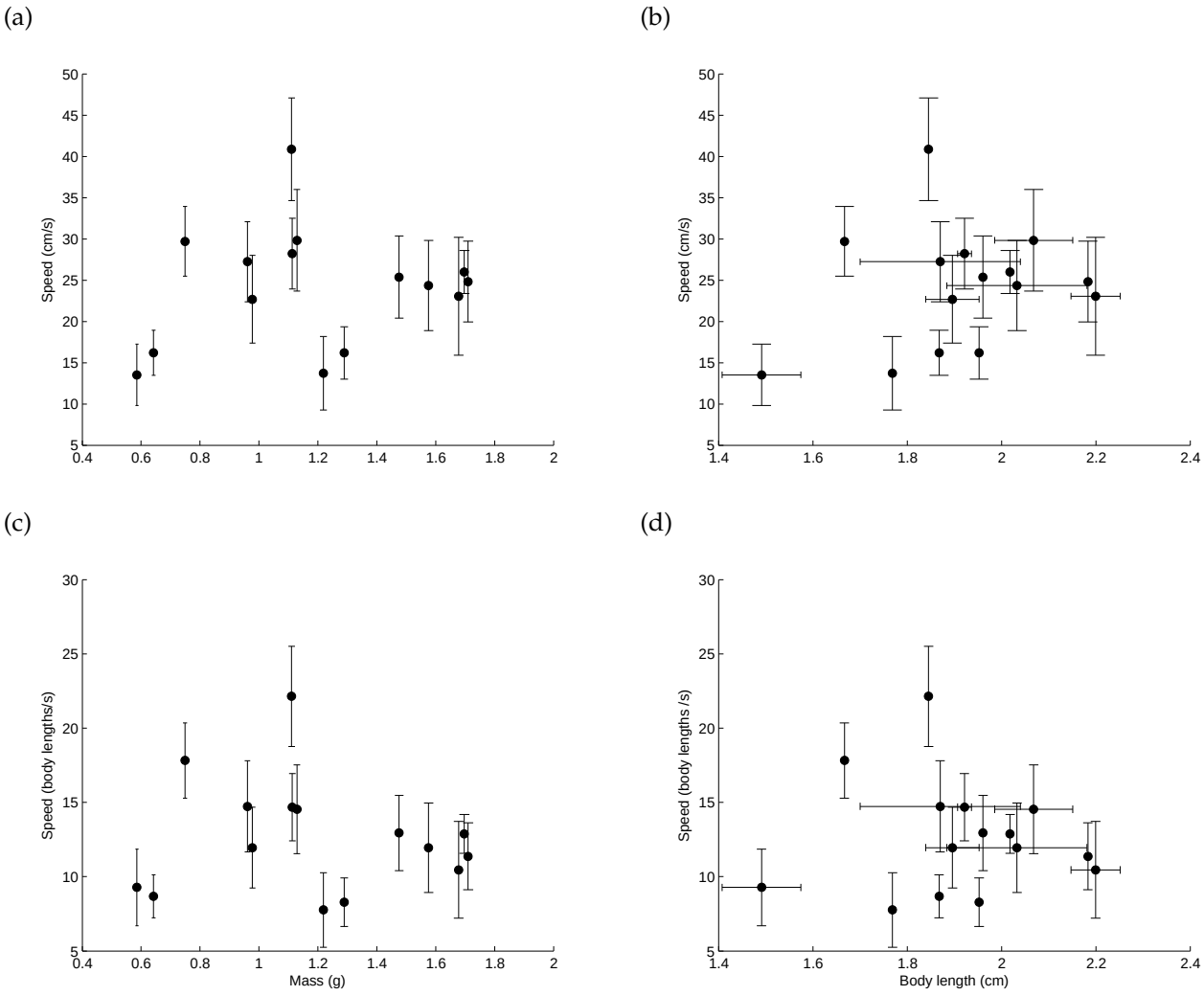

Figure 4.1: Absolute speed (cm s^{-1}) and normalized speed (body lengths s^{-1}) as a function of mass (g) and body length (cm) in the spider *Dolomedes aquaticus*. Data is presented as the mean $\pm$ S.D. Body lengths were estimated during initialization of the spider model for tracking. (a) Absolute speed (cm s^{-1}) vs. mass (g), (b) absolute speed (cm s^{-1}) vs. body length (cm), (c) relative speed (body lengths s^{-1}) vs. mass (g) and (d) relative speed (body lengths s^{-1}) vs. body length (cm). There were no significant trends between average, minimum or maximum absolute or normalized speed and mass or body length.

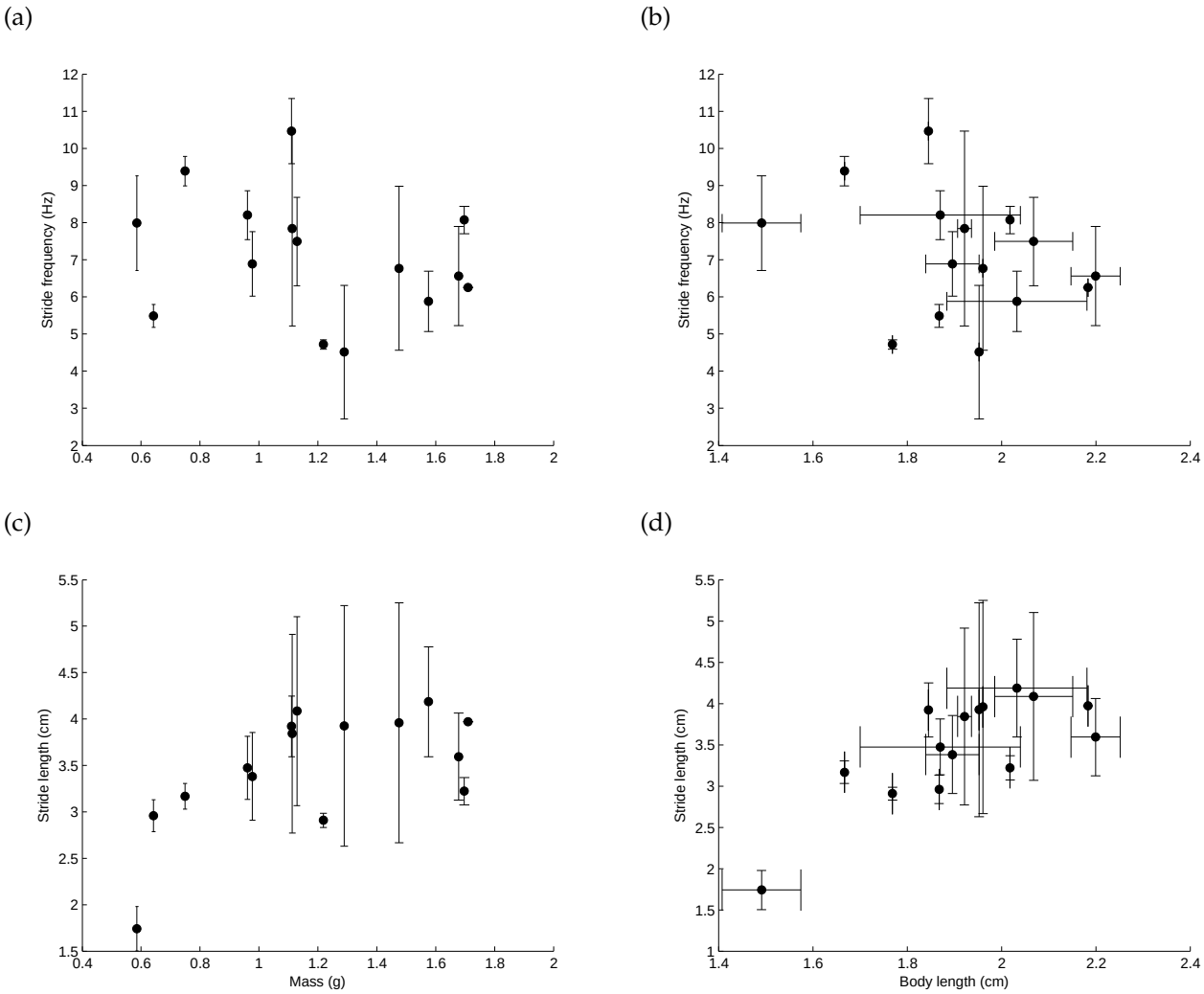

Figure 4.2: Stride frequency and length as a function of mass (g) and body length (cm) in the spider *Dolomedes aquaticus*. Data is presented as the mean $\pm$ S.D. Body lengths were estimated during initialization of the spider model for tracking. (a) Stride frequency (Hz) vs. mass (g), (b) stride frequency (Hz) vs. body length (cm), (c) stride length (cm) vs. mass (g) and (d) stride length (cm) vs. body length (cm). Stride length increased proportionally to mass$^{0.433}$ and body length$^{1.758}$.

Table 4.3: Relationship between locomotion parameters and size parameters in the spider *Dolomedes aquaticus* obtained through ordinary least-squares (OLS) regression on log-transformed data.

	$Y = aX^b$		
	a	b (95% confidence interval)	r^2
Average absolute speed (cm s^{-1})			
mass (g)	23.416	0.267 (-0.251, 0.784)	0.087
body length (cm)	11.642	1.131 (-0.609, 2.870)	0.132
Minimum absolute speed (cm s^{-1})			
mass (g)	11.788	0.409 (-0.524, 1.341)	0.065
body length (cm)	6.179	1.087 (-2.171, 4.345)	0.038
Maximum absolute speed (cm s^{-1})			
mass (g)	32.256	0.243 (-0.174, 0.659)	0.109
body length (cm)	17.661	0.978 (-0.425, 2.381)	0.149
Average normalized speed (body lengths s^{-1})			
mass (g)	12.664	0.019 (-0.485, 0.523)	0.001
body length (cm)	11.960	0.092 (-1.645, 1.829)	0.001
Minimum normalized speed (body lengths s^{-1})			
mass (g)	6.307	0.172 (-0.780, 1.123)	0.012
body length (cm)	6.298	0.039 (-3.259, 3.337)	<0.001
Maximum normalized speed (body lengths s^{-1})			
mass (g)	17.595	-0.009 (-0.421, 0.402)	<0.001
body length (cm)	18.774	-0.102 (-1.520, 1.315)	0.002
Average stride frequency (Hz)			
mass (g)	7.268	-0.162 (-0.561, 0.236)	0.056
body length (cm)	10.570	-0.612 (-1.978, 0.754)	0.067
Minimum stride frequency (Hz)			
mass (g)	6.170	-0.198 (-0.669, 0.272)	0.060
body length (cm)	11.012	-0.939 (-2.514, 0.635)	0.113
Maximum stride frequency (Hz)			
mass (g)	8.682	-0.143 (-0.613, 0.327)	0.032
body length (cm)	11.935	-0.521 (-2.137, 1.095)	0.036
Average stride length (cm)			
mass (g)	3.286	0.433 (0.150, 0.716)*	0.457
body length (cm)	1.110	1.758 (0.958, 2.558)*	0.634
Minimum stride length (cm)			
mass (g)	2.710	0.419 (0.033, 0.805)	0.298
body length (cm)	0.991	1.635 (0.389, 2.882)*	0.382
Maximum stride length (cm)			
mass (g)	3.940	0.409 (-0.011, 0.829)*	0.254
body length (cm)	1.154	1.965 (0.773, 3.158)*	0.494

Values of a were corrected for log transformation following (Sprugel, 1983). * p<0.05

Speed vs. carapace length data obtained from Moya-Laraño et al. (2008) allowed the comparison of *Dolomedes aquaticus* with 38 other species of spider belonging to four families (Fig. 4.3). Regression on log data, without the inclusion of *D. aquaticus*, resulted in the scaling relationship $speed = 58.908 \times carapacelength^{1.094}$ (r^2= 0.609, p< 0.05). Using this equation on the mean carapace length predicts that *D. aquaticus* should have an average running speed of 56.206 cm s^{-1} which is greater than even the fastest speeds observed during our trials. However, examination of Fig. 4.3 reveals that there is a rapid increase in speed in spiders with carapace length between 0.1-0.4 cm long but spiders above this size do not seem to experience any additional gains in speed. Adding our observation to the data set does little to alter the scaling relationship, but results in a slightly larger r^2 value and slightly smaller p-value $speed = 54.666 \times carapacelength^{1.053}$ (r^2= 0.610, p< 0.05).

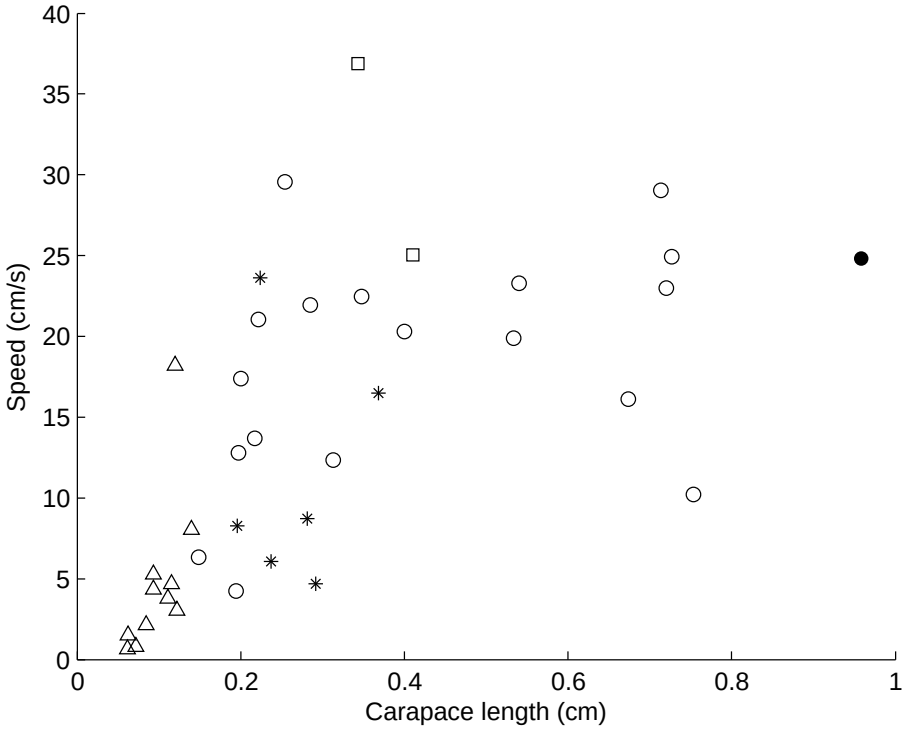

Figure 4.3: Average running speed (cm s^{-1}) as a function of size (carapace length) in 38 species of spider. Families are represented by different symbols: stars, Gnaphosidae; circles, Lycosidae; triangles, Philodromidae; squares, Sparassidae. Note the filled circle shows results from the present study on *Dolomedes aquaticus* which belongs to Lycosidae, remaining results were from (Moya-Laraño et al., 2008).

Overall, maximum running speed was found to increase significantly with increasing body mass (Fig. 4.4; p<0.05). A scaling exponent of 0.175 was obtained through linear regression on the complete selection of data. The majority of the data is from mammals so to ensure that this trend extended across the other animal groupings the analysis was re-

peated without the inclusion of mammals. While this reduced the correlation coefficient from 0.621 to 0.138, there was still a statistically significant trend with speed proportional to mass$^{0.219}$. Further trends between mass and kinematic parameter predicted from vertebrate studies are examined below.

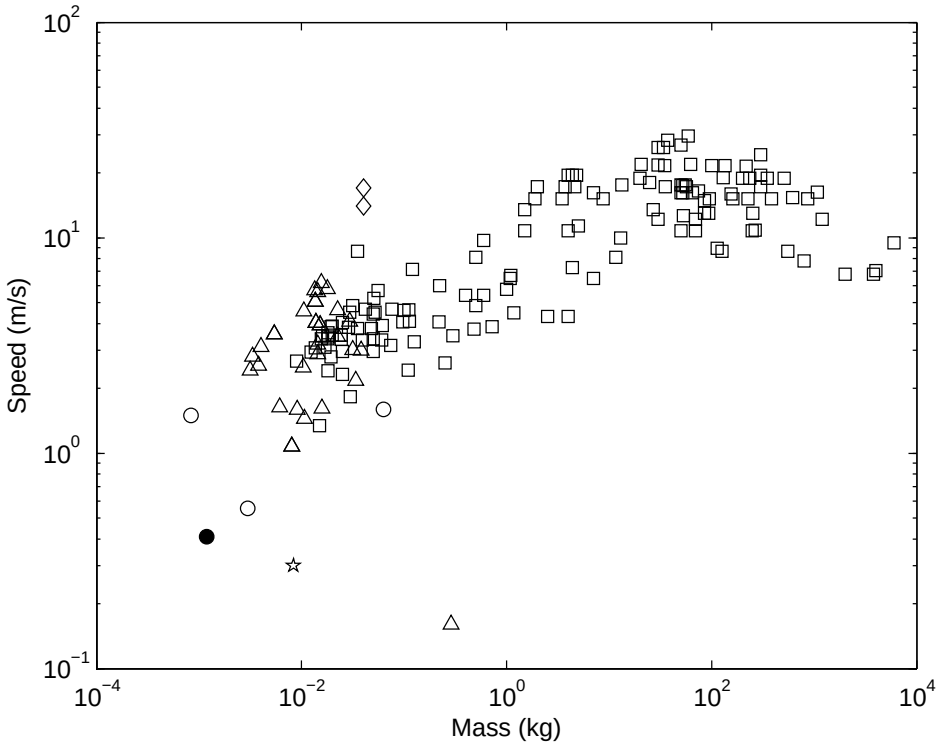

Figure 4.4: Logarithmic plot of maximum speed (m s^{-1}) vs. mass (kg) for terrestrial animals. Squares, mammalia; triangles, reptilia; star, amphibia; diamonds, aves; circles, arthpoda. The filled circle represents data from the present study on *Dolomedes aquaticus*. Additional sources of data were as follows: mammals (Iriarte-Diaz, 2002); lizards (Bonine & Garland, 1999); turtle (Zani & Claussen, 1994); birds (Blanco & Jones, 2005); cockroaches (Full & Tu, 1991; Ting et al., 1994); crab (Blickhan & Full, 1987); frog (Ahn et al., 2004).

Table 4.4 presents a comparison of the results of this study with expected proportions based on other studies (mainly vertebrate). With current results the only significant scaling relationships were between stride length and size; however we include other regression slopes for comparison. Non-significance in some instances was probably due to the inclusion of trials across a wide variety of speeds, rather than just analysing trials near the maximum running speed. None of our results differed significantly from the results predicted in previous research (two-tailed t test, $p>0.05$; Table 4.4). Interestingly, even though the majority of our results were not significant they match very closely with the absolute speed, stride frequency and stride length predicted by (Heglund et al., 1974).

Table 4.4: Scaling of maximal absolute running speed V_a, normalized running speed V_n, stride frequency F_s and stride length L_S determined in the spider *Dolomedes aquaticus*, compared to results in the literature. Observed values were compared to expected using a two-tailed t test where $H_0 : \beta_O = \beta_E$ and $H_A : \beta_O \neq \beta_E$.

	Proportionality			
Relationship	Expected	Source	Observed	Significance
Absolute speed vs. mass	$V_a \propto M^0$	Hill 1950	$V_a \propto M^{0.24}$	p>0.05
	$V_a \propto M^{0.24}$	Heglund et al. 1974		p>0.05
	$V_a \propto M^{0.17}$	Garland 1983		p>0.05
Normalized speed vs. mass	$V_n \propto M^{-0.33}$	Hill 1950	$V_n \propto M^{-0.01}$	p>0.05
	$V_n \propto M^{-0.09}$	Calder 1984		p>0.05
	$V_n \propto M^{-0.17}$	Iriarte-Díaz 2002		p>0.05
Stride frequency vs. mass	$F_S \propto M^{-0.33}$	Hill 1950	$F_S \propto M^{-0.14}$	p>0.05
	$F_S \propto M^{-0.14}$	Heglund et al. 1974		p>0.05
	$F_S \propto M^{-0.17}$	Alexander 1982		p>0.05
Stride length vs. mass	$L_S \propto M^{0.38}$	Heglund et al. 1974	$L_S \propto M^{0.41*}$	p>0.05
	$L_S \propto M^{0.33}$	Hill 1950		p>0.05

* in the observed column indicates significant slope from our regression analysis.

4.2.2 Kinematic variables and speed

A graphical examination of the stepping pattern geometry (Fig. 4.5) reveals that the temporal arrangement of the legs is reasonably regular. For a range of speeds, the stride length and the stride frequency increase as the speed increases (Fig. 4.5). At high speeds the gait approaches an alternating tetrapod gait but at lower speeds a metachronal wave may better describe leg movements. The stepping pattern is highly variable so visual inspection is of little value, therefore a quantitative analysis was made using kinematic variables.

Stride frequency increased linearly with both absolute (Fig. 4.6 (a)) and normalized speed (Fig. 4.6 (b)). Stride length also increased linearly with both absolute (Fig. 4.6 (c)) and normalized speed (Fig. 4.6 (d)). Stride frequency was more highly correlated with normalized speed and stride length was more highly correlated with absolute speed (Table 4.5). This makes sense from a biological perspective because larger animals have longer legs, resulting in longer steps, so if other parameters remain constant this will increase absolute speed. Whereas, when speed is normalized for body length stride length has a reduced role in increasing speed and instead this is achieved by increasing stride frequency. While values for speed reached the expected value for the trot-gallop transition for a spider of mean mass, stride frequency did not exceed the expected value even at highest speeds (Fig. 4.6 (a)). Conversely, stride length was higher than the expected value for the trot-gallop transition in the majority of trials (Fig. 4.6 (c)). Duty factor was generally higher than 0.5 at all speeds, indicating that legs spend more than half of the stride cycle on the ground (Fig. 4.6 (e & f)). There was no trend between increasing speed and duty factor. The duty factor was never beneath the value of 0.375 required for static instability in an eight legged animal (Fig. 4.6 (e & f); Ting et al., 1994).

The positive trend between stride frequency and speed suggests the lengths of the protraction and/or retraction phases may also have a relationship with speed and stride frequency. Both protraction and retraction times increased with absolute and normalized speed (Fig. 4.7 (a-d); Table 4.5). However, there was a much stronger correlation with stride frequency (r^2 protraction=0.827, r^2 retraction=0.690; Table 4.5). Both protraction and retraction decrease by a similar magnitude with protraction decreasing proportionally to -0.013×stride frequency and retraction decreasing proportionally to -0.010×stride frequency (Fig. 4.7 (e & f); Table 4.5). This is consistent with the fact that duty factor remains unchanged across a range of speeds (Fig. 4.7 (e & f)). The longitudinal stability margin is never less than zero, indicating that the animal is statically stable at all times (Table 4.5). An eight-legged arthropod would become less stable as the duty factor decreased to 0.375 (Fig. 4.7 (e & f)) and unstable if it fell below this value.

(a)

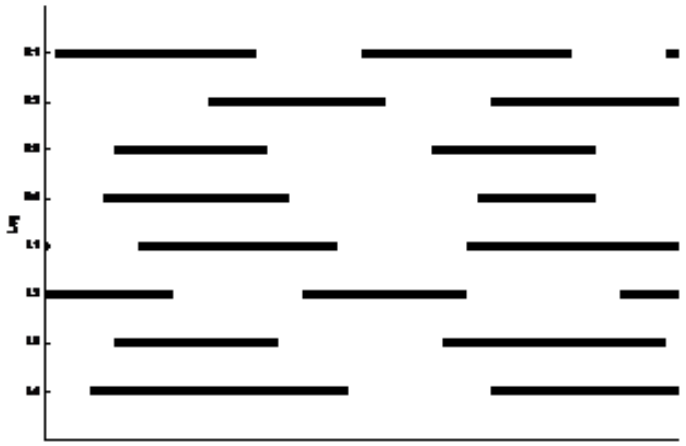

Average absolute speed 15.963 cms^{-1}, stride frequency 5.142 Hz, stride length 3.116 cm.

(b)

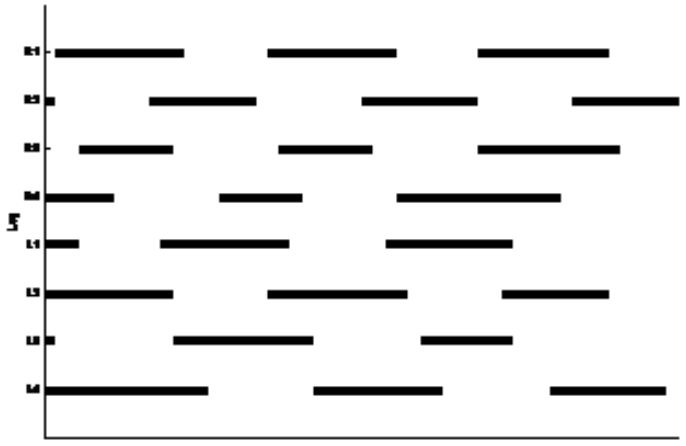

Average absolute speed 24.286 cms^{-1}, stride frequency 6.632 Hz, stride length 3.691 cm.

(c)

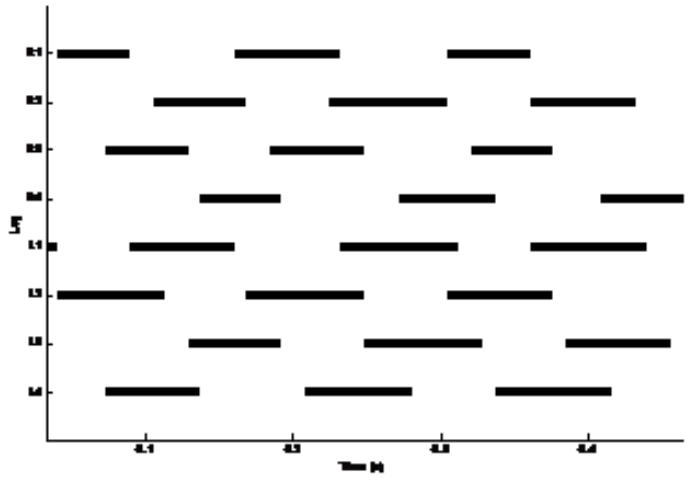

Average absolute speed 33.306 cms^{-1}, stride frequency 8.403 Hz, stride length 3.997 cm.

Figure 4.5: Stepping patterns during locomotion of the spider *Dolomedes aquaticus* at three different speeds(a-c). A heavy black line represents stance phase (retraction), and a space swing phase (protraction). All records last 0.432 sec and are from the same spider to avoid size issues. Scale is located beneath (c) is in intervals of 0.1 s.

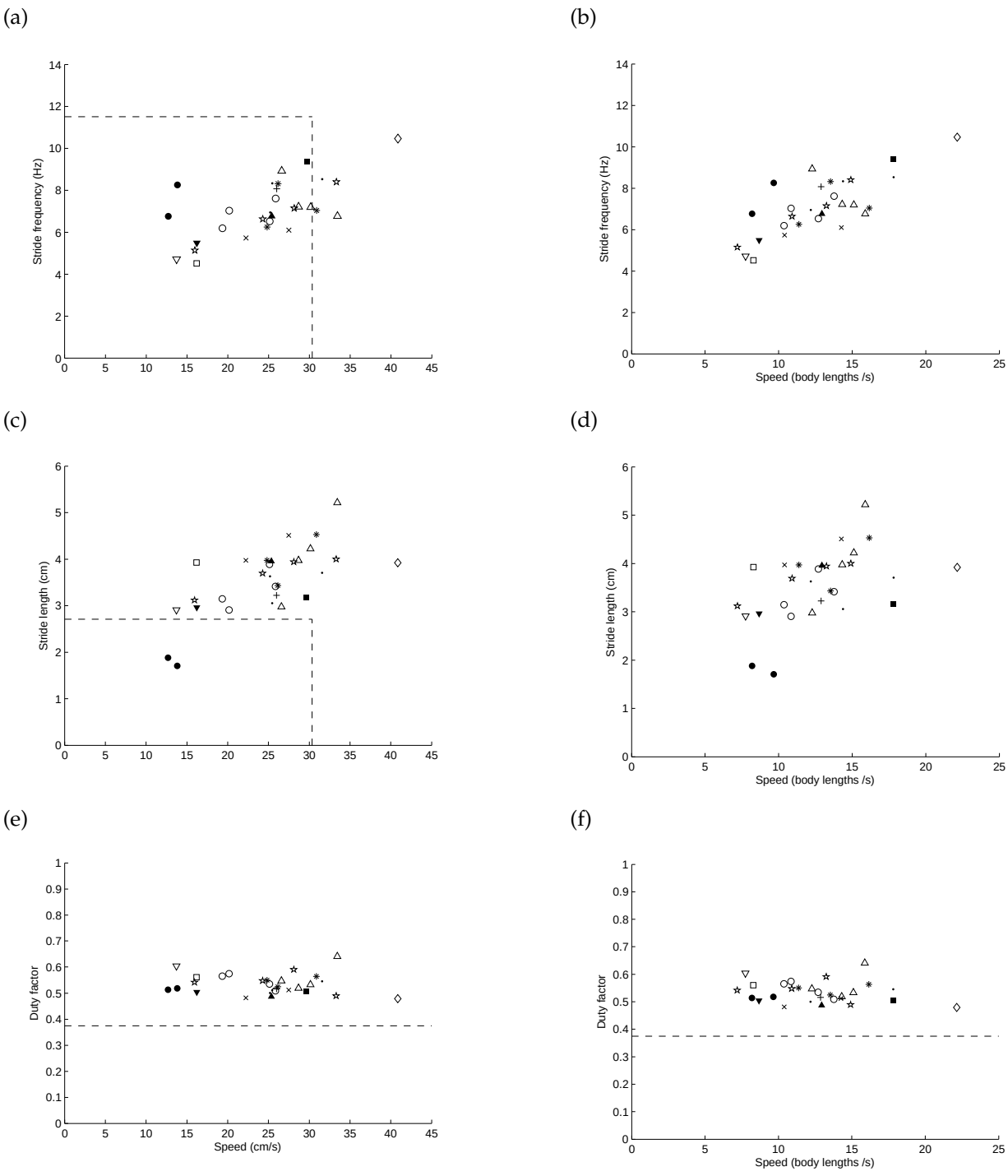

Figure 4.6: Kinematic variables as a function of absolute speed (cm s^{-1}) and normalized speed (body lengths s^{-1}) in the spider *Dolomedes aquaticus*. (a) Stride frequency (Hz) vs. absolute speed, (c) stride length (cm) vs. absolute speed, and (e) duty factor (stance phase/stride duration) vs. absolute speed, (b),(d) and (f) have the same y variable as described above but normalized speed on the x-axis. The dashed line in (a) shows the stride frequency and speed, (c) shows the stride length and speed predicted from the mean spider mass using the allometric equations from mammals for the trot-gallop transition (Heglund et al., 1974) and (e & f) show the duty factor required for static instability predicted by the longitudinal stability margin (Ting et al., 1994). Both stride frequency and stride length increased significantly with increasing absolute speed and normalized speed (a-d). Different shapes represent different individuals.

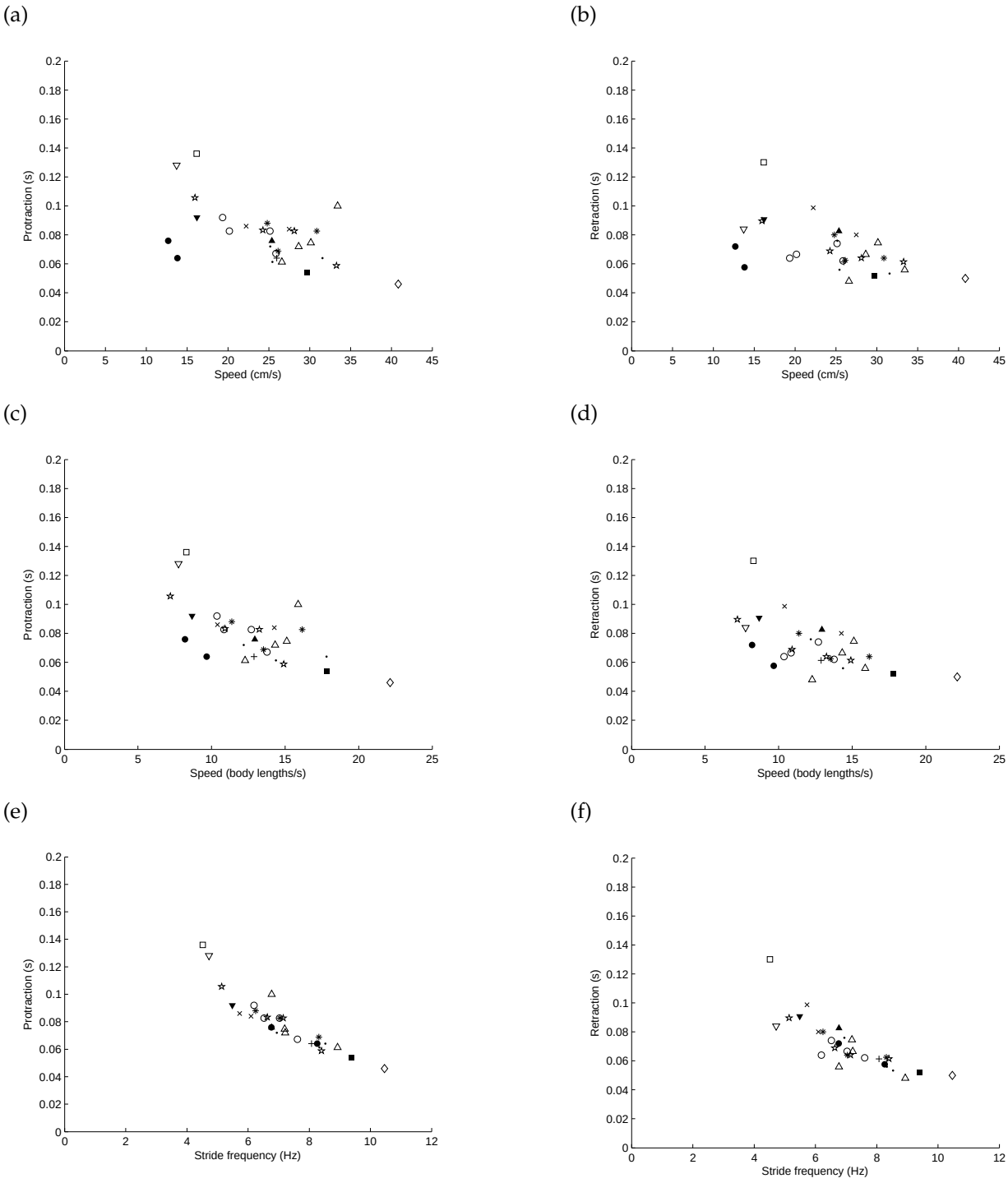

Figure 4.7: Protraction and retraction period (s) as a function of absolute speed (cm s^{-1}), normalized speed (body lengths s^{-1}) and stride frequency (Hz) in the spider *Dolomedes aquaticus*. (a) Protraction vs. absolute speed, (c) protraction vs. normalized speed, and (e) protraction vs. stride frequency, (b), (d) and (f) have the same x variable as previously described but retraction on the y-axis. Both protraction and retraction decrease with absolute speed, normalized speed and stride frequency. Different shapes represent different individuals.

Table 4.5: Relationship between kinematic variables and speed in the spider *Dolomedes aquaticus*, obtained through ordinary least-squares (OLS) regression.

	$Y = a + bX$		
	a	b (95% confidence interval)	r^2
Stride frequency (Hz)			
Absolute speed (cm s^{-1})	3.793	0.134 (0.072, 0.196)*	0.424
Normalized speed (body lengths s^{-1})	3.174	0.309 (0.205, 0.413)*	0.580
Stride length (cm)			
Absolute speed (cm s^{-1})	1.694	0.075 (0.043, 0.107)*	0.464
Normalized speed (body lengths s^{-1})	2.171	0.108 (0.034, 0.182)*	0.249
Protraction (s)			
Absolute speed (cm s^{-1})	0.121	-0.002 (-0.003, -0.001)*	0.323
Normalized speed (body lengths s^{-1})	0.129	-0.004 (-0.006, -0.002)*	0.428
Stride frequency (Hz)	0.173	-0.013 (-0.016, -0.011)*	0.827
Retraction (s)			
Absolute speed (cm s^{-1})	0.105	-0.001 (-0.002, -0.001)*	0.290
Normalized speed (body lengths s^{-1})	0.111	-0.003 (-0.005, -0.002)*	0.386
Stride frequency (Hz)	0.144	-0.010 (-0.013, -0.008)*	0.690
Duty factor			
Absolute speed (cm s^{-1})	0.550	-0.001 (-0.003, 0.002)	0.014
Normalized speed (body lengths s^{-1})	0.560	-0.002 (-0.006, 0.002)	0.034
Longitudinal stability margin			
Absolute speed (cm s^{-1})	0.350	-0.001 (-0.006, 0.003)	0.014
Normalized speed (body lengths s^{-1})	0.370	-0.004 (-0.013, 0.005)	0.034
* $p<0.05$			

The table above shows the duration of protraction is proportional to both speed and stride frequency, but this does little to inform us how the leg is actually moving through space during the swing phase. We now examine the variables relating to the position, velocity and acceleration across the duration of the stride.

4.2.3 Position, velocity and acceleration of the leg

Examination of Fig. 4.8 (a-d) reveals that the angular distance covered in the swing phase by legs 2 and 3 is greater than legs 1 and 4. Legs 3 and 4 showed trends of increasing leg excursion with stride period (leg 3: leg excursion = 52.793Ps + 16.699, r^2 = 0.154, $p < 0.05$, Fig. 4.8 (c); leg 4: leg excursion = 62.555Ps + 1.088, r^2 = 0.230, $p < 0.05$, Fig. 4.8 (d)). Conversely, examination of Fig. 4.9 (a-d) reveals that the average distance covered by the tibia is greater in legs 1 and 4 than legs 2 and 3. Leg 3 showed decreasing distance covered by the tibia with increasing stride period (leg 3: distance = -2.496 P_S+ 0.934, r^2 = 0.214, p <

0.05, Fig. 4.9 (c)).

The scatter plots of average angular velocity during swing phase as a function of stride period reveal the velocity magnitude is larger for legs 2 (Fig. 4.10 (b)) and 3 (Fig. 4.10 (c)) than legs 1 (Fig. 4.10 (a)) and 4 (Fig. 4.10 (d)). Similar results were observed during the stance phase, with velocities of legs 2 (Fig. 4.11 (b)) and 3 (Fig. 4.11 (c)) having larger negative values than legs 1 (Fig. 4.11 (a)) and 4 (Fig. 4.11 (d)). There was no significant trend in average angular velocity during swing phase as a function of stride period for any of the legs (Fig. 4.10). During the stance phase there was a significant trend between average angular velocity and stride period for legs 2 and 3 (Fig. 4.11 (b & c)). The magnitude of negative velocity decreases as stride period increases (leg 2: velocity = $762.938P_S$ - 417.381, $r^2 = 0.136$, $p < 0.05$; leg 3 velocity = $1017.726P_S$ - 474.011, $r^2 = 0.323$, $p < 0.05$).

Fig. 4.12 shows the relationship between the angular positions and velocities of legs 1, 2, 3 and 4 for all sequences. This representation of leg movements in their phase plane allows the examination of temporal stability of leg movement. Whilst subjects and sequences both show variation mainly due to differences in speed, these plots prove useful in examining general cyclic patterns of movement which allow us to infer the relative roles of each leg during locomotion.

The phase portrait of leg 1 (Fig 4.12 (a)) again reinforces that the movement of this leg is much more variable than other legs. It should be noted that this variability is not accumulated as a result of combining different sequences, but was found to exist from one sequence to another. Leg 2 showed reasonably stable cycling which is symmetrically distributed around approximately 20^o (Fig.4.12 (b)). Likewise, leg 3 showed reasonably stable cycling which is symmetrically distributed around approximately -10^o (Fig. 4.12 (c)). Conversely, leg 4 varied considerably suggesting that it is possibly acting under the influence of other legs (Fig. 4.12 (d)).

Leg 1 was highly variable with regards to both its position and speed. Leg 4 values were also variable but this was mainly due to variation in its position with velocity being somewhat more stable. The amplitudes of the cycles, as well as the results for leg excursion (Fig. 4.8), suggest that legs 2 and 3 play the prominent role during locomotion.

Figs 4.13 and 4.14 show the combined acceleration curves for all of the strides of the left set of legs (Note right leg strides were similar but not included to reduce clutter). In these figures, the curves were centred at the point corresponding to maximum angular speed of the leg; these values do not always correspond exactly to the zero acceleration point due to the resolution involved with the frame rate we used. Because strides varied in duration depending on speed, data is presented as a percentage of the swing and stance

phases. The overlapping curves are rather variable due to the inclusion of different trials and animals but general trends can still be observed across the swing (Fig. 4.13) and stance (Fig. 4.14) phases.

Legs 2 and 3 show acceleration and decelerations up to ~ 70000 degrees s^{-2} whereas legs 1 and 4 only reach peaks of ~ 50000 degrees s^{-2} (Fig. 4.13 & 4.14). The duration of the acceleration phase and deceleration phase vary greatly, which is evident in both swing (Fig. 4.13) and stance graphs (Fig. 4.14) requiring x-axes spanning values greater than 100. On average legs in the swing phase appear to spend equal period of time in the acceleration and deceleration phases (Fig. 4.13). However, in the stance phase legs (particularly 1 & 4) appear on average to spend a greater portion of time in the deceleration phase (Fig. 4.14).

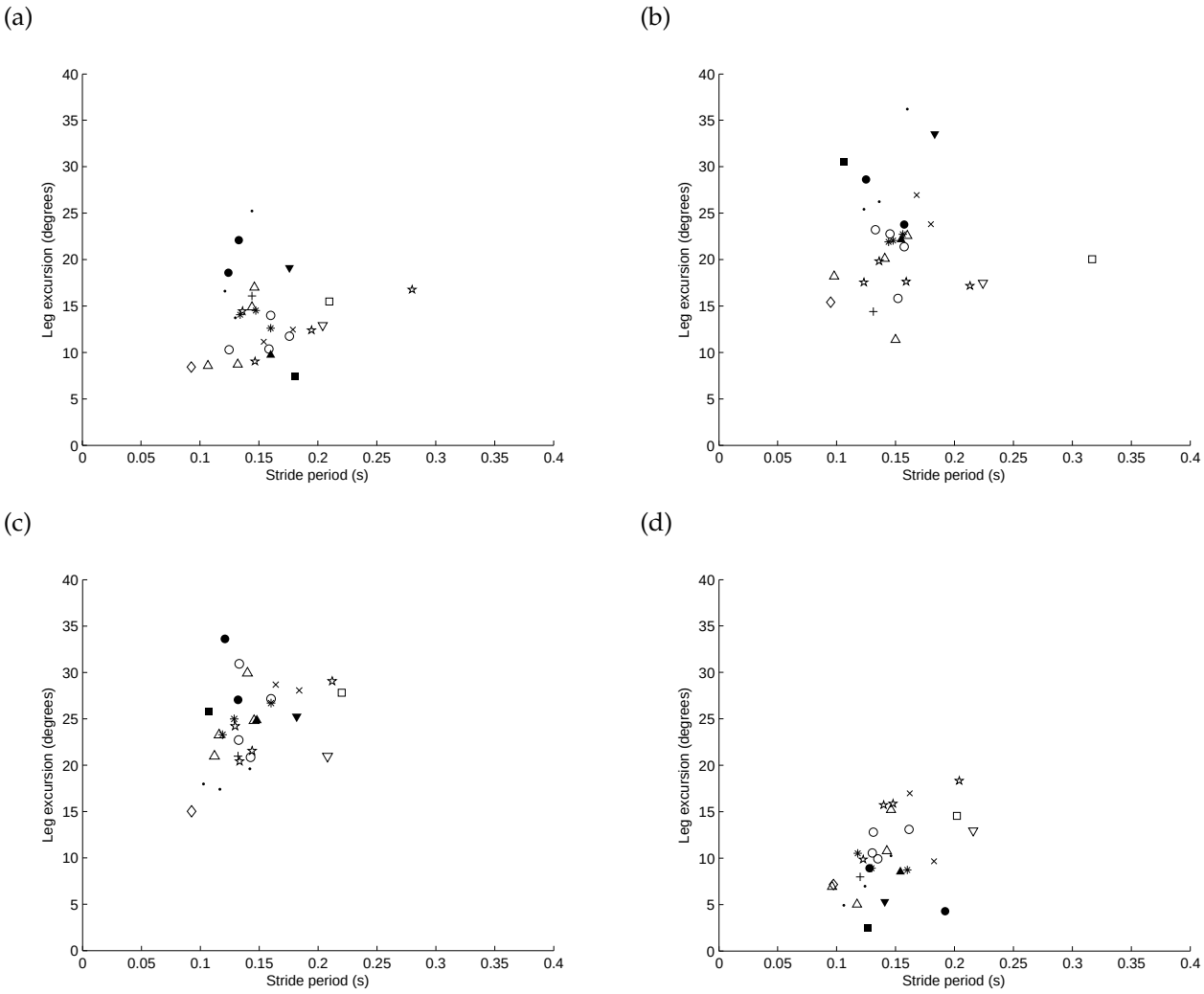

Figure 4.8: Leg excursion (º) during the swing phase as a function of stride period (s) for each leg of the spider *Dolomedes aquaticus*. (a) Leg 1, (b) leg 2, (c) leg 3 and (d) leg 4. Swing phase leg excursion increases significantly with stride period in legs 3 and 4. Different shapes represent different individuals.

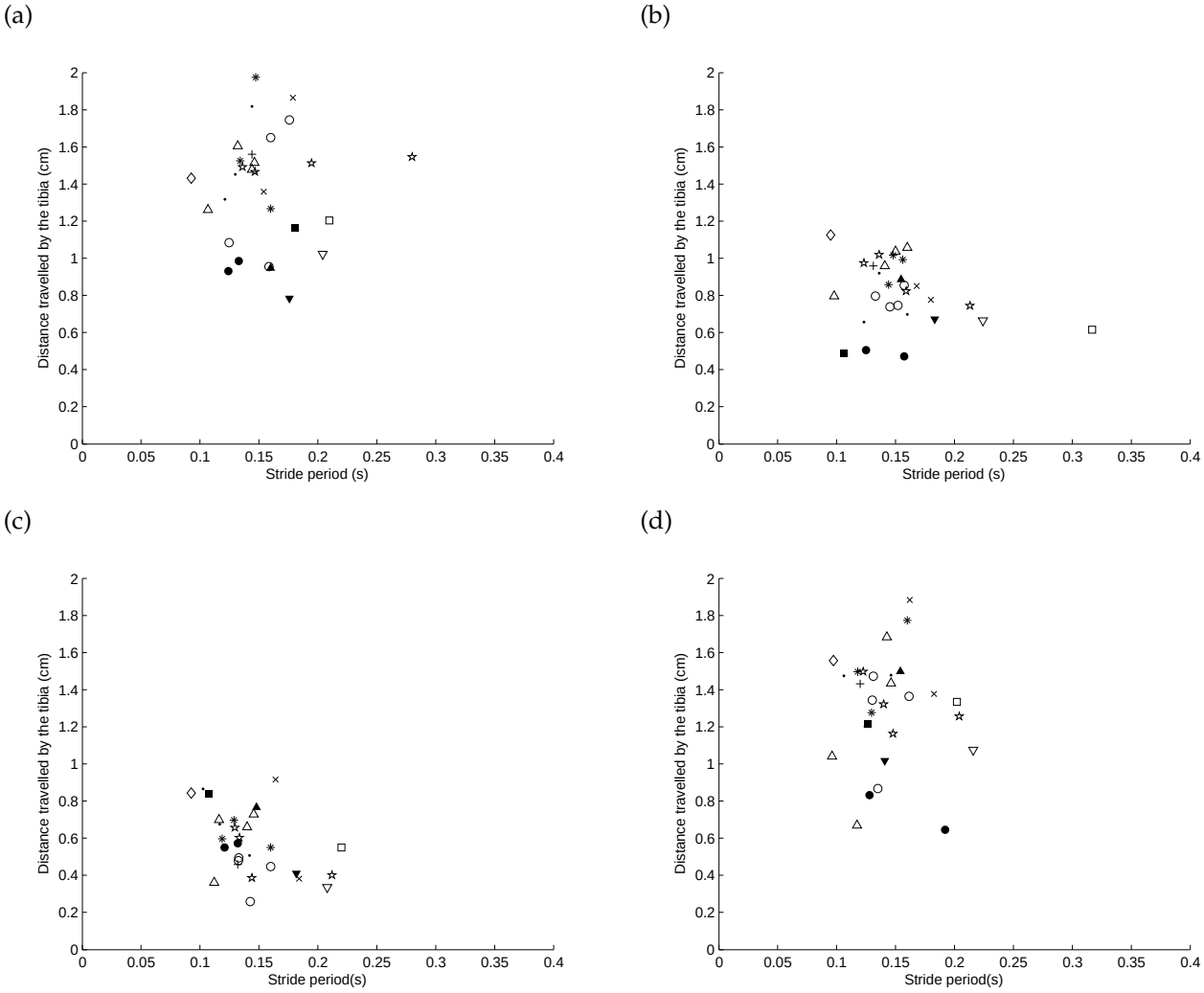

Figure 4.9: Average distance travelled by tibia during the swing phase as a function of stride period (s) for each leg of the spider *Dolomedes aquaticus*. (a) Leg 1, (b) leg 2, (c) leg 3 and (d) leg 4. The distance travelled by the tibia of leg 3 decreases significantly with increasing stride period. Note this differs from tibia excursion (cm) because as the leg was swinging the body is being pulled forward by other legs, so the average distance travelled consists of both tibia excursion and body shift (Jamon & Clarac, 1995). Different shapes represent different individuals.

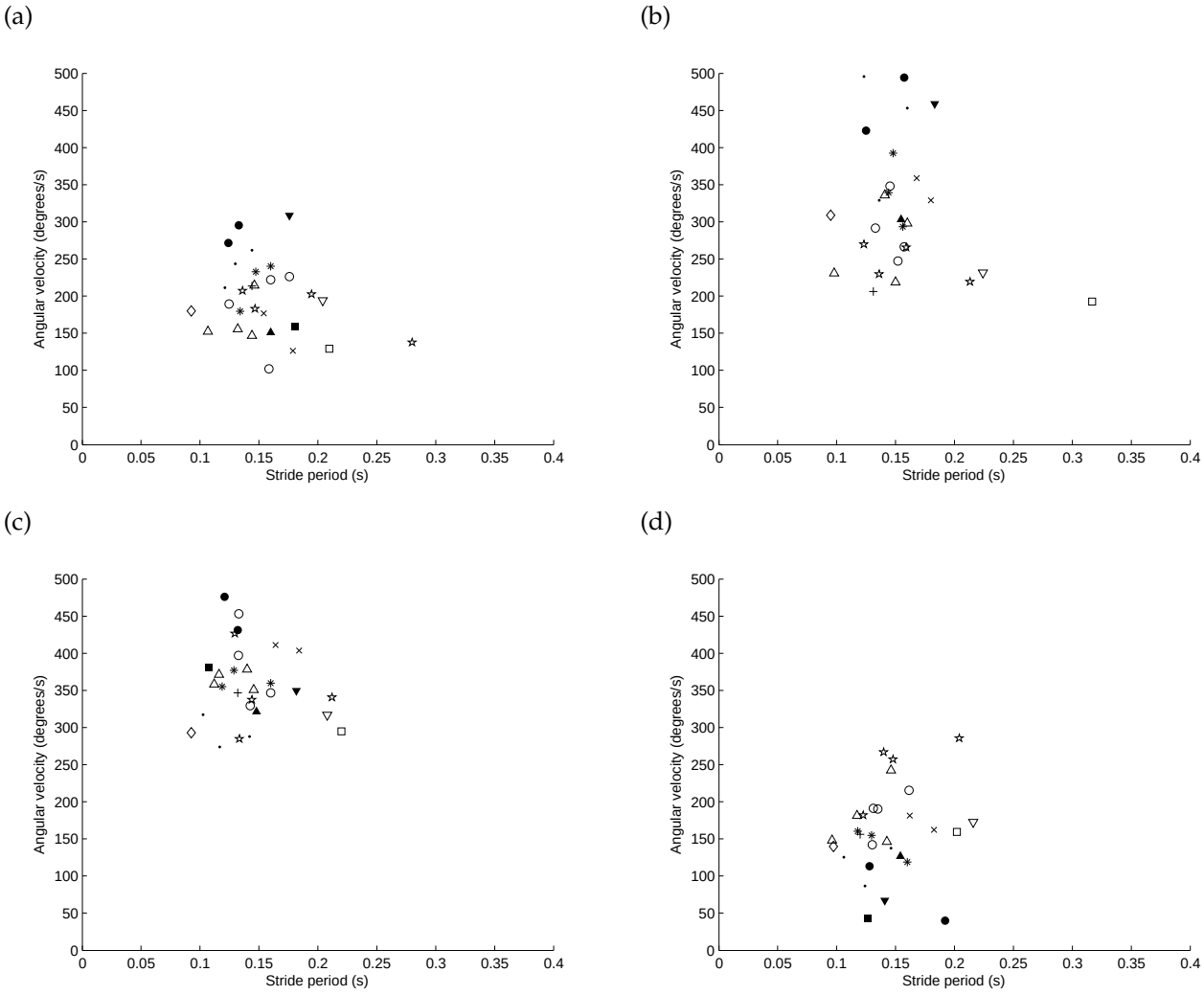

Figure 4.10: Average angular velocity of the leg during the swing phase as a function of stride period (s) for each leg of the spider *Dolomedes aquaticus*. (a) Leg 1, (b) leg 2, (c) leg 3 and (d) leg 4. There was no significant relationship between stride period and average angular velocity of the leg during the swing phase for any legs. Different shapes represent different individuals.

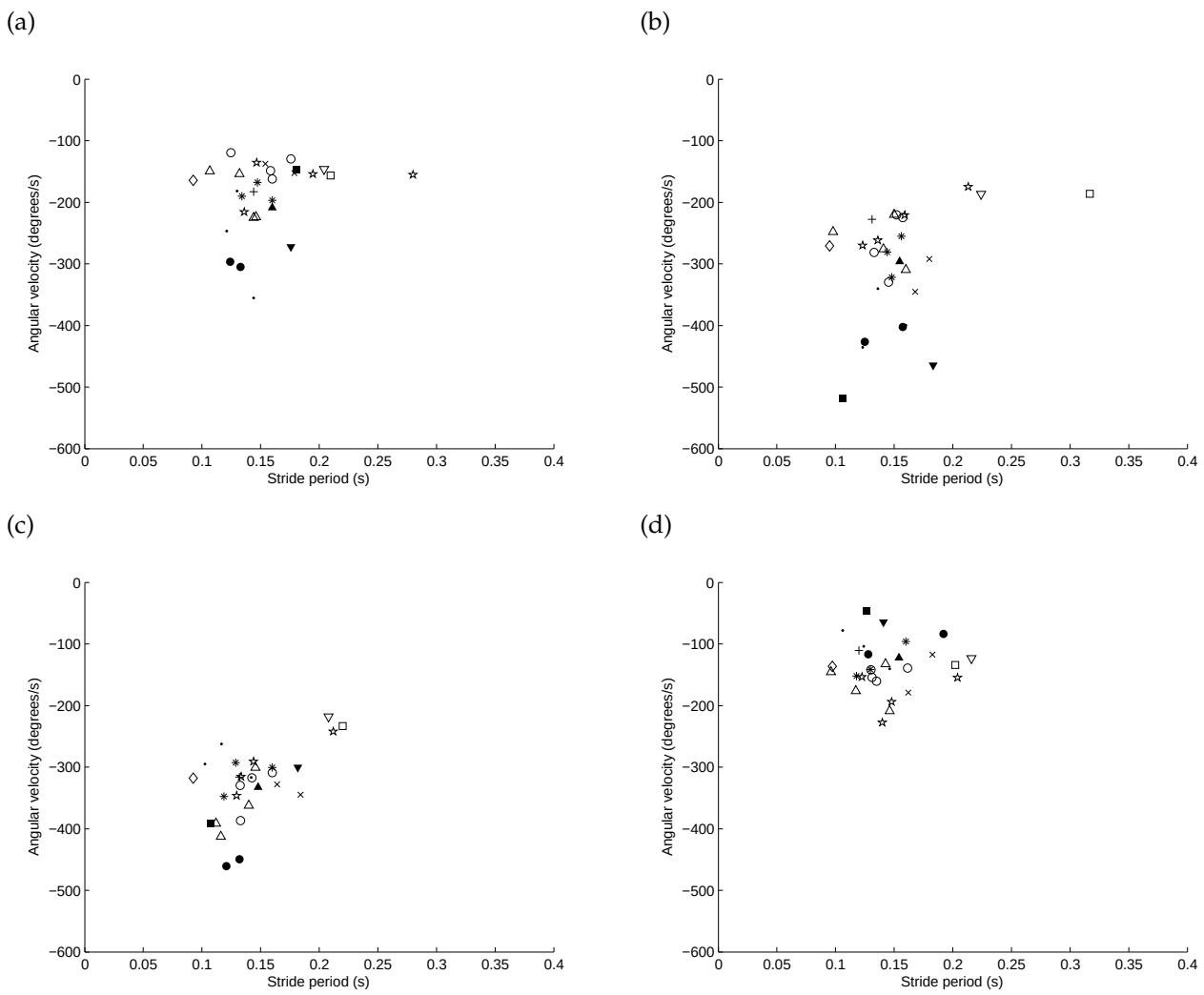

Figure 4.11: Average angular velocity of the leg during the stance phase as a function of stride period (s) for each leg of the spider *Dolomedes aquaticus*. (a) Leg 1, (b) leg 2, (c) leg 3 and (d) leg 4. Average angular velocity of the leg during the stance phase has a significant relationship with stride period in legs 2 and 3. The magnitude of the negative velocity is larger for shorter stride periods in these legs. Different shapes represent different individuals.

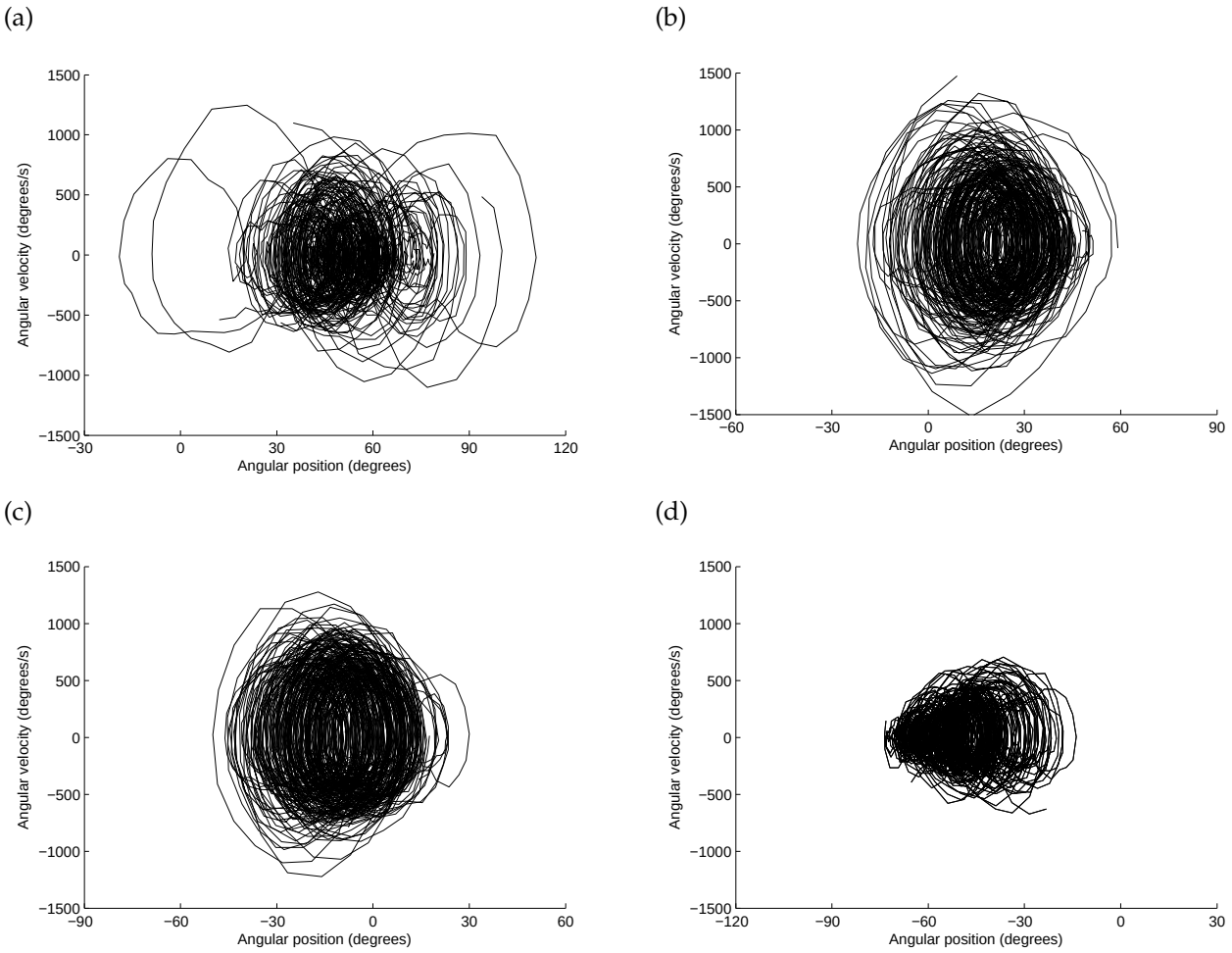

Figure 4.12: Movements of the legs of the spider *Dolomedes aquaticus* in their phase plane (a) leg 1, (b) leg 2, (c) leg 3 and (d) leg 4. Angular speeds plotted as a function of angular positions. Strides occurring during all sequences have been superimposed. Angular position is equal to zero when the leg is perpendicular to the body axis of symmetry, while the x-values differ in magnitude each graph has the same size scale (ticks are at 20^o intervals) and displays a range of 150^o.

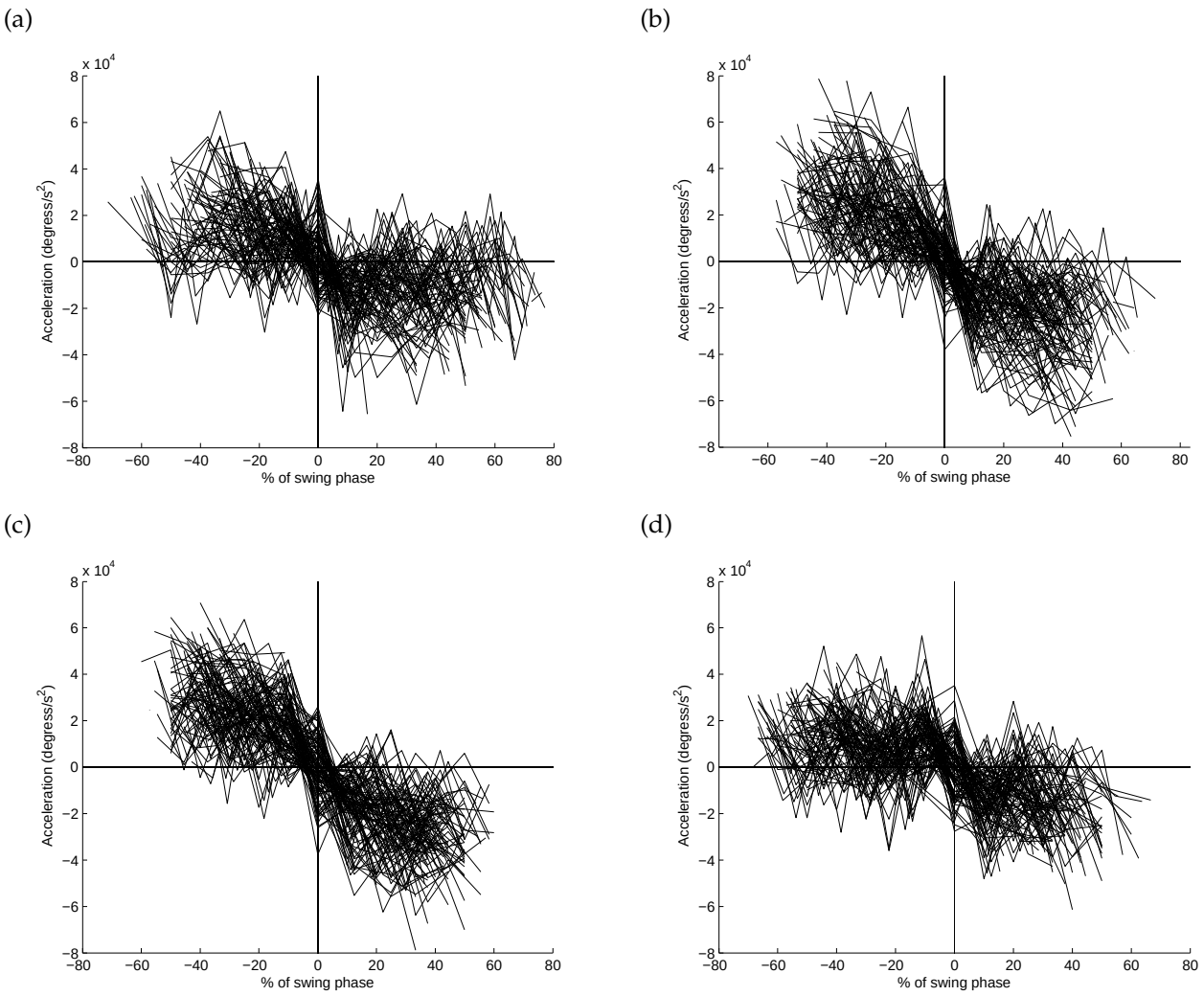

Figure 4.13: Variations in the acceleration amplitude during the swing phase of *Dolomedes aquaticus* locomotion. Patterns of acceleration are shown for left legs only but are representative of results obtained for right legs. (a) leg 1; (b) leg 2; (c) leg 3; (d) leg 4. Each trace represents the swing phase of a single stride, and the strides of all sequences are superimposed. Values on the x-axis represent percentage of the swing phase and zero has been set to the point corresponding to maximum velocity.

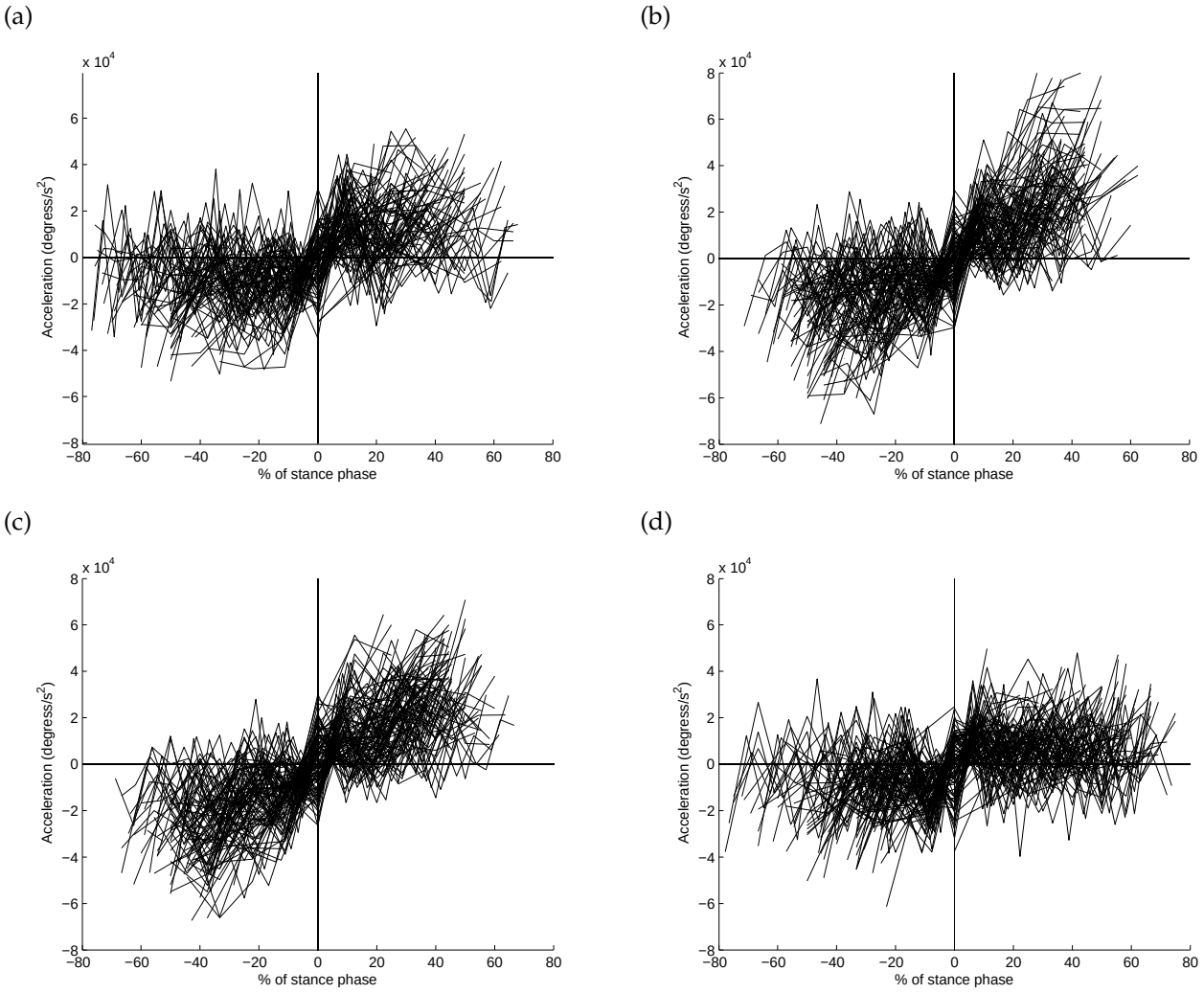

Figure 4.14: Variations in the acceleration amplitude during the stance phase of *Dolomedes aquaticus* locomotion. Patterns of acceleration are shown for left legs only but are representative of results obtained for right legs. (a) leg 1; (b) leg 2; (c) leg 3; (d) leg 4. Each trace represents the swing phase of a single stride, and the strides of all sequences are superimposed. Values on the x-axis represent percentage of the swing phase and zero has been set to the point corresponding to maximum velocity.

4.2.4 Phase relationships between legs

The phase lag distributions of contralateral legs all have a mean of approximately 0.5, the value expected from an alternating tetrapod gait (Fig. 4.15). This result is predicted by Hughes' (1952) rule for contralateral coupling during normal walking, which states that "each leg alternates with the contralateral limb of the same segment". Phase lags in leg pair 1 have a greater spread resulting in the distribution of phase lag L1:R1 being random ($p > 0.05$, Rayleigh test). Leg pairs all have mean phase lags close to 0.5, but appear to have stricter coupling towards the posterior end (mean angle ± circular S.D.: Leg pair 1 = 0.458 ± 0.006, Leg pair 2 = 0.498 ± 0.003, Leg pair 3 = 0.485 ± 0.002, Leg pair 4 = 0.510 ± 0.002; Fig. 4.15).

A similar trend is observed from anterior to posterior in adjacent ipsilateral legs (Fig. 4.16). Phase lag distributions of pairs containing leg 1 have a greater spread than those which do not contain leg 1 (mean angle ± circular S.D.: L1:L2 = 0.368 ± 0.004, R1:R2 = 0.377 ± 0.005, L2:L3 = 0.437 ± 0.002, R2:R3 = 0.461 ± 0.002, L3:L4 = 0.493 ± 0.002, R3:R4 = 0.512 ± 0.002; Fig. 4.16). It is clear that the mean phase value also increased from the anterior to the posterior pairs of adjacent ipsilateral legs. A possible mechanism for this pattern is provided by Hughes' (1952) rule for ipsilateral coupling during normal walking, which states that "no fore or middle leg is protracted until the leg behind has taken up its supporting position".

The remaining couplings for adjacent-but-one and adjacent-but-two ipsilateral legs have probably come about as a result of the above two rules. Again results can be split into groupings based on whether the pairing contains leg 1 or not (mean angle ± circular S.D.: L1:L3 = 0.823 ± 0.005, R1:R3 = 0.654 ± 0.005, L2:L4 = 0.936 ± 0.003, R2:R4 = 0.972 ± 0.003, L1:L4 = 0.207 ± 0.005, R1:R4 = 0.163 ± 0.005; Fig. 4.17). The distribution of R1:R3 is random ($p > 0.05$, Rayleigh test) and the remaining pairs containing either of the front legs have a more varied distribution than pairs which do not contain either of the front legs. Apart from the pairing of R1:R3 the remaining mean angles are all $\mu_\phi > 0.75$ or $\mu_\phi < 0.25$ indicating that these legs are moving in-phase.

The possibility that phase lag might change with speed was investigated by angular-linear regression. Representative plots are shown in Fig. 4.18 and Fig. 4.19 for ipsilateral phase lags as these are more likely to show a change in phase lag with speed. Plots for contralateral phase lags were similar to Fig. 4.18, with leg pairs 1 and 2 showing greater variation similar to Fig 4.18 (a & b) and leg pairs 3 and 4 more tightly clustered around 0.5 similar to Fig 4.18 (c-e). The phase lag between left legs 3 and 4 was correlated with both absolute and normalized speed (absolute speed $r^2 = 0.460$, $p<0.05$; normalized speed $r^2 = 0.494$,

p<0.05; Fig. 4.18 (e)). Likewise the phase lag between left legs 1 and 4 was correlated with both absolute and normalized speed (absolute speed r^2 = 0.488, p<0.05; normalized speed r^2 = 0.425, p<0.05; Fig. 4.19 (e)). The phase lag of right legs 1 and 2 was correlated with absolute speed but not normalized speed (absolute speed r^2 = 0.459, p<0.05; normalized speed R2 = 0.336, p=0.109; Fig. 4.19 (b)).

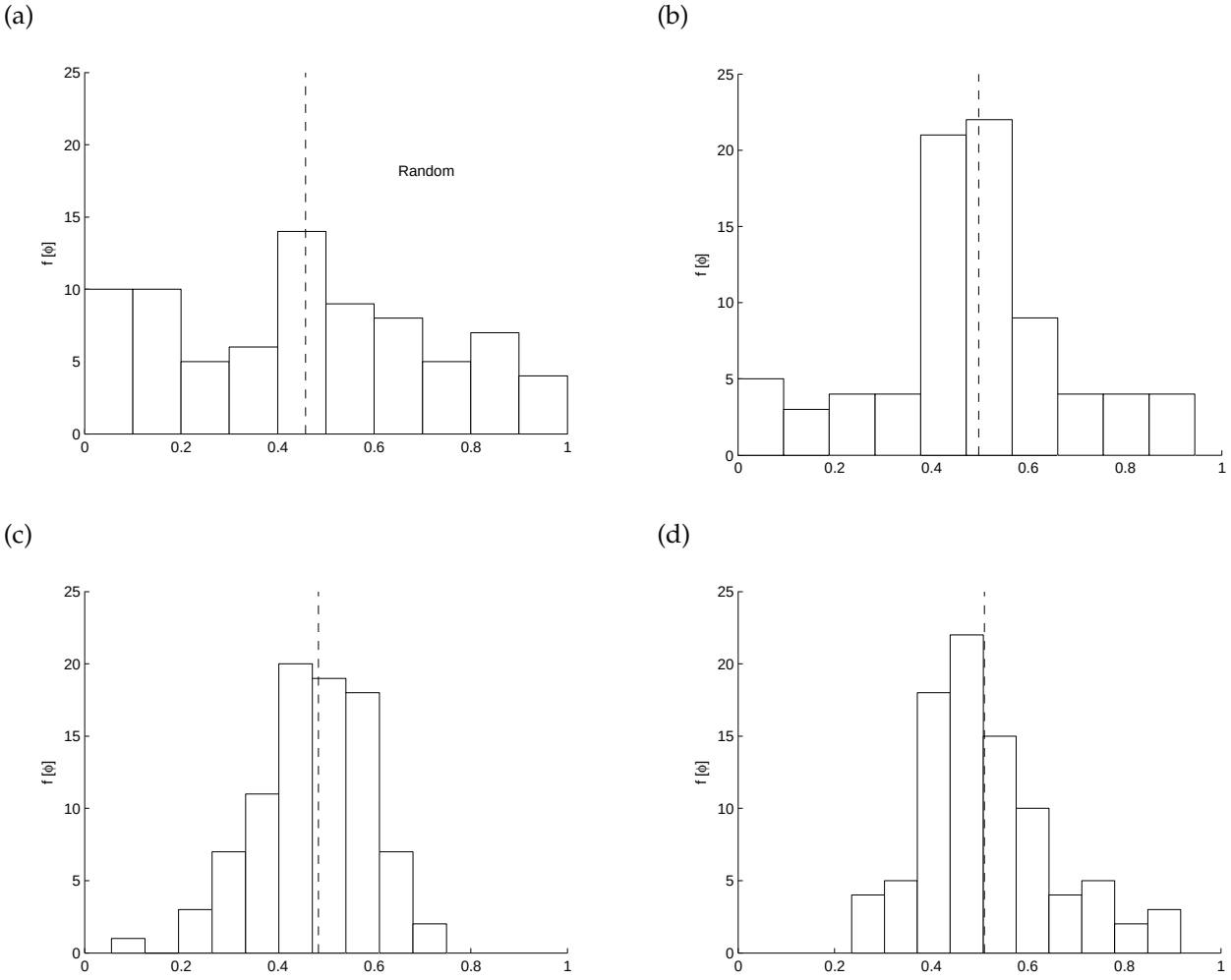

Figure 4.15: Phase-lag ϕ distributions for contralateral leg pairs in the spider *Dolomedes aquaticus*. (a) L1 and R1, (b) L2 and R2, (c) L3 and R3 and (d) L4 and R4. Phase lag values are between 0 and 1, and are described in more detail in the text. Dashed lines represent the circular mean. The phase lag distribution for L1 and R1 is random.

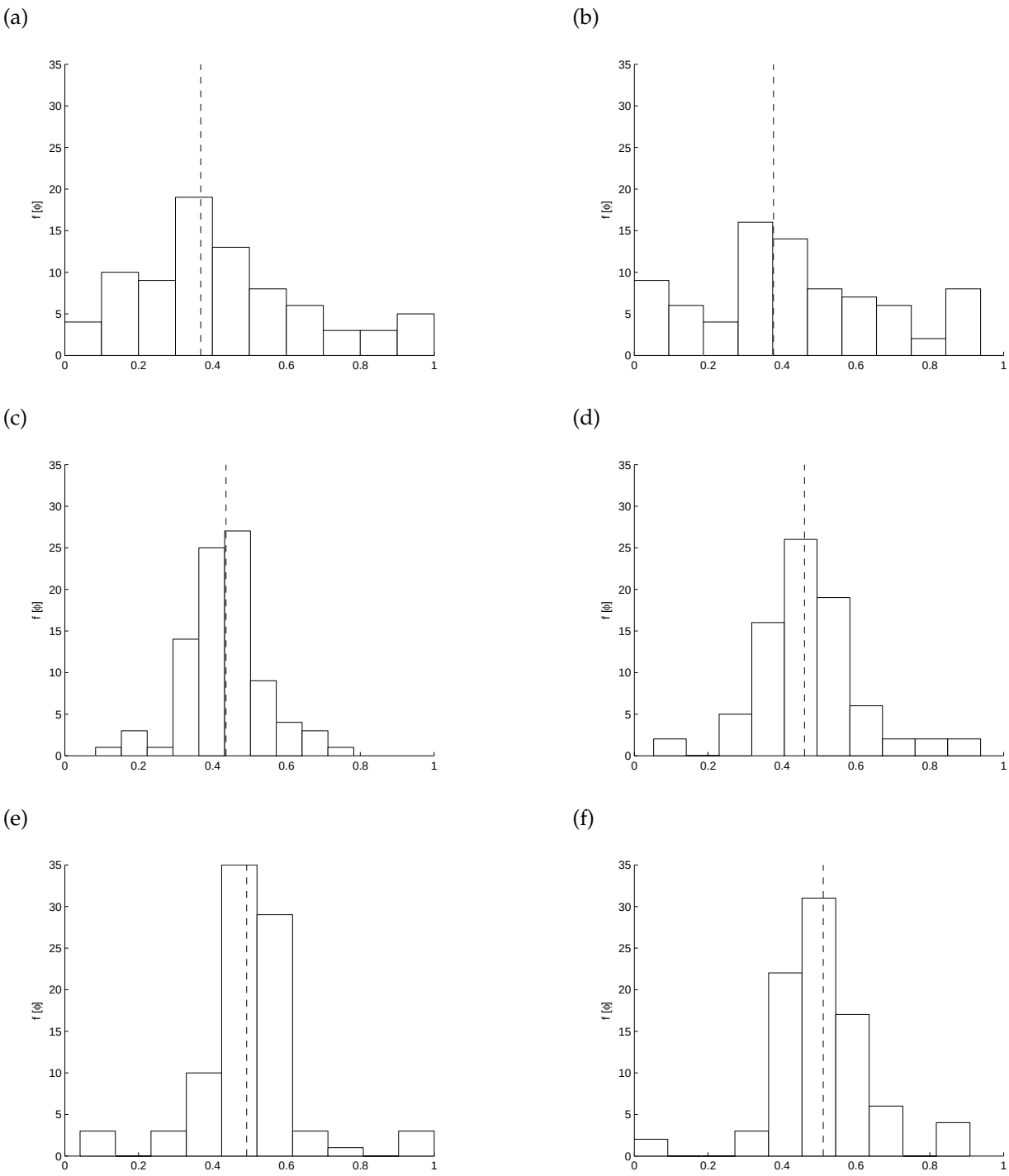

Figure 4.16: Phase-lag ϕ distributions for adjacent ipsilateral leg pairs in the spider *Dolomedes aquaticus*.(a) L1 and L2, (b) R1 and R2, (c) L2 and L3, (d) R2 and R3, (e) L3 and L4 and (f) R3 and R4. Phase lag values are between 0 and 1, and are described in more detail in the text. Dashed lines represent the circular mean.

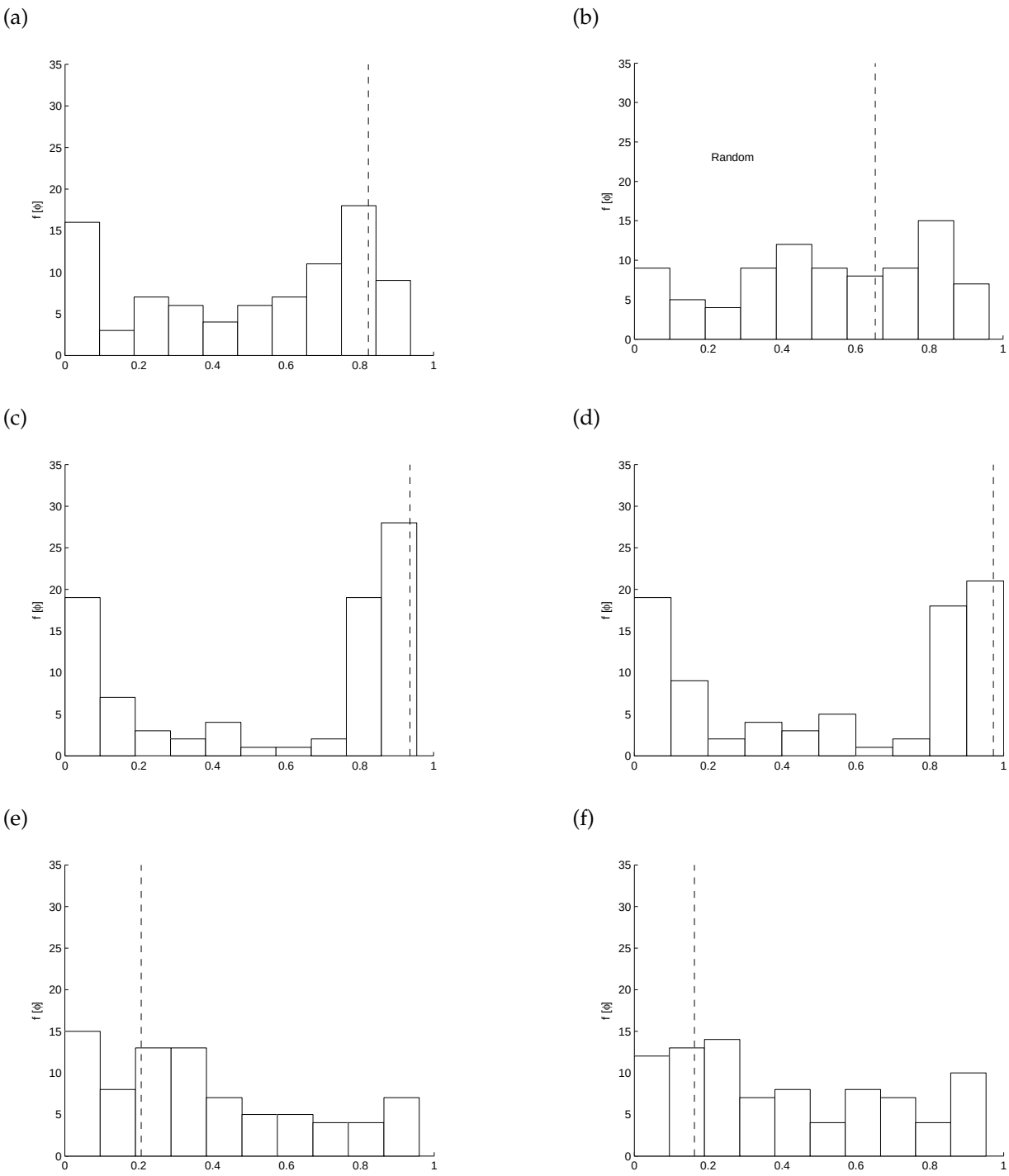

Figure 4.17: Phase-lag ϕ distributions for adjacent-but-one and adjacent-but-two ipsilateral leg pairs in the spider *Dolomedes aquaticus*. (a) L1 and L3, (b) R1 and R3, (c) L2 and L4, (d) R2 and R4, (e) L1 and L4 and (f) R1 and R4. Phase lag values are between 0 and 1, and are described in more detail in the text. Dashed lines represent the circular mean. The phase lag distribution for R1 and R3 is random.

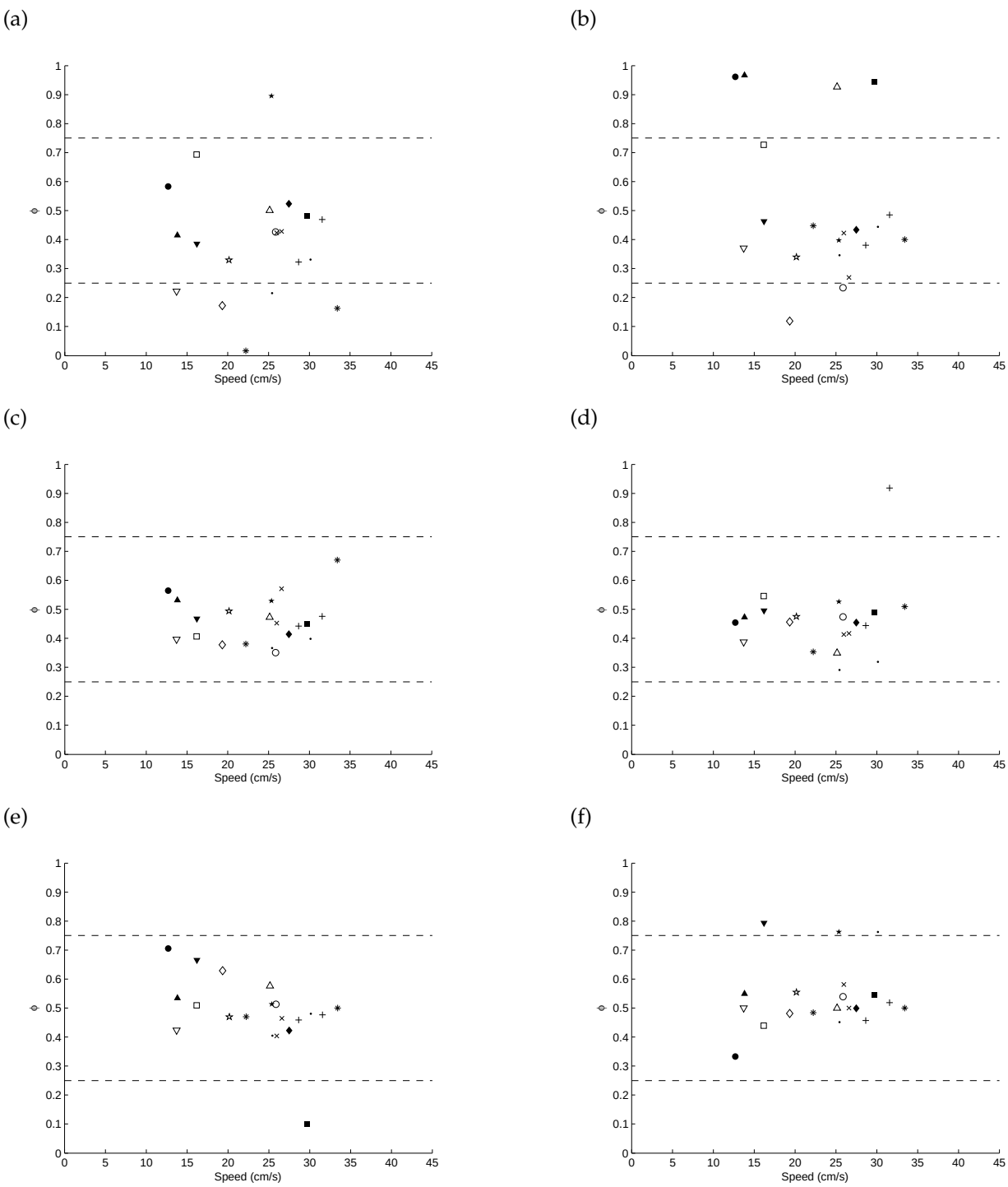

Figure 4.18: Phase-lag ϕ as a function of speed (cm s^{-1}) in adjacent ipsilateral leg pairs in the spider *Dolomedes aquaticus*. (a) L1 and L2, (b) R1 and R2, (c) L2 and L3, (d) R2 and R3, (e) L3 and L4 and (f) R3 and R4. Phase lag values are between 0 and 1, and are described in more detail in the text. Values between the dashed lines are out of phase, values outside are in-phase coupling of legs. Different shapes represent different individuals.

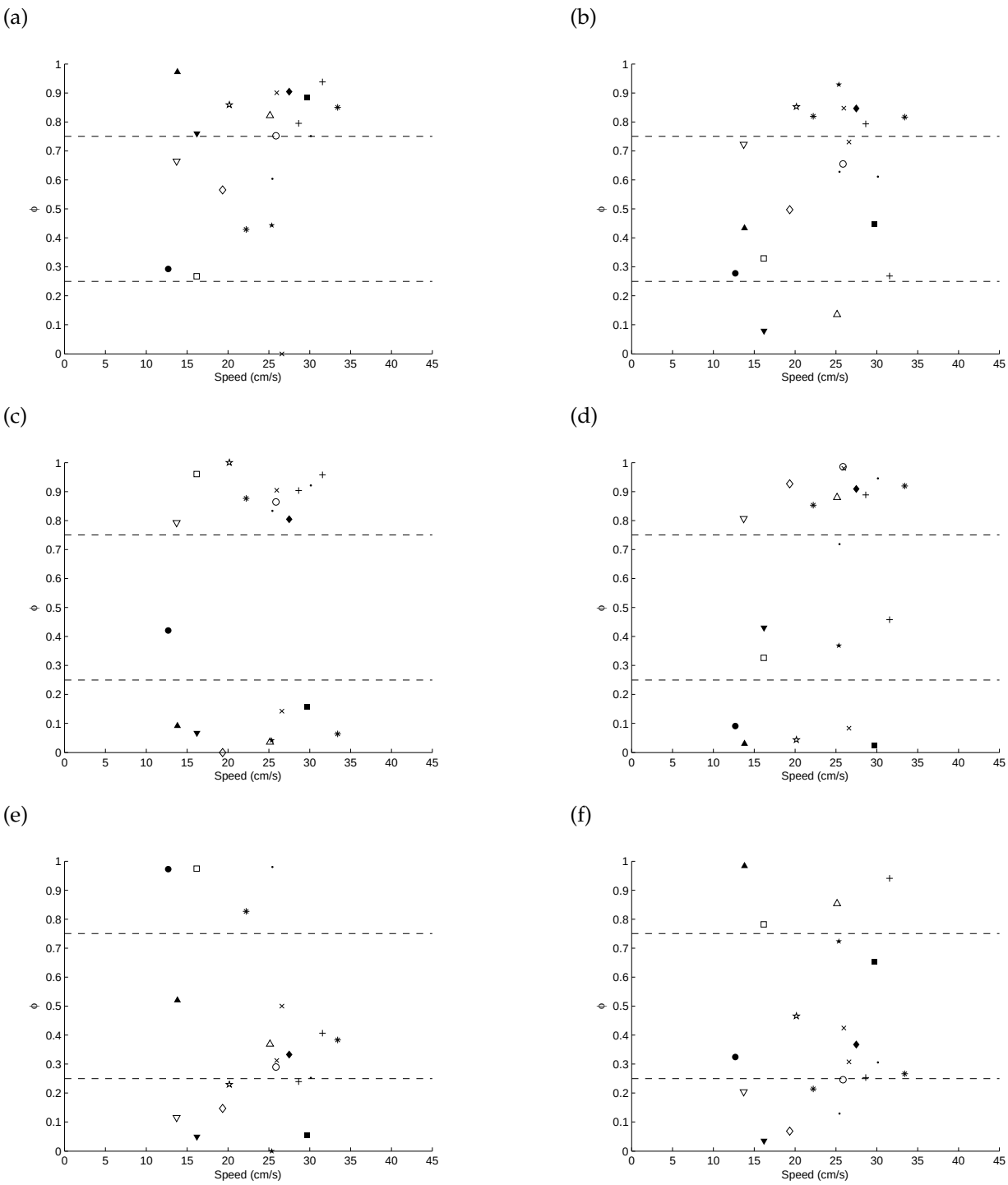

Figure 4.19: Phase-lag ϕ as a function of speed (cm s^{-1}) in adjacent-but-one and adjacent-but-two ipsilateral leg pairs in the spider *Dolomedes aquaticus*. (a) L1 and L3, (b) R1 and R3, (c) L2 and L4, (d) R2 and R4, (e) L1 and L4 and (f) R1 and R4. Phase lag values are between 0 and 1, and are described in more detail in the text. Values between the dashed lines are out of phase, values outside are in-phase coupling of legs. Different shapes represent different individuals.

4.2.5 Maximum and minimum joint angles

Leg 4

The most proximal joint is the body-coxa joint. This joint plays the largest role in overall positioning of the leg. In the fourth pair of legs, this angle had a range averaging 33^o during locomotion and values are always negative (where 0^o is perpendicular to the line of symmetry of the body axis); (Table 4.6). The range of angles covered by the body-coxa joint of leg pair 4 is smaller than the range of all other legs. The coxa-trochanter joint range is 30^o, which again is smaller than all other legs (Table 4.6). In this case the maximum value is just positive (where 0^o is no rotation about the joint axis, positive values indicate rotation in the forward direction of movement) but the majority of the range is negative. The remaining joints (patella-tibia, tibia-metatarsus and metatarsus-tarsus) again all have smaller ranges than other leg pairs but 0^o is about centre of the range of angles (Table 4.6). Not surprisingly the range of the metatarsus-tarsus joint is most variable, since errors in the position of this segment can only lead to small error in the overall position of the spider (Table 4.6).

Leg 3

The body-coxa joint of this leg has a larger range than in other legs (64^o, Table 4.6), which spans both positive and negative values but is mainly skewed towards negative. The remaining joints (coxa-trochanter, patella-tibia, tibia-metatarsus and metatarsus-tarsus) again all have larger ranges than leg pair 4 and are distributed with 0^o approximately middle of the range of angles (Table 4.6). Ranges of movement for coxa-trochanter, patella-tibia and tibia-metatarsus joints of this leg pair show less variation than other leg pairs, suggesting that movement of this leg is reasonably consistent between animals.

Leg 2

Similarly to leg pair 3 the body-coxa joint spans both positive and negative values but in this case is skewed towards positive and has a slightly reduced range of movement (59^o; Table 4.6). Likewise, the range of the coxa-trochanter joint was skewed towards positive values (min=-27^o, max=44^o; Table 4.6). The remaining joints (patella-tibia, tibia-metatarsus and metatarsus-tarsus) showed similar values to leg pair 3 (Table 4.6).

Leg 1

In leg pair 1, the body-coxa angle had an average range of 51^o during locomotion and values are always positive (Table 4.6). This range is less than leg pairs 2 and 3 but greater than leg pair 4 and shows the greatest variation between individuals, mainly due to variation in the minimum value with maximum values being consistent (max=61± 1^o; Table 4.6). The range of the coxa-trochanter joint was skewed towards positive values in a similar trend to leg pair 2 (min=-21^o, max=48^o; Table 4.6). The ranges for all joints except the metatarsus-tarsus joint were more variable than other legs.

Table 4.6: Angular movement of the joints (°) of *Dolomedes aquaticus* during locomotion.

Joint	Leg 1	Leg 2	Leg 3	Leg 4
Body-Co				
Max	61± 1	54 ± 4	11 ± 8	-21 ± 10
Min	10 ± 13	-4 ± 10	-53 ± 8	-54 ± 1
Range	51 ± 13	59 ± 10	64 ± 12	33 ± 10
Co-Tr				
Max	48 ± 5	44 ± 7	22 ± 1	2 ± 14
Min	-21 ± 16	-27 ± 11	-21 ± 2	-28 ± 0
Range	69 ± 17	71 ± 13	43 ± 2	-28 ± 0
Pa-Ti				
Max	22 ± 15	26 ± 9	17 ± 4	7 ± 3
Min	-37 ± 4	-27 ± 9	-16 ± 2	-9 ± 1
Range	59 ± 15	53 ± 10	33 ± 4	15 ± 3
Ti-Me				
Max	6 ± 1	6 ± 1	6 ± 1	3 ± 1
Min	-6 ± 1	-7 ± 1	-6 ± 1	-4 ± 0
Range	13 ± 2	13 ± 1	12 ± 1	7 ± 1
Me-Ta				
Max	29 ± 10	35 ± 20	38 ± 13	28 ± 12
Min	-38 ± 16	-40 ± 15	-40 ± 11	-33 ± 15
Range	67 ± 20	75 ± 24	78 ± 20	61 ± 21
Values are means ± S.D (N=15).				

Chapter 5

Discussion

The aim of my study was twofold: to develop a markerless technique for tracking spider locomotion and to analyse the kinematics of spider locomotion. The basic elements of the tracking approach consist of an articulated body model, extracted features from video sequences and various constraints which are used to solve a CRF. To my knowledge, this the first time a markerless technique has been applied to the investigation of arthropod kinematics. I first review the tracking algorithm, followed by kinematics relating to the organisation of the stride in general, and then discuss inter-leg coordination. By comparing these results to data previously obtained for spiders, other arthropods and vertebrates, it is possible to gain insight into general principles underlying legged locomotion.

5.1 Markerless tracking algorithm

The efficiency of motion capture algorithms is generally evaluated on three criteria: the cost and ease of experimental setup, the manual user intervention required and lastly the accuracy of tracking results (Zakotnik & Dürr, 2005). The presented algorithm requires little in terms of equipment, with the key requirements being some sort of behavioural arena which can be filmed from above using a digital video camera. The resulting video sequence is analysed in MATLAB using a constrained kinematic model. The model in this case was rather basic, consisting of a stick spider based on experimentally determined joint lengths and constrained by experimentally determined joint limits (Reussenzehn, 2008). Knowledge of joint limits is not a prerequisite; it does however help constrain the state space. Currently the algorithm requires that the user initializes the size and position of the spider for a given sequence and specify some parameters relating to the CRF. This is done with relative ease through a graphical user interface and is preferable to stan-

dard marker based techniques which may fail in a given frame due to marker occlusion or marker-like reflections etc and require manual correction and re-analysis of subsequent frames. It is somewhat difficult to assess the accuracy of the algorithm without ground truth data; this is attempted through both qualitative and quantitative techniques. Visual inspection video sequences overlaid with the spider model verify that the algorithm performs reasonably well at finding the pose of the subject. For global position, results were highly repeatable with x-y coordinates differing by less than 1mm in each dimension when data was compared running the sequence of frames in forward then reverse order. Individual joint angles appeared less accurate than total leg angle (Table 4.2). Root mean squared differences between forward and reverse tracking for total leg angle average 4.26^o across the four legs.

5.1.1 Running time

Extracting the subject from the image sequence and estimating its pose is computationally expensive. Graph cuts provide an efficient framework for segmentation and pose estimation once a rough estimate of the pose has been obtained. That being said the present implementation is far from being real time or even fast tracking. Running the program on my dual core 2.11 GHz AMD Athlon™ 64 X2 4000+ with 3 GB ram, we would get running times were ~1-3 minutes per frame, resulting in a typical sequence taking ~ 4 hours to run. Fortunately after initialization had been completed for each of the sequences, the batch processing option meant the computer could just tick away in the background for the next few days.

5.1.2 Shortcomings of the algorithm

Apart from being time consuming, the algorithm suffers several other shortcomings I will briefly discuss. This will be followed by a section which suggests techniques to diminish these issues and generally improve the tracking algorithm.

The log likelihood term based on pixel intensity sometimes resulted in false labelling when the subject ran close to the edges of the arena due to reflections in the glass. This did little to affect pose estimation as the sequence was cropped reasonably tightly to contain only the behavioural arena, causing tracking to terminate when limbs were against the glass sides.

The algorithm involves minimizing an energy term which combines both image segmen-

tation and pose estimation which proved problematic for some poses. Occasionally when legs passed close to each other one leg would get stuck tracking the other leg's trajectory and this would not rectify itself until the two legs crossed paths again. This could generally be avoided by re-analysing the sequence with different input parameters or altering the angle multiplier so that angle changes started at values which were either greater or smaller than 5.

As mentioned previously, individual joints appear somewhat less accurate than the total angle of the leg, suggesting that the optimization framework is causing one angle to increase/decrease and a joint further down the limb to do the opposite. I tried to avoid this by having angular rotations occur from segments closest to the body outwards, but because the angles and corresponding energy term are recalculated several times per frame this was not as successful as anticipated.

Because we are examining 2D data on a process occurring in 3D there are some intrinsic problems. During initialization of the pose, the entirety of all legs of the spider could not necessarily be seen due to loss of depth information. A balance had to be struck between having some of the stick model legs too long and/or short for the limbs in the sequence. Also, since the spider was projected into the 2D image plane, at times joint angles appeared like they could only be obtained by exceeding known joint limits in the X-Y plane. It is more likely however that the joint was rotating about another axis.

The running program is implemented in MATLAB, with a couple of key functions implemented using Jensen's (2008) mex files to stop processing from being prohibitively slow. Another issue with the use of MATLAB is the extensive use of memory. Originally the number of rows and columns in each frame had to be reduced to ¼ of the original image to prevent MATLAB running out of memory. After videos were cropped to only contain the region of interest, frames only needed reducing to ½ their original size. This slows down tracking, since most operations occur on a pixel basis, but increasing resolution does improve accuracy so ideally the original resolution of the video should be used.

5.1.3 Potential improvements to the algorithm

Running time:

As mentioned above implementing more key functions or the entire code in C++ would vastly improve the performance of code. Alternatively, several modifications could be made to the MATLAB code. Currently calculations such as the distance map and labelling are done for the entire frame. A more efficient approach would be to locate the spider and

only perform these calculations on a cut of the frame, which would reduce the number of pixels to approximately ¼ of the current amount. As long as the change between successive frames is small, energy minimization can be calculated dynamically, rather than statically, using graph cuts. The computation of each graph cut was a fraction of a second. This may not seem much, but is rather slow when you consider that for each frame this is recalculated a number of times for different estimates of the pose parameters. This can be made significantly faster by using the dynamic algorithm proposed by (Kohli, 2007). This algorithm re-uses the solution of the previous graph cut in order to solve for a new instance of the problem, which made computation in the order 15-20 times faster (Kohli, 2007).

Accuracy:

Raw data was smoothed using a 4th order, zero-lag Butterworth filter which is widely used in the field of biomechanics to remove the high frequency components which are assumed to be noise. This may also remove high frequency components originating from the movement, which can be an issue, particularly when filming occurs at lower frame rates. Future implementations will have this replaced by smoothing with constrained splines. This technique constructs a spline through data points, while allowing for small deviations to minimize higher order derivatives and has been shown to outperform other smoothing methods (Walker, 1998).

As seen in Fig. 3.5 (b) and Fig. 3.6 (a) the colour distributions were rather undiscriminating with subject distribution overlapping somewhat with the background distribution. The present implementation achieved better results using solely background distribution held against its own mean than two separate distributions for subject and background. A more accurate representation of pixel distributions would be to represent the colour distribution of each pixel position in the video as a Gaussian Mixture Model (Kohli, 2007).

Knowledge about the mechanical properties of spider limbs and the physics involved in locomotion helps constrain the state space required for movement. The more we know about the spiders' mechanical design, the easier the task of tracking becomes. The current tracking algorithm only makes use of the very basic assumption of constant velocity to predict the pose of the spider in the next frame. If we had a correct model of the spider our predictions would be improved, which in turn makes the statistical modelling easier. Research is presently being conducted in our lab relating joint angles to applied torque, investigating the use of hemolymph to hydraulically extend the legs and creating simulated passive dynamic walkers.

Table 4.2 illustrated the difference between running the algorithm in the forward direction compared to the reverse direction. Differences between successive runs will occur even when the algorithm is run in the same direction because all of the joint angles are updated randomly a number of times and the configuration is chosen based on the minimization of energy, rather than spanning the entire state space. If improvements are made to the speed of the algorithm, it becomes feasible to run each sequence a number of times and then calculate pose based on the distribution of results rather than a single run. Similarly, repeated analysis could be done on each frame and a disambiguation method could be used to select one of the poses as the correct solution. Such a technique has been implemented for marker-based motion capture which uses stochastic optimization, rather than relying solely on segmentation, to determine the position of markers (Zakotnik & Dürr, 2005). The disambiguation method described in this research is based on the Viterbi method for Markov chains and works by processing the entire sequence, then selecting the trajectory which is globally smoothest for all joint angles and frames (Zakotnik & Dürr, 2005).

Shape model:

Presently the shape model used is highly simplified and only contains information about the lengths of segments based on measurements obtained from a single spider. It is possible however that leg and/or segment length does not scale isometrically with size, so certain segments and/or legs may be proportionately large or smaller in different sized spiders.

We have obtained a micro CT scan of this species of spider, which could be used a more accurate exemplar. Previous work suggests that sophisticated shape priors are overkill, since simple shape cues and edge information embedded in the image provide accurate results (Kohli, 2007). It would be interesting however to compare results and would produce more realistic looking sequences if motion capture results and the shape model are applied to the animation of spider locomotion.

Extending to 3D:

With monocular techniques, many possible poses can explain the same spider shape observed in the image. Multiple views can be used to reduce the ambiguity in pose. To maintain the simplicity of a single camera setup, the view from the top and side can be simultaneously recorded by arranging a mirror set at 45^o from the animal plane. Using the

POSECUT approach multiple views can be easily incorporated into a single optimization framework (Bray et al., 2006). Specifically the optimization problem becomes:

$$E(x) = \arg\min_{\theta} \left(\min_{x} \sum_{views} \left(\sum_{i} \left(\phi_i \left(x_i, \mathbf{y} \right) + \psi_i \left(x_i | \theta \right) \right) + \sum_{i,j} \left(\left(\phi_{i,j} \left(x_i, x_j, \mathbf{y} \right) + \psi_{i,j} \left(x_i, x_j \right) \right) \right) \right) \right) \tag{5.1}$$

5.2 Kinematics of spider locomotion

There were several consistent changes to kinematic parameters relating to changes in the size of the spider and relating to the speed the spider was travelling.

5.2.1 Kinematic variables and size

It is not surprising to expect animals of different sizes to achieve different maximum speeds during locomotion. In this section we compare how our data matches with the theoretical expectations of how maximum speeds scale with mass. The four competing theories predicting how speed should scale with body mass were mentioned in the introduction. Hill (1950) supports the geometric similarity hypothesis with observations from a narrow size range and concludes that maximum running speed is independent of mass, $V_a \propto M^0$. The dynamic similarity hypothesis predicts a scaling relationship of $V_a \propto M^{0.17}$, which has been supported based on observations on 106 species of mammals (Garland, 1983). The predicted relationship is $V_a \propto M^{0.25}$ for elastic and $V_a \propto M^{0.40}$ for static stress similarity (McMahon, 1975). Our data comparing mass to maximum absolute speed resulted in an exponent of 0.243 (confidence interval of the slope: -0.174, 0.659), which was non-significant (Fig. 4.1 (a); Table 4.3). While our data was closest to the predictions of elastic similarity we cannot eliminate any of the other hypotheses due to the error in fitting, this is also reinforced by comparisons to other results in the literature in Table 4.4.

These hypotheses also make predictions about other kinematic parameters. Stride frequency is predicted as proportional to $M^{-0.33}$, $M^{-0.13}$ and M^0 for the geometric, elastic and static stress models (McMahon, 1975). Again our data was non-significant with a scaling exponent of -0.143 ± 0.470 (Fig. 4.2 (a); Table 4.3). Stride length was the only variable to have a significant scaling relationship with mass. Maximum stride length was found to be proportional to $M^{0.409}$ (Fig. 4.2 (c); Table 4.3), where we would expect va-

lues of $M^{0.33}$,$M^{0.38}$ and $M^{0.40}$ in the geometric, elastic and static stress models (McMahon, 1975). The dynamic similarity hypothesis predicts that stride period $\propto$ shoulder height$^{0.5}$ (Alexander & Jayes, 1983), assuming shoulder height $\propto$ mass$^{1/3}$ we can extrapolate to get stride frequency $\propto M^{-0.17}$ and stride length $\propto M^{0.34}$.

While our data is in closest agreement with the predictions of elastic similarity it is unreasonable to draw any conclusions since the majority of these results were non-significant. A potential confounding factor in the research was that analysis of locomotion occurred across a broad range of speeds. In order to elucidate whether any relationships do indeed exist between these variables and mass, trials should be selected where the spider is running at near maximal speed. As mentioned multiple times in the literature these models are useful in comparing the movements of animals of different sizes, in reality however no animal is precisely the scale of another.

Plotting the maximal speed observed in *D. aquaticus* along with species spanning the range terrestrial locomotors shows confirms that these spiders do appear to agree with the general scaling relationship in animals (Fig. 4.4). While this data is skewed towards vertebrates, in particular mammals, the speed of these spiders does fit with expected results, particularly when looking at animals less than 1 kg in mass. Another obvious trend in the graph is that very large animals do not run as fast as intermediate sized animals (Fig. 4.4).

A similar trend is seen when *D. aquaticus* is compared to 38 other species of spider (Fig. 4.3). In this case the data is skewed towards smaller species of spider but the trend that largest spiders do not run as fast as intermediate sized spiders is still apparent. Research on locomotion of fishing spiders, *D. triton*, found that small spiders could achieve rowing velocities as high as large spiders during locomotion on the water surface despite a 600-fold difference in mass (Suter, 2000). In this case relationships were best predicted by the geometric similarity hypothesis, with $V_a \propto M^{0.02}$ and $V_n \propto M^{-0.31}$. Observations show relative velocities of small spiderlings can be attributed to high stride frequency ($F_S \propto M^{-0.43}$) and high angular velocity of propulsive legs ($\omega \propto M^{0.02}$) (Suter, 2000). It is hypothesized that relative velocity may be more 'ecologically relevant' than absolute velocity, if this is true the surprising locomotory performance would aid spiderlings by making them more successful in evading predators than their larger parents (Suter, 2000).

5.2.2 Kinematic variables and speed

As noted above, being able to move quickly is advantageous when it comes to escaping predators. As *D. aquaticus* does not construct a web or tunnel, agile locomotion is also of particular importance in hunting prey. *D. aquaticus* sense their prey both on water and

land by detecting vibrations using the two front pairs of legs (Forster & Forster, 1999). They then chase down their prey with rapid burst of speed. We examine observations on which kinematic parameters can be attributed with increasing speed in *D. aquaticus*.

Speed can be calculated as stride length multiplied by stride frequency; thus speed may be increased by increasing either stride frequency and/or stride length. Depending on the gait being used the relative importance of the two trends differs (Biewener, 2003). The observation that stride length has a greater correlation with absolute speed than normalized speed (Fig. 4.6 (c & d); Table 4.5), along with the fact that stride length was the only relationship to have a significant trend with mass (Table 4.3) suggests that larger animals are able to attain greater speeds by having long limbs move at lower frequencies. Conversely, stride frequency had a greater correlation with normalized speed than absolute speed (Fig. 4.6 (a & b); Table 4.5), suggesting that smaller animals have shorter limbs that move at higher frequencies. In terms of the relative importance of the two parameters, it appears that stride frequency is the more important factor, with the slope of the trend greater for both absolute and normalized speeds (Table 4.5).

In analyses of quadrupedal mammals, there is typically a distinct change in the slope of speed as a function of stride length and/or stride frequency associated with transitions between gaits (Biewener, 2003). Birds, humans and non-mammalian quadrupeds (i.e. lizards etc) show consistent slopes across the range of speeds with speed increasing by both stride length and frequency increasing (Biewener, 2003). The few invertebrate species studied (crabs and cockroaches) appear to increase speed by increases to both stride frequency and length at lower speeds, but in order to attain highest speeds rely mainly on increases in stride length in a similar manner to quadrupedal mammals (Biewener, 2003). In *D. aquaticus,* however, stride frequency and length vary linearly and continuously with speed (Fig. 4.6 (a-d), Table 4.5). This result matches better with the trend shown for lizards than other arthropods. That is, as these animals approach their fastest speeds increases in speed are more dependent on stride frequency, as illustrated by the slope of the lines (Biewener, 2003). Some alternative explanations for the trend are: because our data is a bit sparse at faster running speeds, we are simply failing to see the levelling off of stride frequency that is exhibited by other arthropods, or our data consists solely of one gait and does not contain a gait transition. Spiders are indeed capable of exhibiting multiple gaits. During locomotion on the water *D. triton* exhibit two different gaits. At speeds up to 0.2 m s^{-1}, the spiders use a "rowing" gait with oar-like movements of the 2nd and 3rd legs propelling the spiders forward while the front and back legs are held stationary relative to the body (Suter, 1999). At faster speeds up to 0.7 m s^{-1}, the spiders use a "galloping" gait where only the 4th legs remain motionless and the remaining pairs of legs move nearly simultaneously resulting in a series of leaps (Suter, 1999).

Another indicator of gait transitions is the trend between duty factor and speed. In general, duty factors were greater than 0.5, indicating that legs spend more than half of the stride cycle in contact with the ground (Fig. 4.6 (e & f)). The duty factor did not vary with speed (Table 4.5). The period of a stride consists of one protraction phase and one retraction phase. As stride cycle period decreases, the stride frequency, or walking speed, increases. Therefore, it follows that in order to decrease the stride cycle period, either one or both of the phase durations must be shortened. Analysis revealed stride frequency was the best predictor of protraction and retraction and that both phases did indeed decrease with similar slopes of -0.013 and -0.010 respectively (Fig. 4.7 (e & f); Table 4.5). This is also reinforced by the unchanging duty factor. Similar results were observed in the vagrant wolf spider, *Trochosa ruricola*, where both protraction and retraction decrease with increasing stride frequency (Ward & Humphreys, 1981). This relationship is contrary to the relationship frequently observed in insects, where only retraction decreases with stride frequency and protraction remains constant (reviewed in Wilson, 1966). Examination of two other species of spider, *D. triton* (semi-aquatic) and *Lycosa rabida* (terrestrial), found that retraction changes more rapidly than protraction during increases in frequency for terrestrial locomotion (Shultz, 1987). Interestingly, this relationship is reversed for all legs of *D. triton* during locomotion on the water surface but only leg 3 in *L. rabida* (Shultz, 1987).

5.3 Spider leg movements

In this present study, we performed detailed analysis of locomotory behaviour in freely moving spiders without the imposition of having to attach physical or painted on markers for each joint. A previous study, in which walking legs were autotomized, revealed that spiders are capable of adaptive changes and can replace the role of each other during locomotion (Wilson, 1967). Despite this plasticity, the biomechanics of joints are important and our results suggest that each leg plays a distinct role in locomotion. Analysis of the leg trajectories through phase diagrams (Fig. 4.12) show that each leg exhibits a distinctive pattern. Legs 1 and 2 show mainly positive angular position values, suggesting these legs are used to pull the body forward. Conversely, legs 3 and 4 show mainly negative values so are likely used to push the body. Comparisons between the amplitude of angular velocity of each leg show that legs 2 and 3 undergo much larger positive and negative velocities throughout the cycle. This supports the hypothesis that it is predominantly legs 2 and 3 that are generating propulsive thrust, through pulling and pushing respectively, throughout the locomotory cycle.

The conclusions drawn above are supported by additional experimental results defining leg movement. Analysis of legs during the swing phase (Fig. 4.8) found that legs 2 and 3 undergo larger excursions than legs 1 and 4. Additionally, excursion during the swing phase shows a positive relationship with stride duration in legs 3 and 4, suggesting that in order to increase speed these legs decrease the size of excursion and instead increase frequency. The average distance travelled by the tibia during the swing phase show somewhat opposite results between legs. The tibia of legs 1 and 4 on average travels a greater distance than legs 2 and 3 (Fig. 4.9). In this case the measurement also includes thrust from other legs because as the leg of interest is swinging the body is being pulled forward by other legs. This result is likely due to the positioning of the neutral orientation of legs 1 and 4 being in front and behind the body respectively, whereas legs 2 and 3 are closer to perpendicular to the body.

Reinforcing the results of the phase diagrams, legs 2 and 3 produced velocities of greater magnitude than legs 1 and 4 in both the swing and stance phases (Fig. 4.10 & 4.11). For each leg there was no difference in these magnitudes relative to stride period in the swing phase. However, in the stance phase legs 2 and 3 had negative velocities which were larger in magnitude for shorter stride periods (Fig. 4.11). This suggests that legs 2 and 3 may be decelerating more rapidly than legs 1 and 4, which is confirmed by comparison of variations in acceleration patterns between legs during the swing and stance phases (Fig. 4.13 & Fig. 4.14). We plotted acceleration/deceleration as a percentage of a given phase, with zero on the x-axis equal to the maximum velocity. These plots show that acceleration in both phases is highly variable with the x-scale needing to be 160 to fit all trials rather than the 100 expected from a percentage. This is likely a consequence of the relative durations of acceleration and deceleration differing between trials of different speed and possibly animals of different size.

Specialization in the role of different legs is reasonably common in other arthropods. Jamon & Clarac (1995) found that legs 3 and 4 were the main legs used during crayfish locomotion, although in some animals these patterns were altered so legs 4 and 5 played the dominant role instead. In the rapidly running cockroach, *Periplaneta americana*, different gaits utilize different number of legs generating propulsion. Full & Tu (1991) found that at slow speeds these cockroaches use the alternating tripod gait typical of insect walking, but in order to overcome limitations in stride length, and thus increase speed, animals run primarily on their two hind legs. These findings raise the issue of inter-leg coordination during locomotion, which will be examined in detail below.

5.4 Phase relationships between legs

The spider gaits shown as stepping pattern in Fig. 4.5 are best described in terms of the phase relationships between ipsilateral and contralateral leg pairs. There is great variation in phases and in some cases this is correlated with speed (Fig. 4.18 & 4.19). While there were significant trends with speed for L3:L4, L1:L4 and R1:R2, some relationships are only significant with absolute and not normalized speed and due to the fact that these relationships were not consistent across right and left ipsilateral pairings these results are difficult to interpret as fundamental patterns in locomotory behaviour.

If *D. aquaticus* were to use an alternating gait we would expect phase lag values for contralateral legs all to be equal to 0.5. Our results found that the coupling of legs 2-4 was approximately equal to 0.5. However, the phase lag distribution for front legs was found to be random. This suggests that *D. aquaticus* is actually only utilizing an alternating tripod gait analogous to insects. The alternating tripod gait predicts that contralateral and adjacent ipsilateral legs are anti-phase (i.e. have phase lags of 0.5) and adjacent-but-one legs are in phase (i.e. have phase lags of 0 or 1). Figs 4.15-4.17 investigate these phase relationships and found that as hypothesised the phase lags of L2:L3, R2:R3, L3:L4 and R3:R4 have values reasonably close to 0.5; and the phase lags of L2:L4 and R2:R4 have values reasonably close to 1. This seems to be a phenomenon which occurs to various extents in different spider species which are examined below.

Previous analysis shows the burrow dwelling wolf spider, *Lycosa tarantula*, exhibits very similar phase lag relationships to the ones described here. The mean contralateral and adjacent ipsilateral phase lags were close to 0.5 for the three hind legs, whereas the mean adjacent-but-one where close to 1 (Ward & Humphreys, 1981). In this case however, while the relationships between ipsilateral legs and leg 1 were random the anti-phase contralateral coupling between left 1 and right 1 was maintained. The same study also investigated the vagrant wolf spider, *Trochosa rurico*. Phase lag trends were similar for the three hind leg pairs; in this case however phase lag comparisons containing leg 1 were non-random (Ward & Humphreys, 1981). In both species, leg 1 exhibited more erratic movements than other legs but, in *T. rurico* this did not prevent the spider from coming close to an alternating tetrapod gait (Ward & Humphreys, 1981). Likewise comparisons between semi aquatic, *D. triton*, and terrestrial, *Lycosa rabida*, yielded differing results. During terrestrial locomotion the contralateral phase lag was random for both of the front two leg pairs in *D. triton*, but these values were close to 0.5 in *L. rabida*, with coupling approximating an alternating tetrapod gait (Shultz, 1987). Analysis of the tarantula shows progressively weaker contralateral coupling in leg pairs from posterior to anterior, with reasonably

random phase lag distributions in the front leg pair, however this distribution was not verified statistically (Wilson, 1967). This did not appear to affect ipsilateral coupling with phase lags between leg1:leg2 close to 0.5, and leg1:leg 3 close to 1 (Wilson, 1967).

The minimum requirement for static stability is three legs in a tripod on the ground at all times, analogous to a stool. Thus spiders can attain stability with a set of legs to spare, allowing the function of front legs to potentially be modified for functions other than support. The range of results suggests species are adapted to use front legs for purposes other than support to varying extents. Ward & Humphreys (1981) hypothesised that a possible purpose for these legs is as a sensory apparatus. This was supported by observations by Blickhan & Barth (1985) from tarantulas, which found that the power stroke of the front leg is shorter and the vertical excursion is higher, suggesting that front legs are acting as "feelers" during locomotion. Likewise, this "feeler" function was hypothesised in stick insets, with front legs producing smaller forces than other legs, as well as being seen making groping movements (Cruse, 1976). Research on the crickets found that forces exerted by the front legs during locomotion were smaller in magnitude and forces were more random than observations from other legs, suggesting legs may have been involved in "searching" behaviour (Harris & Ghiradella, 1980). Whip spiders, which despite their name are non-spider arachnids, have taken this specilization to the extreme. These animals also walk only on their three most posterior pairs of legs, but their front pair of legs has become highly elongated 'antenniform legs' and are specialised for sensory function (Santer & Hebets, 2009). While waiting for prey, *D. aquaticus* use the front two pairs of legs to detect vibrations both on the water and land (Forster & Forster, 1999). Many species of spider are nocturnal; in the majority of these species, vision is believed to play a reduced role, or no role at all, in mediating behavioural responses (Foelix, 1982). Thus it becomes particularly advantageous to use front legs as feelers when hunting at night.

During passive dynamic walking, there is an impulsive foot-ground collision within each stride, this impact results in loss of energy. The forces involved in the collision are the major determinant of locomotor efficiency (Garcia et al., 2000), thus providing a significant constraint on gait generation. When applied to locomotion in more complex conditions, passive dynamic simulations find it is more efficient to be able to predict ground compliance and preemptively modify gait parameters accordingly, rather than recover the trajectory after the collision (Paulin, pers. comm.). This implies that if spiders are indeed operating under passive dynamic principles, sensory information would allow disturbances to normal locomotion to be anticipated and compensated for. Therefore, front legs acting as sense organs would play a crucial role in locomotor agility.

An alternative, but less probable explanation, is that the function of these legs has been

modified due to habitat usage. Our study species, *D. aquaticus* and *D. triton* are semi-aquatic spiders. During locomotion on the water, a rowing gait involving the legs 2 and 3 is predominately used by *D. triton* (Suter, 1999). Lack of use of the front pair of legs during terrestrial locomotion may be as a result of adaptations relating to the aquatic environment. The fact that *L. tarantula* also exhibits some adaptation in front legs makes this unlikely since this species more or less stays in its burrow waiting for prey to pass (Ward & Humphreys, 1981). Thus, the most likely explanation is that the front pair of legs is being used as a sensory apparatus.

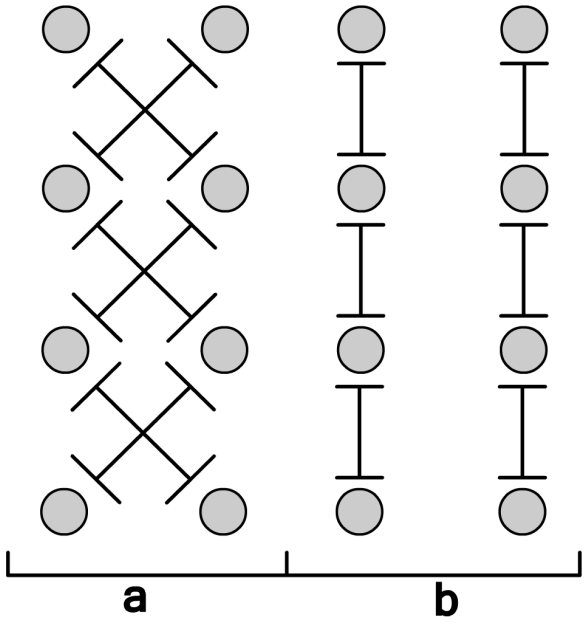

Figure 5.1: Diagrams showing the direction of inter-segmental coupling predicted by (a) the alternating tetrapod (diagonal) model and (b) the metachronal (ipsilateral) model. Created after (Shultz, 1987).

As mentioned above, *D. triton* and *L. rabida* exhibit slightly different inter-leg coupling during terrestrial locomotion. Inter-leg coupling was also investigated during locomotion on the water surface. In *L. rabida*, contralateral phase values were similar to terrestrial locomotion. However instead of an alternating gait, the ipsilateral legs assumed a metachronal stepping pattern (Shultz, 1987). *D. triton* used a "rowing" gait during water surface locomotion, as described in the previous paragraph (Shultz, 1987). The observation that ipsilateral and contralateral coordination between segments was altered in both proximate (i.e. differences between aquatic and terrestrial trials) and evolutionary time scales (i.e. differences between the two species), suggested to Shulz (1987) that inter-leg coupling is controlled by both inter- and intra-segmental mechanisms. There are two general models of pattern generation in arthropods which are illustrated in Fig. 5.1. The

alternating tetrapod model (Fig. 5.1 (a)), suggests that walking is governed by diagonal inter-segmental coupling; whereas the metachronal model (Fig. 5.1 (b)), suggests it is governed by longitudinal inter-segmental coupling (Shultz, 1987). By comparing observed phase values from *L. rabida* with values predicted using each of the models of inter-segmental coordination based on observed data from *D. triton*, it was determined that coupling was stronger between adjacent ipsilateral legs than contralateral legs, indicative of metachronal organisation (Shultz, 1987). The variation found in our phase lag data supports this conclusion, with ipsilateral pairings, not containing leg 1, all having standard deviations less than or equal to standard deviations of contratateral pairings, not containing leg 1 (Fig. 4.15 & 4.16).

5.5 Range of angular movement of joints

The entire range of mechanically possible angles is not necessarily exploited to generate the propulsive force required for locomotion. Table 5.1 compares the mechanically possible range from Reussenzehn (2008) with the range of angles utilized during locomotion. The angles observed in body-coxa joints of the front pair of legs spanned the entire range of mechanically possible angles. In fact, apart from the tibia-metatarsus joint, which has an extremely limited range of movement, the joint which used the greatest proportion of its mechanically possible range across all legs was the body-coxa. More than half of all leg muscles are located in the proximal leg segments of the spider (Seyfarth et al., 1985). The major movements involved in stepping are caused by small changes in these muscles to produce protraction/retraction, levation/depression and rotation about the leg axis. The body-coxa joint was shown to have an important role in modifying leg trajectory during climbing in the cockroach (Watson et al., 2002) and during defensive kicking in locusts (Burrows & Morris, 2001). Conversely, while the metatarsus-tarsus joint is capable of greatest range, the proportion of the range of angles that animals actually utilize is the least. The tarsus is free of muscles and instead is activated by tendons. This reduces active manoeuvrability but errors in the position of this segment can only lead to small errors in the overall position of the spider (Blickhan & Barth, 1985).

Examination of range of joint angles utilized compared to the mechanically possible range across leg pairings also reveals several trends (Table 5.1). In terms of proportions of the mechanically possible range utilized during locomotion, leg 3 exploits the greatest, followed by in successively smaller proportions leg 2, leg 1 and leg 4. Leg 4 exhibits a high degree of dragging as part of the protraction phase (Ward & Humphreys, 1981), so it is likely that the entire range is not required as this relatively smaller cycle requires less active

Table 5.1: Percentage of each joints maximum mechanical range utilized in locomotion of *Dolomedes aquaticus*. Maximum mechanical range was determined by Reussenzehn (2008).

Joint	Leg 1	Leg 2	Leg 3	Leg 4
Body-Co	100	91	96	61
Co-Tr	68	70	93	54
Pa-Ti	71	78	92	88
Ti-Me	93	100	92	88
Me-Ta	58	63	66	44

input from leg muscles. Legs 2 and 3 undergo larger and quicker angular movements, suggesting they play a more dominant role in generating propulsive force. Thus, it is not surprising that legs 2 and 3 utilize a greater proportion of their mechanically possible range compared to the less dominant pairs of legs.

5.6 Conclusions

The markerless tracking algorithm proved successful in tracking spiders during locomotion. This represents a step away from the traditional marker based techniques towards computer vision based approaches, which helps avoid some of the difficulties of marking small animals.

Stride length was found to increase significantly with spider size. This was the only kinematic parameter to yield significant results, however non-significant slopes were similar in magnitude to those in the literature. Stride frequency showed a greater correlation with normalized speed than absolute speed and stride length showed a greater correlation with absolute speed than normalized speed. This suggests that larger animals increase their speed by increasing stride length, whereas it is possible for smaller animals to increase their speed by increasing stride frequency. Contrary to the relationship frequently observed in insects, both protraction and retraction periods decreased with speed.

Each leg was found to contribute in a specific manner to locomotion. Movements of front legs were random suggesting they play some other role, possibly sensory, rather than contributing to stability. Legs 2 and 3 appeared to play a more dominant role in generating propulsive force, with hind legs probably contributing more to stability than propulsion.

Now that there is a basic understanding of the biomechanics behind terrestrial locomotion, it is possible to begin exploring how locomotion varies under different conditions and how the nervous system produces these changes.

References

Ahn, A. N., Furrow, E., & Biewener, A. A. (2004). Walking and running in the red-legged running frog, *Kassina maculata*. *Journal of Experimental Biology*, **207**, 399-410.

Alexander, R. McN. (1982). *Locomotion of Animals*. Glasgow: Blackie & Son Limited.

Alexander, R. McN. (2003). *Principles of Animal Locomotion*. Princeton: Princeton University Press.

Alexander, R. McN., & Jayes, A. S. (1983). A dynamic stability hypothesis for the gaits of quadrupedal mammals. *Journal of Zoology*, **201**, 135-152.

Anderson, B. D., Shultz, J. W., & Jayne, B. C. (1995). Axial kinematics and muscle activity during terrestrial locomotion of the centipede *Scolopendra heros*. *Journal of Experimental Biology*, **198**, 1185-1195.

Biewener, A. A. (2003). *Animal Locomotion*. New York: Oxford University Press.

Biewener, A. A. , & Full, R. J. (1992). Force platform and kinematic analysis. In A. A. Biewener, *Biomechanics: Structures and Systems A Practical Approach* (pp. 45-73). New York: IRL at Oxford University Press.

Blanco, R. E., & Jones, W. W. (2005). Terror birds on the run: a mechanical model to estimate its maximum running speed. *Proceedings of the Royal Society B*, **272**, 1769-1774 .

Blickhan, R., & Barth, F. (1985). Strains in the exoskeleton of spiders. *Journal of Comparative Physiology A*, **157**, 115-147.

Blickhan, R., & Full, R. J. (1987). Locomotion energetics of the ghost crab II. Mechanics of the center of mass during walking and running. *Journal of Experimental Biology*, **130**, 155-174.

Bonine, K. E., & Garland, T. (1999). Sprint performance of phrynosomatid lizards, measured on a high-speed treadmill, correlates with hindlimb length. *Journal of Zoology*, **248**, 255-266 .

Bowerman, R. F. (1975). The control of walking in the scorpion. *Journal of Comparative Physiology A*, **100**, 183-196.

Bowerman, R. F. (1981). Arachnid locomotion. In C. F. Herreid II, & C. R. Fourtner, *Locomotion and Energetics in Arthropods* (pp. 73-102). New York: Plenum Press.

Boykov, Y., & Jolly, M. P. (2001). Interactive graph cuts for optimal boundary and region segmentation of objects in N-D images. *Proceedings of International Conference on Computer Vision*. **1**, pp. 105-112. Vancouver: IEEE.

Boykov, Y., & Kolmogorov, V. (2004). An experimental comparison of min-cut/max-flow algorithms for energy minimization in vision. *IEEE Transactions on Pattern Analysis and Machine Intelligence*, **26**, 1124 - 1137.

Bray, M., Kohi, P., & Torr, P. H. (2006). POSECUT: Simultaneous segmentation and 3D pose estimation of humans using dynamic graph-cuts. *European Conference on Computer Vision* (pp. 642-655). Graz: Springer, Heidelberg.

Burrows, M., & Morris, G. (2001). The kinematics and neural control of high-speed kicking movements in the locust. *Journal of Experimental Biology*, **204**, 3471-3481.

Calder, W. A. (1984). *Size, Function and Life History*. Cambridge: Harvard University Press.

Cartmill, M., Lemelin, P., & Schmitt, D. (2002). Support polygons and symmetrical gaits in mammals. *Zoological Journal of the Linnean Society*, **136**, 401-420.

Cavagna, G. A., Thys, H., & Zamboni, A. (1976). The sources of external work in level walking and running. *Journal of Physiology*, **262**, 639-657.

Cook, C. E., Smith, M. L., Telford, M. J., Bastianello, A., & Akam, M. (2001). Hox genes and the phylogeny of the arthropods. *Current Biology*, **11**, 759-763.

Cruse, H. (1976). The funciton of legs in the free walking stick insect, *Carausius morosus*. *Journal of Comparative Physiology*, **112**, 235-262.

Dickinson, M. H., Farley, C. T., Full, R. J., Koehl, M. A., Kram, R., & Lehman, S. (2000). How animals move: An integrative view. *Science*, **288**, 100-106.

Farley, C., & Taylor, C. (1991). A mechanical trigger for the trot-gallop transition in horses. *Science*, **253**, 306-308.

Fedak, M., Heglund, N., & Taylor, C. (1982). Energetics and mechanics of terrestrial locomotion. II. Kinetic energy changes of the limbs and body as a function of speed and body size in birds and mammals. *Journal of Experimental Biology*, **97**, 23-40.

Fisher, N. (1995). *Statistical Analysis of Circular Data*. Cambridge University Press.

Foelix, R. F. (1982). *Biology of Spiders*. Cambridge, Massachusetts: Harvard University Press.

Forster, R., & Forster, L. (1999). *Spiders of New Zealand and their Worldwide Kin*. Dunedin: University of Otago Press.

Full, R. J., & Tu, M. S. (1990). Mechanics of six-legged runners. *Journal of Experimental Biology*, **148**, 129-46.

Full, R. J., & Tu, M. S. (1991). Mechanics of a rapid running insect - 2-legged, 4-legged and 6-legged locomotion. *Journal of Experimental Biology*, **156**, 215-231.

Garcia, M. S., Chatterjee, A., & Ruina, A. (2000). Efficiency, scaling, and speed in two dimensional passive-dynamic walking. *Dynamics and Stability of Systems*, **15**, 75-99.

Garland, T. J. (1983). The relation between maximal running speed and body mass in terrestrial mammals. *Journal of Zoology*, **199**, 157-170.

Gasparetto, A., Vidoni, R., & Seidl, T. (2008). Kinematic study of the spider system in a biomimetic perspective. *Proceedings of the IEEE/RSJ International Conference on Intelligent Robots and Systems*, (pp. 3077-3082). Nice: IEEE/RSJ.

Goyen, P. (1887). Descriptions of new species of New Zealand Aranea. *Transactions and Proceedings of the Royal Society of New Zealand*, **20**, 133-140.

Graham, D. (1983). Insects are both impeded and propelled by their legs during walking. *Journal of Experimental Biology*, **104**, 129-137.

Greig, D. M., Porteous, B. T., & Seheult, A. H. (1989). Exact Maximum A Posteriori estimation for binary images. *Journal of the Royal Statistical Society B*, **51**, 271-279.

Griffin, T. M., Main, R. P., & Farley, C. T. (2004). Biomechanics of quadrupedal walking: How do four-legged animals achieve inverted pendulum-like movements? *Journal of Experimental Biology*, **207**, 3545-3558.

Harris, J., & Ghiradella, H. (1980). The forces exerted on the substrate by walking and stationary crickets. *Journal of Experimental Biology*, **85**, 263-279.

Hedrick, T. L. (2008). Software techniques for two- and three-dimensional kinematic measurements of biological and biomimetic systems. *Bioinspiration and Biomimetics*, **3**, 034001.

Heglund, N., Cavagna, G., & Taylor, C. (1982a). Energetics and mechanics of terrestrial locomotion. III. Energy changes of the centre of mass as a function of speed and body size

in birds and mammals. *Journal of Experimental Biology*, **97**, 41-56.

Heglund, N., Fedak, M., Taylor, C., & Cavagna, G. (1982b). Energetics and mechanics of terrestrial locomotion. IV. Total mechanical energy changes as a function of speed and body size in birds and mammals. *Journal of Experimental Biology*, **97**, 57-66.

Heglund, N., Taylor, C. R., & McMahon, T. A. (1974). Scaling stride frequency and gait to animal size: mice to horses. *Science*, **186**, 1112-1113.

Hildebrand, M. (1985). Walking and running. In M. Hildebrand, D. M. Bramble, K. Liem, & D. B. Wake (Eds.), *Functional Vertebrate Morphology* (pp. 38-57). Cambridge: Harvard University Press.

Hill, A. V. (1950). The dimensions of animals and their muscular dynamics. *Science Progress*, **38**, 209-230.

Hoyt, D. F., & Taylor, C. R. (1981). Gait and the energetics of locomotion in horses. *Nature*, **292**, 239-240.

Hughes, G. M. (1952). The co-ordination of insect movements. I. The walking movements of insects. *Journal of Experimental Biology*, **29**, 267-284.

Iriarte-Diaz, J. (2002). Differential scaling of locomotor performance in small and large terrestrial mammals. *Journal of Experimental Biology*, **205**, 2897-2908.

Jamon, M., & Clarac, F. (1995). Locomotor patterns in freely moving crayfish (*Procambarus clarkii*). *Journal of Experimental Biology*, **198**, 683-700.

Jensen, R. R. (2008). *Human Gait Analysis Using Markerless Tracking*. MSc thesis: Technical University of Denmark.

Jensen, R. R., Paulsen, R., & R., L. (2009). Analyzing gait using a Time-of-flight camera. *Proceedings of the Scandinavian Conference on Image Analysis* (pp. 21-30). Oslo: Springer, Heidelberg.

Koditschek, D. E., Full, R. J., & Buehler, M. (2004). Mechanical aspects of legged locomotion control. *Arthropod Structure and Development*, **33**, 251-272.

Kohli, P. (2007). *Minimizing Dynamic and Higher Order Energy Functions Using Graph Cuts*. PhD Thesis, Oxford Brookes University.

Kohli, P., & Torr, P. (2007). Efficiently solving dynamic markov random fields using graph cuts. *IEEE Transactions on Pattern Analysis and Machine Intelligence*, **29**, 2079-2088.

Kohli, P., Rihan, J., Bray, M., & Torr, P. (2008). Simultaneous segmentation and pose estimation of humans using dynamic graph cuts. *International Journal of Computer Vision*, **79**, 285-298.

Kumar, M., Torr, P., & Zisserman, A. (2005). OBJCUT. *Computer Vision and Pattern Recognition*, **1**, 18-25.

Kumar, S., & Hebert, M. (2003). Discriminative fields for modeling spatial dependencies in natural images. In *Advances in Neural Information Processing Systems* (16 ed., Vol. 16).

Lempitsky, V., Blake, A., & Rother, C. (2008). Image segmentation by branch-and-mincut. *European Conference on Computer Vision* (pp. 15-29). Marseille: LNCS.

Li, J., Wan, C. K., Zhang, D. Y., Miao, Z. J., & Yuan, B. Z. (2009). Markerless human motion capture by Markov random field and dynamic graph cuts with color constraints. *Science in China, Series F: Information Sciences,* **52**, 252-259.

Li, S. (1994). Markov random field models in computer vision. *Proceedings of the European Conference on Computer Vision* (pp. 361-370). Stockholm: Springer-Verlag.

Loeb, G. (1989). Neural control of locomotion. *BioScience*, **39**, 800-804.

McGeer, T. (1990a). Passive dynamic walking. *International Journal of Robotics Research*, **9**, 62-82.

McGeer, T. (1990b). Passive bipedal running. *Proceedings of the Royal Society of London B*, **240**, 107-134.

McLeod, P., & Dienes, Z. (1996). Do fielders know where to go to catch the ball or only how to get there? *Journal of Experimental Psychology: Human Perception and Performance*, **22**, 531-543.

McMahon, T. (1975). Using body size to understand the structural design of animals: quadrupedal locomotion. *Journal of Applied Physiology*, **39**, 619-627.

Moeslund, T. B., & Granum, E. (2001). A survey of computer vision-based human motion capture. *Computer Vision and Image Understanding*, **81**, 231-268.

Moeslund, T., Hilton, A., & Krüger, V. (2006). A survey of advances in vision-based human motion capture and analysis. *Computer Vision and Image Understanding*, **104**, 90-126.

Moya-Laraño, J., Vinkovic, D., De Mas, E., Corcobado, G., & Moreno, E. (2008). Morphological evolution of spiders predicted by pendulum mechanics. *PLoS ONE*, **3**, e1841.

Parry, D. A., & Brown, R. H. (1959). The hydraulic mechanism of the spider leg. *Journal of Experimental Biology*, **36**, 423-433.

Paulin, M. (pers. comm.). Associate professor, University of Otago.

Perez, P. (1998). Markov random fields and images. *CWI quarterly*, **11**, 413-437.

Reussenzehn, S. (2008). *Analysis of ranges of movement for leg joints of the hunting spider Dolomedes aquaticus*. PgDip Sci Dissertation, University of Otago.

Ritzmann, R. E., Gorb, S., & Quinn, R. D. (2004). Arthropod locomotion systems: From biological materials and systems to robotics. *Arthropod Structure and Development*, **33**, 183-185.

Rother, C., Kolmogorov, V., & Blake, A. (2004). "GrabCut" - Interactive foreground extraction using iterated graph cuts. *ACM Transactions on Graphics*, **27**, 309-314.

Santer, R., & Hebets, E. (2009). Tactile learning by a whip spider, *Phrynus marginemaculatus*, C.L. Koch (Arachnida, Amblypygi). *Journal of Comparative Physiology A*, **195**, 393-399.

Sensenig, A. T., & Shultz, J. W. (2006). Mechanical energy oscillations during locomotion in the harvestman *Leiobunum vittatum* (opiliones). *Journal of Arachnology*, **34**, 627-633.

Seyfarth, E., Eekweiler, W., & Hammer, K. (1985). Proprioceptors and sensory nerves in the legs of a spider, *Cupiennius salei* (Arachnida, Araneida). *Zoomorphology*, **105**, 190-196.

Shultz, J. W. (1987). Walking and surface-film locomotion in terrestrial and semiaquatic spiders. *Journal of Experimental Biology*, **128**, 427-444.

Sidenbladh, H. (2001). *Probabilistic tracking and reconstruction of 3D human motion in monocular video sequences*. Ph.D. Thesis, KTH Royal Institute of Technology.

Sprugel, D. G. (1983). Correcting for bias in log-transformed allometric equations. *Ecology*, **64**, 209-210.

Stockard, C. R. (1908). Habits, reactions and mating instincts of the walking stick. *Papers from the Tortugas Lab of the Carnegie Institution of Washington*, **103**, 45-59.

Suter, R. B. (1999). Locomotion on the water surface: hydrodynamic constraints on rowing velocity require a gait change. *Journal of Experimental Biology*, **202**, 2771-2785 .

Suter, R. B. (2000). Spider size and locomotion on the water surface (Araneae, Pisauridae). *The Journal of Arachnology*, **28**, 300-308.

Taylor, C. R. (1978). Why change gaits? Recruitment of muscles and muscle fibers as a function of speed and gait. *American Zoologist*, **18**, 153-161.

Taylor, C. R., Heglund, N. C., & Maloiy, G. M. (1982). Energetics and mechanics of terrestrial locomotion. I. Metabolic energy consumption as a function of speed and body size in birds and mammals. *Journal of Experimental Biology*, **97**, 1-21.

Ting, L. H., Blickhan, R., & Full, R. J. (1994). Dynamic and static stability in hexapedal runners. *Journal of Experimental Biology*, **197**, 251-269.

Walker, J. A. (1998). Estimating velocities and accelerations of animal locomotion: a simulation experiment comparing numerical differentiation algorithms. *Journal of Experimental Biology*, **201**, 981-995 .

Ward, T. M., & Humphreys, W. F. (1981). Locomotion in burrowing and vagrant wolf spiders (lycosidae). *Journal of Experimental Biology*, **92**, 305-321.

Watson, J. T., Ritzmann, R. E., Zill, S. N., & Pollack, A. J. (2002). Control of obstacle climbing in the cockroach, *Blaberus discoidalis*. I. Kinematics. *Journal of Comparative Physiology A*, **188**, 39-54.

Wilson, D. (1966). Insect walking. *Annual Review of Entomology*, **11**, 103-122.

Wilson, D. M. (1967). Stepping patterns in tarantula spiders. *Journal of Experimental Biology*, **47**, 133-151.

Zakotnik, J., & Dürr, V. (2005). Motion analysis using stochastic optimisation and posture disambiguation. In H. Witte (Ed.), *Third International Symposium on Adaptive Motion of Animals and Machines* (pp. 1-6). Ilmenau: ISLE Verlag.

Zakotnik, J., Matheson, T., & Dürr, V. (2004). A posture optimization algorithm for model-based motion capture of movement sequences. *Journal of Neuroscience Methods*, **135**, 43-54.

Zani, P. A., & Claussen, D. L. (1994). Voluntary and forced terrestrial locomotion in juvenile and adult painted turtles, *Chrysemys picla*. *Copeia* , **2**, 466-471.

Zar, J. H. (1996). *Biostatistical Analysis* (3rd ed.). London: Prentice-Hall.

Zollikofer, C. (1994a). Stepping patterns in ants I. Influence of speed and curvature. *Journal of Experimental Biology*, **192**, 95-106.

Zollikofer, C. (1994b). Stepping patterns in ants II. Influence of body morphology. *Journal of Experimental Biology*, **192**, 107-118.

Appendix A. Locomotion terminology

Term	Description
Absolute velocity	Velocity in absolute measurements i.e. cm s^{-1}.
Anterior extreme position	The leg reaches its most anterior position. Transition from the swing phase to the stance phase occurs at this point.
Contralateral	On the opposite side (used with reference to legs).
Double support	All legs in contact with the ground.
Duty factor	Percentage of the stride cycle for which a leg is in the stance phase.
Ipsilateral	On the same side (used with reference to legs).
Leg phase	Describes a given leg phase with respect to a reference leg.
Normalized velocity	Velocity in normalized for body size i.e. body lengths s^{-1}.
Posterior extreme position	The leg angle reaches its most posterior position. Transition from the stance phase to the swing phase occurs at this point.
Stability margin	Longitudinal stability margin of a wave gait normalized for stride length is $S = \frac{n_{legs}}{4}\beta - \frac{3}{4}$ where β is duty factor and n_{legs} is the number of legs. When S<0, the animal is statically unstable.
Stance phase	Also referred to as power stroke or support phase. Period where the leg is on the ground providing support and propulsion for the animal. The horizontal component of the swing phase is retraction.
Stride frequency	Number of strides per second, 1/stride period.
Stride length	The distance the trunk translates during one stride. Calculated by average velocity divided by stride frequency.
Stride period	Time for a complete cycle of locomotion. This begins and ends with the reference leg footfall. We take it to be two successive anterior extreme positions of the second left leg unless analysis is occurring on a specific leg.
Swing phase	Also referred to as return stroke or transfer phase. Period in which the leg is off the ground moving from one foothold to the next. The horizontal component of the swing phase is protraction.

Appendix B. Tracking GUI

Following is a section of figures showing the key components of the graphical user interface set up to facilitate tracking of different spiders in multiple video files. The corresponding code can be found on the DVD provided. To capture images which allowed high resolution images of various menus, we use screen-capture software (SnagIt, version 9.0; TechSmith, East Lansing, MI; www.snagit.com).

(a) File menu: New Project, Load, Save, Batch Process, Quit.

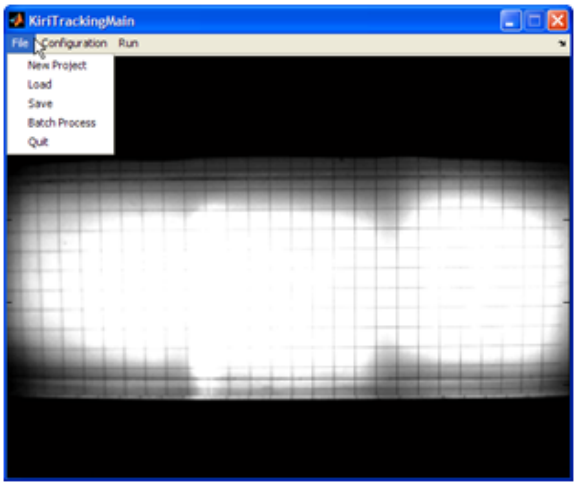

(b) Configuration menu: Configure Video, Configure Model, Configure Optimization.

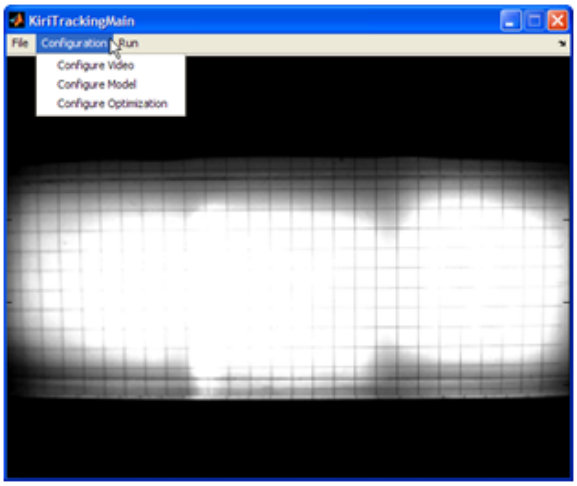

(c) Run menu: Track, Filter.

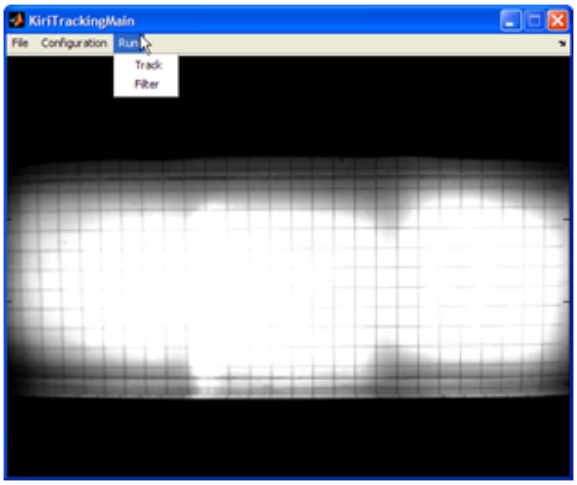

Figure B.1: The main display of the tracking GUI and the various menus. The File menu (a) contains options relating to file input and output, the configure menu (b) allows any of the tracking parameters to be adjusted and the run menu (c) runs tracking and filtering of raw data.

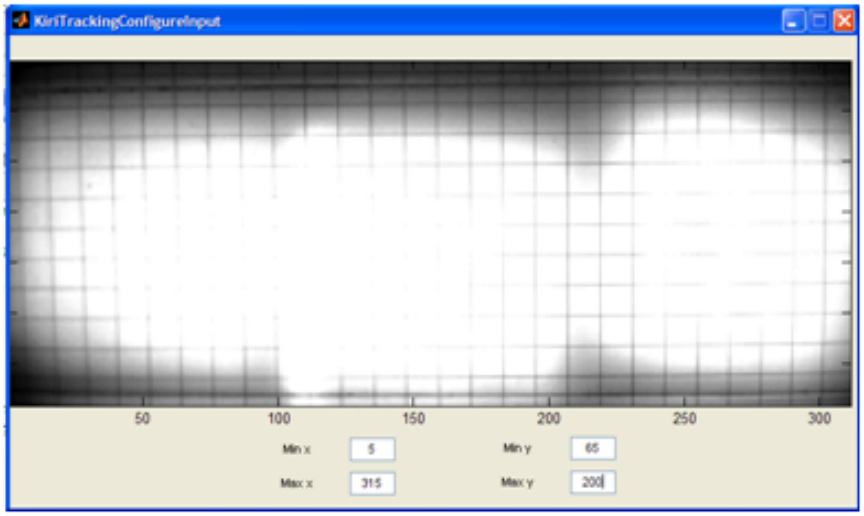

Figure B.2: The configure input display pops up when the video file is loaded. This allows the user to select the rectangular region of interest for tracking analysis.

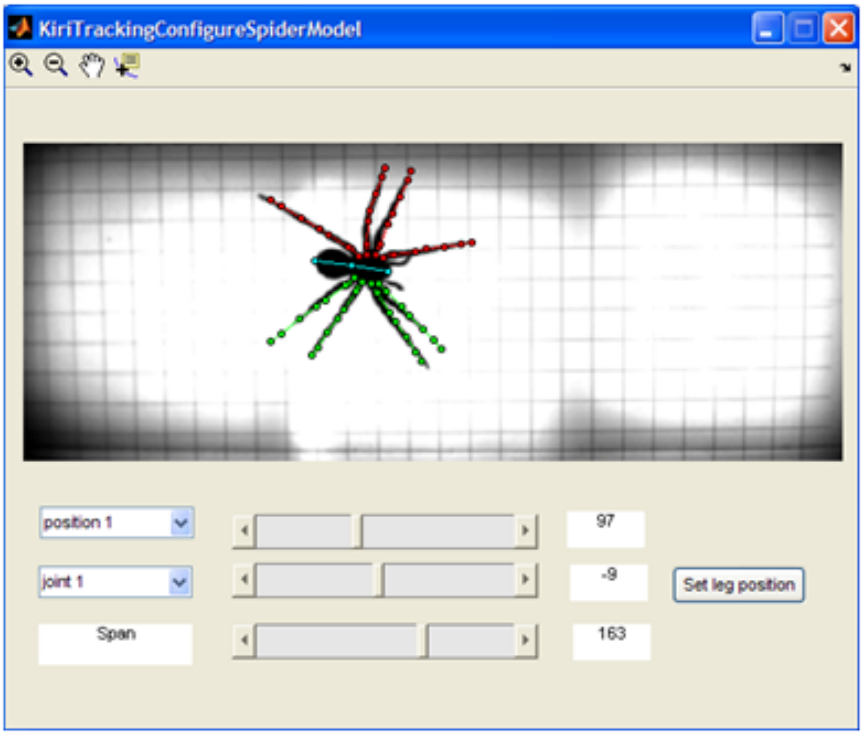

Figure B.3: The configure model display pops up when Configure>Configure Model is selected. This allows the user to initialize the position, joint angles and leg span of the spider and displays the resulting stick spider.

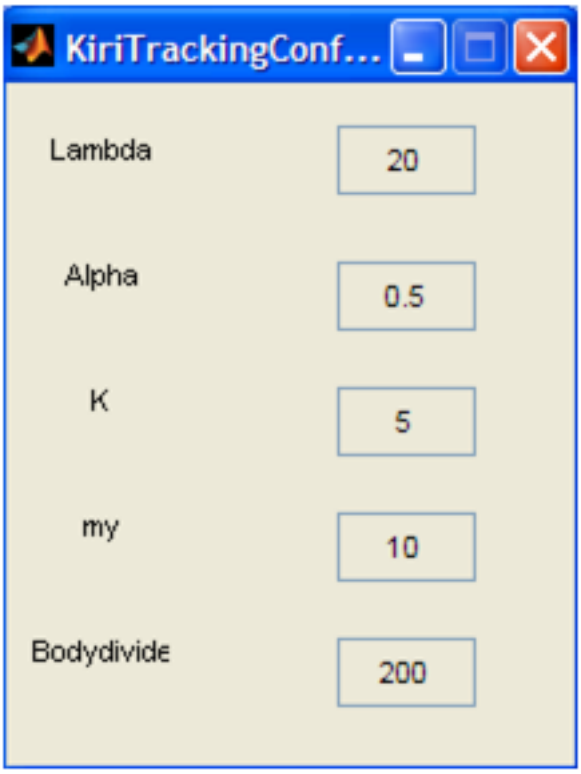

Figure B.4: The configure optimization display pops up when Configure>Configure Optimization is selected. This allows the user to alter the various input parameters controlling penalties etc. for tracking.

Appendix C. Description of files on CD

The CD contains three folders: tracking code, analysis code and videos. Files in the first two folders are presented such that they contain the name of the person who wrote the code followed by the function name. Code on markerless tracking of humans using a time-of-flight camera was acquired via personal communication with Rasmus Jensen. The majority of my tracking code works at adapting these techniques to intensity images (normal video stream) of spider locomotion. All code acquired from other sources contains information regarding its source in the comments at the top of the function. The student version of MATLAB gives access to several toolboxes, from memory my code uses functions from the Image Processing toolbox and Statistics toolbox. The Bouguet Camera Calibration Toolbox for MATLAB available at http://www.vision.caltech.edu/bouguetj/calib_doc/, is used for calculating the conversion factors from pixels to cm. This present use is somewhat overkill for the simple task, but it is implemented in the hope we will soon be tracking in 3D. The key file for tracking is KiriTrackingMain which opens the GUI and all other functions are called through this. The key file for analysis and statistics is kiri_statisticalAnalysis which again calls all other required functions.

The videos folder contains an example of the original video, segmentation, tracking results, animation of the shape model and analysis of stationary frames. Segmentation was included to show how this technique accurately segments the video stream into spider and background. Tracking results illustrate the success of pose estimation by overlaying the original video with the stick spider in its estimated pose. Stick spider again proves the correctness of pose estimation with the resulting movement of the shape model looking "spider-like" and also hints at the applicability of motion capture results to animation. Finally, tracking of the stationary frames that were used to estimate accuracy is included.